THE DEVELOPMENT AND USE OF THE RAYLEIGH INTERFEROMETER TO STUDY MOLECULAR DIFFUSION IN AN APPLIED MAGNETIC FIELD

by

STEVEN KELLEY HOWELL

B.Sc., Southern Methodist University, 1976
M.Sc., Southern Methodist University, 1977

A THESIS SUBMITTED IN PARTIAL FULFILLMENT OF

THE REQUIREMENTS FOR THE DEGREE OF

DOCTOR OF PHILOSOPHY

in

THE FACULTY OF GRADUATE STUDIES

(Department of Chemical Engineering)

We accept this thesis as conforming

to the required standard

THE UNIVERSITY OF BRITISH COLUMBIA

July, 1983

In presenting this thesis in partial fulfilment of the requirements for an advanced degree at the University of British Columbia, I agree that the Library shall make it freely available for reference and study. I further agree that permission for extensive copying of this thesis for scholarly purposes may be granted by the head of my department or by his or her representatives. It is understood that copying or publication of this thesis for financial gain shall not be allowed without my written permission.

Department of Chemical Engineering

The University of British Columbia
1956 Main Mall
Vancouver, Canada
V6T 1Y3

Date 25,November, 1983

ABSTRACT

The purpose of this work was to investigate the effects of an externally applied homogeneous steady magnetic field on liquid phase diffusion through a porous membrane. A physico-chemical model was developed to describe the effect of a magnetic field on magnetically anisotropic molecules diffusing through a porous membrane. An applied magnetic field is expected to cause a reduction in the diffusivity of an anisotropic molecular system. Orientation of the molecule in the magnetic field (Cotton-Mouton effect) will change the effective cross-sectional area of the molecule, increasing the viscous drag between the molecule and membrane pore surface thereby reducing the diffusion coefficient.

An optical interferometric technique was used to measure diffusion coefficients which offered advantage over other methods since concentration profiles could be locally observed adjacent to the membrane surface without disturbing the diffusive flows. A Rayleigh interferometer was designed and constructed to be placed between the pole pieces of a 30 cm electromagnet. The diffusion of an aqueous sucrose solution through General Electric Nucleopore membranes (pore diameters 0.8 μm and 8.0 μm) was measured in applied field strengths from 0 to 12.5 kGauss. This combination of membrane and solution was selected for this initial work because of potential applications to biological systems and to verify the validity of the measurement technique since widely accepted diffusion data for this system are

available in the literature for comparison. A computer program was developed to account for errors introduced by wavefront deflection in a refractive index gradient and to numerically calculate mass fluxes and diffusivities from interference fringe data.

Within the limits of experimental error a slight decrease (1% to 2%) in the diffusion coefficient of sucrose through the membrane has been observed for applied magnetic fields up to 12.5 KG. Free diffusion coefficients measured at no field conditions compared to accepted values measured at identical concentration and temperature to within ± 3%.

While these results indicate some alignment of the sucrose-water clusters in an applied magnetic is taking place, further work is needed to improve the accuracy of the experimental technique and to study molecules possessing a higher degree of anisotropy than sucrose and water. Recommendations are made for modifications to the diffusion cell which should significantly reduce experimental errors. Magnetically anisotropic molecular systems are also recommended for study which should show a greater degree of magnetic orientation than sucrose and water.

TABLE OF CONTENTS

LIST OF TABLES

LIST OF FIGURES

ACKNOWLEDGMENTS

I would like to thank my research supervisor, Professor Janis Lielmezs, for his guidance, support, and inspiration during this work.

Acknowledgment is made to the Natural Sciences and Engineering Research Council of Canada for their financial support and to the University of British Columbia for a Graduate Student Research Fellowship which made this work possible.

A special thanks to Mrs. Hana Aleman for the many useful suggestions and ideas and timely assistance in proofreading this manuscript.

I appreciate the assistance of Mr. Paddy Jarvis of the UBC Chemical Engineering Workshop for the excellent fabrication of the experimental equipment.

None of this would have been possible without the loving support and encouragement from my wife, Debra.

CHAPTER 1

INTRODUCTION

In recent years a great deal of interest has been generated in magnetic field effects on various chemical and biological processes. With the advent of manned space flight in the 1960's, researchers became interested in the effects of the absence of a magnetic field on the living organism with respect to extended outer space flight.[1] Barnothy[2] performed some of the earliest research in magnetic effects on the living organism. In 1948 he found that young female mice, when placed in a $(3 - 6) \times 10^3$ Oersted magnetic field, underwent a temporary retardation of growth. He also reports[3] that a magnetic field can have a retardation effect on the growth rate of cancer cells in mice. Several researchers have also investigated the effect of an applied magnetic field on the healing rate of bone fractures.[4-7] A slight increase in the rate of healing has been observed when low frequency alternating magnetic fields are applied to the fracture. This method is currently being used on an experimental basis at the UBC Sports Medicine Centre to influence the healing rate of athletic stress fractures.[8] Barnothy[9] has compiled an extensive survey of other interesting applied magnetic field effects to living systems including changing the germination rate of seeds, altering the navigational ability of homing pigeons, and changing the pulse rates and metabolism of rats. No satisfactory agreement has been reached on a biochemical explanation for these effects. Bhatnager and Mathur[10] propose that these effects can be explained by a change in reaction rates within the cell, while Gross[11]

attributes these changes to alterations in the chemical bond formations due to the presence of a magnetic field. Liboff[12] proposes that the growth rate changes observed in cells in an applied magnetic field result from a change in the diffusion rate of dissociated salts across the plasma membrane and nuclear membrane of the cell.

In addition to the magnetic effects on living systems, several researchers have reported a magnetic field effect on various other physical and chemical dynamic processes. Lielmezs et al. have studied magnetic effects on liquid transport properties and the diffusion rate of several aqueous salt solutions.[13-20] They also report a change in the viscosity of calf thymus DNA[21] during the thermal denaturation process which they relate to magnetic inhibition of the double helix-coil unwinding during denaturation. Changes in transport properties of gases in an applied magnetic field have also been observed.[22-39] The kinetic theory of gases has been extended to provide a theoretical basis for these observations. These results will all be discussed in greater detail in Chapter 2.

This experimental evidence indicates that a magnetic field applied to many dynamic chemical and biological processes changes the dynamics of that process. While the kinetic theory of gases has been successfully applied to predict these effects in gases, very little theoretical basis exists for the prediction of magnetic effects in the liquid state. The effects of a magnetic field on the living organism has intrigued researchers for many years, but at this time no clear understanding of the molecular mechanisms responsible for these effects

has been reached. Therefore, it is the purpose of this work to study the effects of an applied magnetic field on the diffusion rate of organic molecules through a membrane. A simple theory of molecular diffusion in a magnetic field through a porous membrane is developed with application to molecules which possess a magnetic anisotropy. A system was selected for investigation which consists of a common organic molecule; sucrose, in an aqueous solution diffusing through a porous membrane. The membrane used consists of straight cylindrical pores in a thin (10 micron) polycarbonate film. This combination of membrane and solution has potential application to biological systems, yet provides a simple system for analysis since the pores of the membrane act as capillaries for the diffusing molecules. In addition, data are readily available in the literature for this system in the absence of a magnetic field, providing a reference point for this work.[40]

Optical interferometry was selected as the technique to measure these diffusion coefficients. This method was chosen because it provides a tool which gives a continuous concentration profile of the diffusing molecules at all locations in the test cell. If the diffusing medium is transparent to the optical wavelength used, then no energy is absorbed by the diffusing molecules and it is possible to measure the diffusion rate without disturbing the diffusive flows. Therefore, this technique is desirable for measuring local diffusion coefficients through a membrane in a magnetic field, since the only perturbations to the diffusion process will be due to the applied magnetic field and not from the measurement technique itself.

The work described in this thesis consists of: I) previous work and literature survey — a survey of previous studies made on magnetic effects observed on transport properties of gases and liquids, and a review of experimental techniques used to measure liquid system diffusion coefficients; II) theoretical considerations - development of a theory describing molecular diffusion in a magnetic field and a review of the theory of interferometry; III) experimental method - a detailed description of the experimental setup and method; IV) data analysis - a method of interpreting interference fringes and reducing them to concentration profiles and mass fluxes, including a technique to allow for errors introduced by optical ray bending in a refractive index gradient; V) results - a discussion of experimental data in terms of the theory described in Part II and VI) recommendations for areas of further research and conclusions.

CHAPTER 2

HISTORICAL BASIS AND PREVIOUS WORK

2.1. Magnetic Field Effects on Transport Properties of Gases

The earliest work examining magnetic effects on the transport properties of gases and liquids was performed in 1930 by Senftleben when he discovered that an applied magnetic field changes the viscosity of oxygen.[41] He observed a decrease in viscosity up to a maximum of 0.4% as a function of H/P, where H was the applied magnetic field strength and P the pressure of O_2. Magnetic effects have since been observed on the thermal conductivity and kinematic viscosity of a member of polyatomic gases[22-39] including HCl, DCl, N_2O, CO_2, OCS, SF_6, CH_3F, CH_3, CN, CHF_3, CDF_3, NH_3, ND_3, NF_3, PH_3, PF_3, AsH_3, O_2, NO, N_2, CH_4, CF_4, CO, nH_2, HD, oD_2, ND_2, pH_2, and CD_4. Beenakker and McCourt[39] give an excellent review of all work done prior to 1970, describing the various magnetic effects on the transport properties of gases.

The kinetic theory of gases has been successfully applied to explain these results and elucidate several aspects of the interactions of polyatomic molecules. In the presence of a magnetic field, any molecular anisotropy will precess around the field direction due to the interaction of the field with the rotational magnetic moment. This precession causes the axis of the molecule to spin about the magnetic field axis much as a rotating gyroscope "wobbles" about the gravitational vector. The frequency and magnitude of the precession is dependent upon the strength of the applied field, the molecular

rotational magnetic moment, and angular momentum of the molecule. This precessional motion has the effect of changing the cross-sectional area of the molecule for collisions with other molecules in the gas phase. The net result is an overall polarization of the cross-sectional areas of the molecules with respect to the direction of the applied field.

This effect can best be visualized by considering Einstein's model for the transport of heat in a gas. For a monatomic gas the heat flow q is defined as

$$q = \int f^M \, 1/2 \, m\vec{V}^2 \, \vec{V} d\vec{V} \tag{2.1}$$

in which f^M is the distribution function, m the particle mass, and $\vec{V}$ the velocity. A temperature gradient $\nabla\vec{T}$, produces a deviation of the distribution function away from the ideal Maxwellian distribution function $f^{(0)}$, which results in a transport of heat through the gas. In the first order, this deviation is proportional to the temperature gradient.

$$f^M = f^{(0)} \, (1 + \vec{A} \, \nabla\vec{T}) \tag{2.2}$$

For a polyatomic gas the vector $\vec{A}$ depends both upon the molecular velocity and the angular momentum of the molecule. When a magnetic field is applied to the gas the angular momentum is polarized in space. This polarization causes an anisotropic distribution of energy in the gas which is observable as an anisotropic thermal conductivity for the gas. Therefore, measurements of these anisotropies provide a test of

the kinetic theory of gases for molecules with internal degrees of freedom.

2.1.2 Magnetic Field Effects on Liquid Transport Properties

Unfortunately, experimental research in magnetic field effects on liquid transport properties is much more limited than for the gaseous state. While many aspects of the kinetic theory of gases are fairly well established and have been reasonably defined or derived such is not the case for a kinetic theory of liquids.[42] In the liquid state a molecule interacts simultaneously with several neighbors, whereas in the gaseous state molecules generally react with only one other molecule at a time. Therefore a theoretical basis for predicting a magnetic effect on liquid transport properties and diffusion is very limited at this time.

Brenner[42a] derives a theoretical expression for the effects of an applied magnetic field on a dilute suspension of spherical particles which possess a magnetic dipole. He discusses how an applied field hinders the free rotation of the particles and hence how the apparent viscosity becomes anisotropic with respect to the direction of applied field.

Lielmezs and Musbally,[43] and Camp and Johnson[44] have chosen to deal with magnetic effects on liquid diffusion on a macroscopic level using the principles of irreversible thermodynamics. They define another driving force term in the thermodynamic force-flux relationships which is the Lorentz force exerted on a diffusing ion in a magnetic field.

This force is defined as

$$\vec{F}_K = Z_K(\vec{V}_K \times \vec{B}) \tag{2.3}$$

where Z_K is the electric charge on the diffusing ion, $\vec{V}_K$ its average drift velocity and $\vec{B}$ the magnetic induction. This force term is included with the other diffusive driving forces and applying the principles of irreversible thermodynamics they solve for the ratio of diffusion coefficients with and without an applied field as,

$$\frac{D^H}{D^o} = \left[1 + \frac{(\vec{V}_1 \times \vec{B}) - (\vec{V}_2 \times \vec{B})}{\mu_{ss} \qquad \text{grad}C_s}\right] \tag{2.4}$$

where $\vec{V}_1$ and $\vec{V}_2$ are the average drift velocities for the two ions, μ_{ss} is the partial derivative of chemical potential with respect to concentration, $\frac{\partial \mu_s}{\partial C_s}$, and $\text{grad}C_s$ is the salt concentration gradient.

O'Brien and Santhanan[45] observed this Lorentz force in an aqueous solution of copper sulfate during electrodeposition in an applied magnetic field. They used a multiple beam interferometer to observe the concentration profile in the electrodeposition cell. When a magnetic field of 6.12 kG was applied to the cell the Lorentz force resulting from the motion of the ions in the applied magnetic field produced a convective driving force. This convection was observable as disturbances in the concentration gradient in the cell producing interference fringes.

Lielmezs and Aleman[15-20] have studied the diffusion of various aqueous solutions of chloride salts (LiCl, NaCl, KCl, and CsCl) through a fritted glass diaphragm in an applied magnetic field. Some of their results are depicted in Figure 1. In an applied field of 5 kG the integral diffusion coefficients for LiCl and CsCl show a slight decrease, while for the other salts they show an increase, the most notable being KCl. The exact cause of these changes cannot be decided with any degree ofcertainty. They note, however, that the KCl-H_2O system, showing the largest magnetic effect, also shows the greatest structural disorder. These results are intriging and of a qualitative nature, and at this time no definite conclusions have been reached explaining them.

Lielmezs et al.[13,14] have also observed a viscomagnetic effect for water and various aqueous solutions of paramagnetic salts ($Mn(NO_3)$, $Cu(NO_3)$, $Ni(NO_3)$ and $Co(NO_3)$). At a transversally applied field strength of 10 kG, they measured an increase in the viscosity of water between 0.1 and 0.2 %.[46,47] They proposed that the magnetic field caused a slight change in the angle of the hydrogen bonds in water which in turn affects the translational and reorientational motion of the molecules and the viscosity. They observed a slight decrease in the viscosity of the various water-paramagnetic salt solutions. They found that the viscosity decreased at high salt concentrations, yet at low concentrations the observed viscosity increases, approaching that of pure water in an applied magnetic field, leading them to propose the existence of two competing microstructural interaction mechanisms; the dipolar interactions associated with pure diamagnetic water, and the

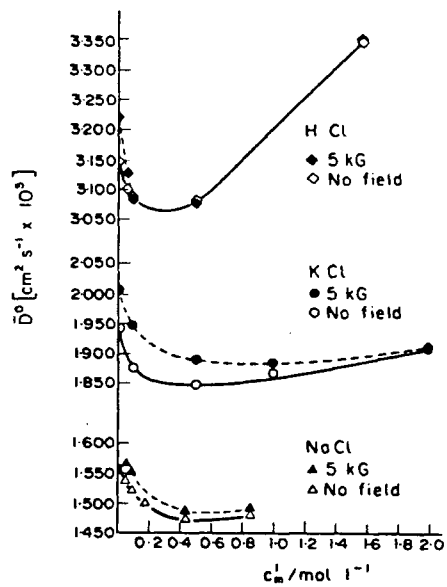

Arithmetic mean integral diffusion coefficient and concentration plot at 25°C temperature for HCl–, NaCl– and KCl–H_2O solutions at the ambient earth field (solid curve) and at the applied external transverse magnetic field (dashed curve) condition.

Figure 1 - Lielmezs' et al.[15] Results for the Diffusion of Aqueous Chloride Salts in an Applied Magnetic Field. (used by permission).

spin-exchange mechanism characterizing the paramagnetic ion-water solution. All of these experiments were performed isothermally at room temperature for several different concentrations.

2.2 Historical Review of Interferometry

Optical interferometry is a technique which will yield a continuous profile of the refractive index of the medium through which the light is being transmitted. In the case of liquid diffusion the refractive index of the diffusing liquid system can be observed continuously in space and time which can be related to concentration of the diffusing molecule or ion. With the advent of modern coherent laser light sources this technique has evolved to a powerful, sensitive tool for measuring small concentration changes in any diffusing molecular system.

2.2.1 Early Work

Optical interferometry was first applied to liquid diffusion measurements of Philpot and Cook[48] in 1947. To do this they modified the Rayleigh interferometer with the introduction of a cylinder lens, which would focus a set of interference fringes representing the refractive index as a function of position in the test cell. Philpot and Cook used this original equipment to measure the diffusion of sodium thiosulfate in water. Longsworth[49] was working concurrently with Philpot and Cook and applied the Gouy method of interferometry to measure diffusion coefficients of KCl dissolved in water at 0.5°C. This method is similar to the one used by Philpot and Cook, except he had no cylindrical lens to focus the interference fringes as a function of position in the test

cell. This equipment produced interference fringes which were a function of refractive index gradient in the cell. At the same time Longsworth was pioneering the applications of Gouy interferometry to diffusion measurements, Ogston[50] was working independently using the same method, applying it to measure binary diffusion coefficients of glycine, KCl, sucrose, and lactoglobulin dissolved in water. In 1949 Gosting and Morris,[51] continuing the development of the Gouy interferometric method published diffusion coefficients for an aqueous sucrose solution at 25°C and 1°C. In 1951, Gosting and Akeley[52] continued this work using the same method to evaluate diffusion coefficients for urea in water at 25°C.

While these workers were developing and using the Gouy method of interferometry, Svenson[53] and Longsworth[54] were extending the original work done by Philpot and Cook with the Rayleigh interferometer. They were both applying it to the measurement of aqueous sucrose diffusion coefficients at 25°C.

This early work was all performed before the advent of modern, laser light sources. These workers all used either sodium vapor or mercury vapor sources of light. The quality of interference fringes they reported is remarkable considering the poor coherence of those light sources as compared with the gas laser used today. All of these workers estimated the values of free diffusion coefficients they measured were accurate to 0.2% or less.

2.2.2 Later Work

The advent of the continuous gas laser in the mid nineteen

sixties provided an intense monochromatic coherent light source previously unobtainable with the conventional vapor lamps. A laser light source is essentially one frequency with the light waves in phase across the output beam cross section. This level of coherence produces interference fringes with a clarity and intensity unobtainable from a vapor light source. Principles of coherence will be dealt with in more detail in Chapter 3.

In the early sixties O'Brien[55] and O'Brien et al[56] pioneered the use of multiple beam interferometry for mass transport measurements. They used a wedge interferometer, which was designed with the light beam passing through the diffusing substance many times, in contrast to a single pass as in the Gouy or Rayleigh interferometric methods. This technique produced a set of interference fringes which were much more sensitive to small refractive index changes than the other single pass systems. They applied this method to measure the concentration gradients at the electrode surfaces of a $Zn/ZnSO_4/Zn$ and $Cu/CuSO_4/Cu$ electrochemical cell.

In 1969 Duda, Sigelko, and Vrentas[57] developed a multiple pass wedge interferometer to measure sucrose-water diffusion coefficients at 25°C. They estimate an accuracy of ±3% with this technique. Multiple beam interferometry has since been applied to diffusion measurements for many different systems including the measurement of diffusion of O_2,N_2,H_2 and Ar into water.[58]

Rard and Miller[59-61] have used Rayleigh interferometry with a laser light source to measure the diffusion of $BaCl_2$, KCl, CsCl, $SrCl_2$,

NaCl, and $CaCl_2$ in aqueous solutions at room temperature. They measured free diffusion coefficients of very dilute solutions (.01 moles/l) to high concentration solutions (5.5 moles/l). They estimate an accuracy of 0.1% to 0.2% for their results.

Sorell and Myerson[62] used a Gouy interferometer with laser light source to measure the diffusivity of an aqueous urea solution in a saturated and supersatured solution. They estimate an error of less than 5% for their results.

Renner and Lyons[63] developed a novel method of improving the data reduction techniques for interferometric measurements. They used an electronic photomultiplier scanner to electronically measure the fringe spacing of the interference fringes produced from a Gouy interferometer applied to the measurement of KCl-water diffusion coefficients. The output of this device was input directly to a digital computer which converted the fringe spacing to refractive index profiles and mass fluxes and diffusivities. This method minimized human errors introduced when manually measuring fringes through a microscope.

More recently double exposure holography has found applications to mass transport problems. Holography has the primary advantage that abberrations in the optical components are "cancelled out" during the reconstruction process, enabling an experimenter to work with less expensive, more readily available lenses, mirrors, and optical components. In this method a three dimensional hologram is made of the test cell during its initial condition. Then, after the mass transport process begins another "double exposure" hologram is made of the object,

with virtually no movement allowed in either the object or photographic film. An interference fringe will appear at every location on the reconstructed image of the test cell where an optical path difference of one wavelength occurred between the two exposures. The fringe results from an optical path length change where the light was transmitted through the object, thus enabling one to measure an index of refraction change at a particular location on the test cell. Gabelman-Gray and Fenichel[64] used double exposure holography to measure the diffusion coefficients of a 10% aqueous sucrose solution at 25°C. Their results are within 10% of other values measured by other methods. O'Brien, Langlais, and Seufort[65] used holography to measure the diffusion coefficients of respiratory gases into a synthetic blood substitute, a perfluorocarbon liquid.

Interferometric techniques which directly measure concentration profiles have been widely applied to the study of free diffusion in liquids. The opaque characteristics of membranes have inhibited the direct measurement of concentration profiles in the membrane itself. However, Bollenbeck and Ramariz in 1972[40,66] first applied interferometry to the measurement of diffusion through membranes. They used a Rayleigh interferometer to measure concentration profiles surrounding a membrane surface in an aqueous sucrose solution. They developed a technique to evaluate the mass flux at each membrane solution interface and therefore the diffusion coefficient through the membrane itself. An error of ±3% is estimated for their work. A modification of their technique is applied in this work to measure

membrane diffusion coefficients in an applied magnetic field. Details concerning this technique are contained in appropriate sections of this thesis.

Min et al[67] and Forgacs et al[68] applied a wedge interferometer to the study of membrane diffusivities in a cellophane and ion exchange membrane respectively. Min et al studied the steady state diffusion of ethyl alcohol and water through a cellophane membrane at room temperature. They estimate an accuracy of at least ±3% for their results. Forgacs et al studied the diffusion of an aqueous KCl solution through an ion-exchange membrane with an applied electric current following current reversal.

The applications of interferometry to diffusion process measurements have been more widely applied to the measurement of free diffusion coefficients rather than membrane diffusion coefficients. The presence of a membrane in the diffusing medium presents several measurement problems not encountered with free diffusion measurements. The membrane is opaque to the transmitted light so it is not possible to actually observe the concentration profile through the membrane. Simplifying assumptions must be made concerning the mass fluxes and concentration gradients through the membrane. In addition, wavefront deflection of light transmitted through a refractive index gradient occurs near the membrane surface which produces a distortion of the measured concentration profile and membrane shadow, so techniques must be developed to correct for deflection effects.

CHAPTER 3

THEORETICAL CONSIDERATIONS

This chapter presents the theoretical basis for molecular diffusion through a membrane. Fick's law is reviewed with application to a simple porous membrane. The effects of a magnetic field on diffusion is discussed with a review of the basic theory of magnetism. A theoretical model is developed describing the effect of a magnetic field on the diffusion rate of molecules through a membrane consisting of cylindrical pores. In addition, the theory of optical interferometry is presented, with applications to diffusion measurements.

3.1 Theory of Molecular Diffusion in a Magnetic Field

3.1.1 Fick's Law of Binary Diffusion

Diffusion is the transfer of a substance through a homogenous solution resulting from a difference in concentrations at two different regions in the mixture. Diffusion is a result of the random Brownian motion of the molecules arising from the thermal energy of the molecule. In terms of this assumption, the motion of the molecule may be considered random. Therefore the net molecular motion of the diffusing species will be from the direction of higher concentration to lower concentration in the absence of any temperature or pressure gradients. Fick's law of binary diffusivity expresses the molecular flux, J, as a linear function of concentration gradient $\frac{\partial C}{\partial x}$

$$J = D \frac{\partial C}{\partial x} \tag{3.1}$$

where D is the constant of proportionality; the diffusion coefficient. Eq. 3.1 is Fick's first law and defines the flux at steady state conditions. This equation is valid for isothermal conditions at constant pressure and with no volume change on mixing. Expressing Fick's first law equation in terms of the conservation of mass (i.e. the change in concentration per unit time in a given volume is equal to the difference of the flows into and out of the volume) gives

$$\frac{\partial C}{\partial t} = \frac{-\partial J}{\partial x} = \frac{D\partial C^2}{\partial x^2} \qquad (3.2)$$

which is Fick's second law. The work presented in this thesis will only consider a concentration gradient in one dimension, so the partial derivatives in Eqs. 3.1 and 3.2 will become ordinary derivatives.

3.1.2 Kinetic Interpretation of Diffusion

Einstein[69] used the molecular kinetic theory of heat to develop a theory of Brownian motion and provide a physical picture to describe the diffusion process in dilute solutions.

According to the molecular kinetic theory, heat is simply a manifestation of the motion of the molecules in a system. The average translational kinetic energy, $1/2\ m\bar{v}^2$ is proportional to the absolute temperature, T, of the system;

$$1/2\ m\bar{v}^2 = 3/2\ KT \qquad (3.3)$$

where K is Boltzman's constant and $\bar{v}$ is the mean square transit velocity in any direction. Einstein showed that the mean square Brownian displacement along an axis, $\bar{\delta}_x^2$, for some time interval Δt is

$$\bar{\delta}_x^2 = \frac{2KT}{f} \Delta t \tag{3.4}$$

where f is a frictional coefficient of a solute molecule. The diffusion coefficient, D, is related to the motion of the particle per unit time by

$$D = \frac{\bar{\delta}_x^2}{2\Delta t} \tag{3.5}$$

Substituting Eq. 3.4 into 3.5 gives

$$D = \frac{KT}{f} \tag{3.6}$$

which is an Einstein diffusion coefficient. According to Stokes,[70] the frictional coefficient f, of a rigid sphere of diameter d moving through a medium of viscosity η is

$$f = 3\pi\eta d \tag{3.7}$$

This relationship is valid only if the fluid medium is continuous and if no slip occurs between it and the sphere.[42] Therefore, combining Eqs. 3.6 and 3.7 yields the classical Stokes-Einstein equation for diffusivity;

$$D = \frac{KT}{3\pi\eta d} \tag{3.8}$$

which is valid only in very dilute solutions of spherical molecules, which are large compared to the size of solvent molecules.

3.1.3 Molecular Diffusion Through a Membrane

Application of Fick's laws to mass transport through porous membranes will be discussed in this section. The following assumptions will be made: 1) Membrane pores are essentially cylindrical (details concerning Nucleopore membranes used in these experiments are given in Chapter 4), 2) membrane is thin (10 μm) and concentration difference through membrane is small (less than 1% by weight), therefore mass flux into one membrane surface equals mass flux out the other surface, and 3) membrane presents a simple cross sectional area reduction to diffusion, i.e., there are not chemical or physical interactions between membrane and solution; diffusion proceeds freely through membrane pores.

If concentration difference is the only driving force through the membrane, then the mass flux through the membrane is

$$J = -D_F A_p \frac{\Delta C}{\Delta x} \tag{3.9}$$

where D_F is the free diffusion coefficient, A_p is the pore cross-sectional area, ΔC is the concentration difference across the membrane which has a thickness of ΔX. This ignores the driving force due to osmotic pressure. In a system where the membrane permeability is different for the solvent and solute molecules, an osmotic pressure, π, exists across the membrane as,

$$\pi = \sigma RT \Delta C \tag{3.10}$$

where σ is Staverman's reflection coefficient which accounts for the difference in permeability between the solvent and solute. R is the gas constant and T is absolute temperature. Renkin[72] proposes an expression for σ for cylindrical pores which is based entirely on the geometry of the membrane,

$$\sigma = 1 - \frac{[2(1-\beta)^2 - (1-\beta)^4][1-2.104\beta + 2.09\beta^3 - 0.95\beta^5]}{[2(1-\gamma)^2 - (1-\gamma)^4][1-2.104\gamma + 2.09\gamma^3 - 0.95\gamma^5]} \qquad (3.11)$$

where $\beta = R_s/R_p$ and $\gamma = R_w/R_p$ with R_s, R_w, and R_p being the radius of the solute, solvent, and pore, respectively. For sucrose in water $R_s = 5.3$ Å,[73] $R_w = 1.9$ Å,[73] and $R_p = 0.4$ μm and 4.0 μm. Therefore

$$\sigma = 1.797 \times 10^{-3} \text{ for } 0.4 \ \mu\text{m pore radius}$$

$$\sigma = 1.7886 \times 10^{-4} \text{ for } 4.0 \ \mu\text{m pore radius}$$

Using the reflection coefficients calculated from Eq. 3.11 for a 1% by weight concentration difference at a temperature of 25°C, Eq. 3.10 predicts a maximum osmotic pressure difference of .10 centimeters of mercury for the .8 μm diameter pore size and 0.01 centimeters of mercury for the 8.0 μm diameter pore size. This osmotic pressure is only a potential for water flow so there cannot be a water flux due to osmotic effects if the volume is physically constrained. The membrane provides a physical barrier to volume change in the cell if it does not stretch during the diffusion process, so any water flow in the cell will only be due to diffusion and not osmotic effects.

Faxen[74] derived an expression for the ratio of the diffusion coefficient in a cylindrical pore to the bulk diffusion coefficient. He

used a frictional drag model based on a sphere falling in a tube to predict this ratio. The Faxen equation is

$$D_p = D_F\ (1 - 2.104\beta + 2.09\beta^3 - 0.95\beta^5) \qquad (3.12)$$

where D_p is the pore diffusion coefficient, D_F is the coefficient in bulk and β is the same as for Eq. 3.11. Therefore the diffusion coefficient observed through the membrane is reduced due to the viscous drag between the diffusing molecule and pore wall surface. Iberall et al[42] supports this observation by measuring the diffusion of different sized molecules through a porous membrane with cylindrical pores. The membrane permeability decreased as the value of β increased. Williamsen, et al.,[75] observed a decrease in the diffusion rate of sucrose through a porous membrane which confirmed the Faxen and Renkins equations. This observation becomes important when considering the diffusion of anisotropic molecules in a magnetic field discussed in Section 3.2.

3.2 Magnetic Field Effects on Diffusion

3.2.1 Basic Magnetochemistry

The most fundamental concept of magnetochemistry is that of magnetic susceptibility, which is the response of a substance to a magnetic field. It is commonly known that some substances are attracted to a magnetic field while others are repelled from it. When a substance is placed in a field of $\vec{H}$ Oersteds, the magnetic induction (expressed in Gauss) is given by the sum of the applied field ($\vec{H}$) plus a contribution $4\pi\vec{M}$, where $\vec{M}$ is the intensity of magnetization or the magnetic moment

per unit volume in the substance itself. The induction $\vec{B}$ is defined as the density of lines of force per unit area A in the substance.

$$\vec{B} = \vec{H} \times 4\pi\vec{M} \tag{3.13}$$

The magnetic susceptibility, χ, is defined as the scalar ratio of the magnetization and applied field;

$$\chi = \frac{\vec{M}}{\vec{H}} \tag{3.14}$$

If a Cartesian coordinate system is chosen within a specimen, the magnetic susceptibility tensor is diagonal, with χ_x, χ_y, χ_z being referred to as the principal susceptibilities. If a substance is magnetically isotropic, the magnetic induction is independent of orientation in the field and the magnetic susceptibility tensor is equal, $\chi_x = \chi_y = \chi_z$. If a substance is anisotropic the magnetic susceptibility depends upon the orientation of the molecule with respect to the direction of the applied magnetic field. Anisotropic susceptibility can only be observed in a substance when all the molecules are oriented with respect to the magnetic field, as in a single crystal. If a powder is measured, the bulk magnetic susceptibility χ_b, is isotropic and is equal to the average of the three principal magnetic susceptibilities.

$$\chi_b = \frac{\chi_x + \chi_y + \chi_z}{3} \tag{3.15}$$

Most substances can be classified as either dia or para - magnetic depending upon the sign of χ. The sign of the magnetic

susceptibility usually depends on whether the ground state electrons are paired or unpaired. The substance is said to be diamagnetic if the sign of χ is negative, i.e., it causes a reduction in the lines of force permeating the substance. This is equivalent to the substance producing a magnetic flux in a direction opposite to the applied field. In the presence of an inhomogeneous field, the molecule will be repulsed from the region of higher field. Diamagnetism arises due to the motion of the electrons in their atomic and molecular orbits. An electron carrying a negative charge and moving in a circular orbit is the equivalent to a circular current. If a magnetic field is applied perpendicularly to the plane of the orbit, the revolving electron experiences a force along the radius. Lenz's law,[75] which predicts the direction of motion of a current-carrying conductor placed in a magnetic field; predicts that the system as a whole will be repelled away from the applied field. The degree of diamagnetism associated with an atom or molecules depends upon the size and shape of the orbiting electrons, the outermost electrons contributing the most to the diamagnetic susceptibility.

Paramagnetism, on the other hand, is characterized by the magnetic induction being larger than the applied magnetic field. The sign of χ is therefore positive and a paramagnetic substance is attracted to a region of higher magnetic field strength. Paramagnetism is exhibited by substances which have unpaired electrons in the ground state. It is generated by the tendency of magnetic angular momentum to orient itself in a magnetic field. The magnetic angular momentum arises from the orientation of the unpaired electrons with the magnetic field. Therefore, the magnitude of paramagnetic susceptibility is a function of

the numbers of unpaired electrons in an atom or molecule.

Most organic molecules are diamagnetic, including sucrose and water, the system studied in this work.

3.2.2 Molecular Orientation in a Magnetic Field and Diffusion

A magnetic field will exert a force upon any molecule which possesses a magnetic anisotropy. This force will tend to give a preferential alignment of the molecular dipole in the direction of the applied magnetic field. The degree of alignment is a function of the anisotropy of the molecule, the magnetic field strength, the interaction of the molecule with its neighbors, and the thermal kinetic energy of the molecule. This section will discuss how this alignment affects the diffusion process.

The orientation of diamagnetically anisotropic molecules in a magnetic field is termed the Cotton-Mouton effect.[77-83] An applied magnetic field produces a force on the molecule if the molecular susceptibility is anisotropic. This force tends to orient the molecule parallel to the directions of magnetic force which is counteracted by the translational and vibrational motion of the molecule. The degree of orientation is inversely related to the thermal energy of the system, since the random Brownian motion tends to disorient the molecules. The degree of orientation, δ_o, is given by

$$\delta_o = (\chi_{11} - \chi_{\perp})\, H^2/KT \qquad (3.16)$$

with K being the Boltzmann constant, T the absolute temperature, H the

applied magnetic field strength, and χ_{11}, $\chi_{\perp}$ being the diamagnetic susceptibilities parallel and perpendicular to a rotational symmetry axis, respectively. The degree of orientation has been measured by observing the magnetically induced birefringence

$$\Delta n = n_{11} - n_{\perp} = CM\ \lambda\ H^2 \simeq \delta(\alpha_{11} - \alpha_{\perp})C \qquad (3.17)$$

where n_{11}, $n_{\perp}$ is the refractive index for light of wavelength λ, when polarized parallel and perpendicular to H, respectively. α_{11}, $\alpha_{\perp}$ are the molecular optical polarisabilities parallel and perpendicular to the molecular symmetry axis, C is the concentration and CM is the Cotton-Mouton constant for that molecule. This technique has been used to observe the orientation of some biological macromolecules such as DNA[84], liquid crystals,[78-82] and micelles in a soap-water system.[83]

If a degree of orientation is achieved in a non-symmetrical molecule or molecular cluster, a change will be observed on the diffusion rate of that molecule through a porous membrane. Equation 3.12 predicts a decrease in the diffusion coefficient of a molecule as β, the ratio of molecule to pore diameter increases. If the axis of an anisotropic molecule is oriented orthogonal to the direction of the pore axis then the effective cross-sectional area of this molecule is increased, increasing β and thereby reducing D_p, the membrane diffusion coefficient. Conversely, if a molecule is oriented parallel to the pore

axis direction the effective cross-sectional area of the molecule is decreased, resulting in an increase in D_p. Therefore, this effect can be used to observe and quantify the degree of anisotropic orientation of a solute in a magnetic field. This is depicted in Figure 2.

3.2.3 Aqueous Sucrose Solution Diffusion in a Magnetic Field

One objective of this work was to demonstrate the use of optical interferometry to measure diffusion coefficients in a magnetic field of organic molecules with applications to living systems. A sucrose-water solution was selected for these initial experiments because it is a simple organic solution for which diffusion measurements have been taken extensively using interferometry. Sucrose is a naturally occurring carbohydrate consisting of two monosaccharides bonded together to form this common disaccharide, table sugar.[85] A glycoside link joins one carbon of fructose with one carbon atom of glucose as shown in Figure 3. When in an aqueous solution it forms hydration clusters as water molecules form hydrogen bonds with the H and OH groups on each ring.[86-89] The geometry, bond angles and bond dimensions have been determined from X-ray[90] and neutron diffraction studies.[91] The radius of a sucrose molecule in water is 5.3 Å.[73]

The magnetic properties of sucrose have not been measured to any great extent. The bulk magnetic susceptibility of sucrose has been calculated using Pascal's system, where the contributions to magnetic susceptibility from individual atoms and bonds is simply summed to yield

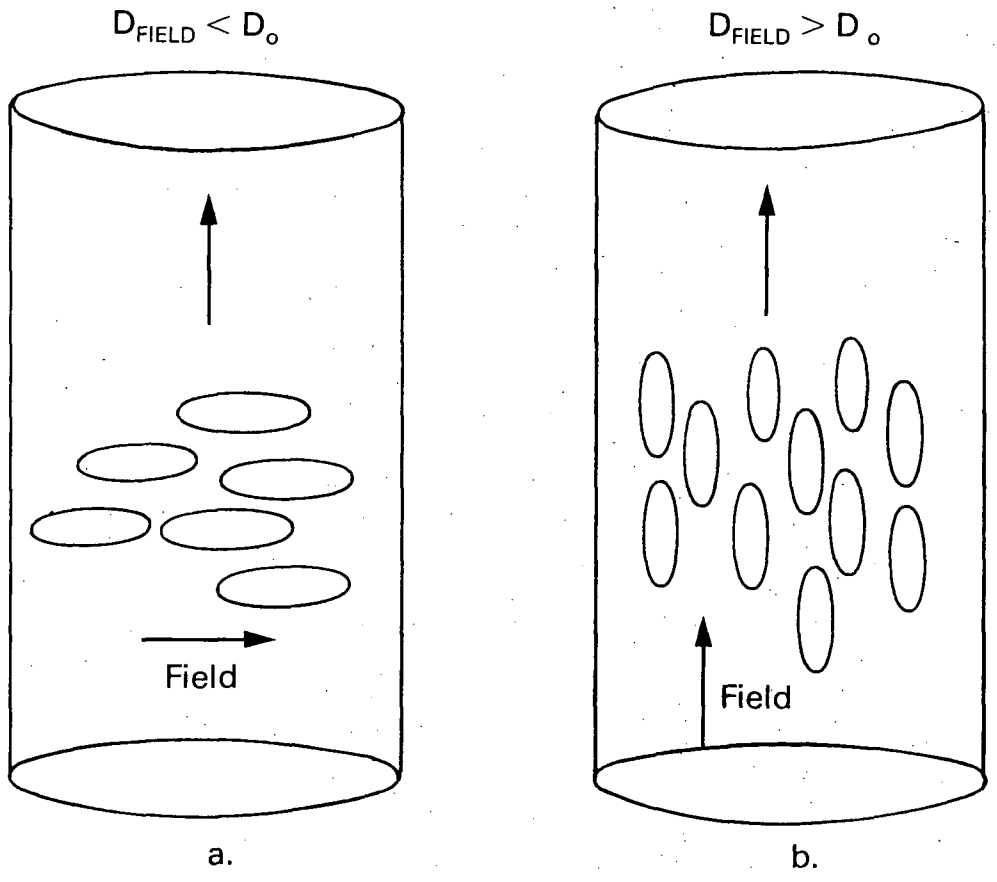

Fig. 2. Molecular Diffusion Through a Porous Membrane in a Magnetic Field:

a. Field Applied Transverse to Pore Direction
b. Field Applied Parallel to Pore Direction

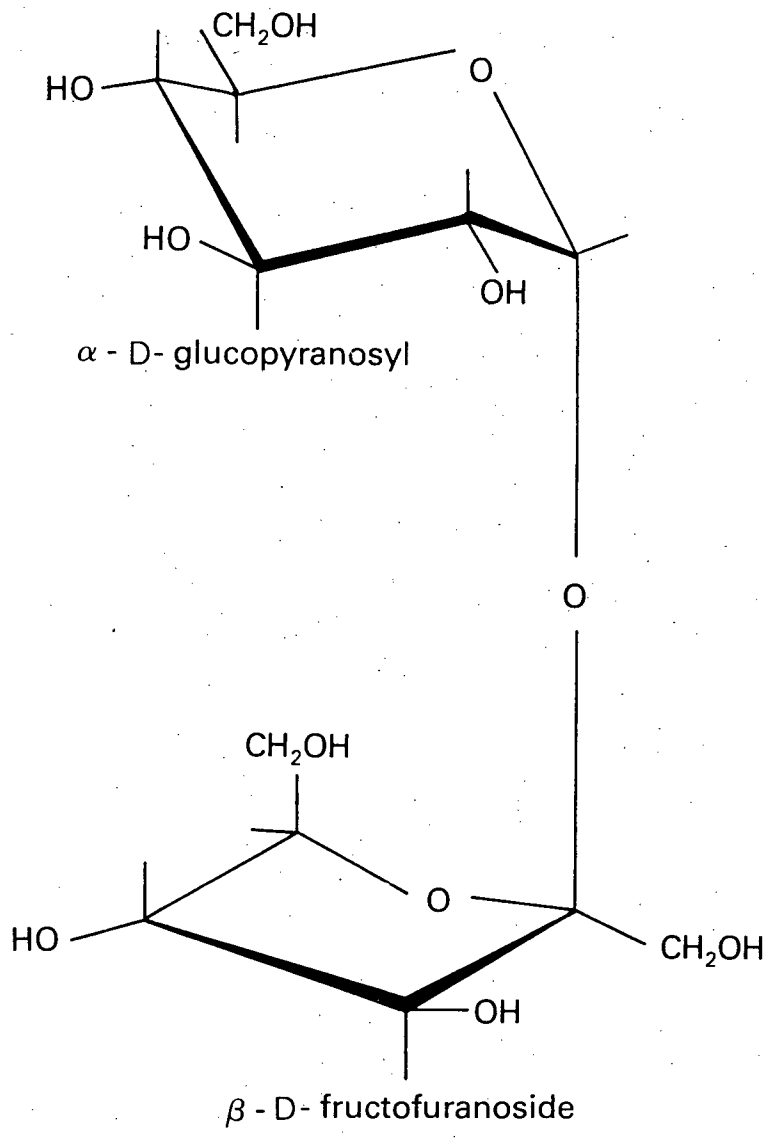

Fig. 3. Structure of Sucrose, $C_{12}H_{22}O_{11}$

the susceptibility for the moleculse as a whole.[92] This value is $\chi_b = -187.06 \times 10^{-6}$ emu/mole. Pascal's method has been applied to predict the magnetic susceptibility of complex organic molecules to better than 5% agreement with experimental values.[92] At this time no measurements are available for sucrose regarding magnetic susceptibility anisotropies, so one objective of this research is to evaluate any anisotropy by observing if the degree of orientation in a magnetic field effects the membrane diffusion rate.

Equation 3.16 predicts the degree of orientation of any molecular magnetic anisotropy in an applied magnetic field. While the bulk magnetic susceptibility for sucrose is readily available ($\chi_b = -187.06$ emu/mole) data regarding the principal susceptibilities, χ_{11} and $\chi_{\perp}$ are not available. A highly anisotropic molecule such as benzene has principal susceptibilities approximately two to one,[92] i.e., the force exerted on the molecules in a homogenous field is twice as large in the parallel plane as the perpendicular plane. If the same degree of anisotropy were observed for sucrose, then $\chi_{11} \simeq -62 \times 10^{-6}$ emu/mole and $\chi_{\perp} \simeq -124.7 \times 10^{-6}$ emu/mole. Using these values Equ. 3.16 predicts that the degree of orientation for a single sucrose molecule in an applied magnetic field equal to 10 kG at 25°C would only be $\simeq 10^{-7}$. This is clearly beyond the limits of sensitivity for most experimental methods. However, δ_o can be increased dramatically when a great number N of such molecules are fixed together parallel to one another, since the effective diamagnetic anisotropy of such a molecular cluster is

proportional to N[84]

$$\delta_o = N(\chi_{11} - \chi_{\perp})H^2/KT \tag{3.18}$$

This situation is applicable in certain long macromolecules and almost full magnetic alignment has been observed for various polymers, large biological molecules such as nucleosides, chloroplasts, retinal rods,[84] and various liquid crystals.[77-82] This effect would also be observable in an aqueous sucrose solution if long molecular clusters existed. Sucrose in water forms hydration clusters as water molecules bind to the sucrose through hydrogen bonds. Shporer et al.,[93] Packer,[94] and Resing[95] discuss the "ordering" of water near a solid surface in an applied magnetic field. Using NMR techniques, they believe partial ordering of water occurs in porous membranes placed in a magnetic field, observed by the splitting of the proton NMR spectrum. Therefore, if an ordering of the sucrose hydration clusters occurs in a similar fashion it should be observable as a decrease in the membrane diffusivity sucrose with a field applied orthogonal to the pores.

The Faxen equation (Eq. 3.12) predicts that the membrane diffusivity will decrease as β, the ratio of molecular radius to pore radius, increases. This is due to increased drag between the diffusing molecule and pore surface. Any ordering of sucrose molecular clusters in the magnetic field would have the same effect as increasing the effective cross-sectional area of the molecule thereby increasing the drag between it and the pore surface. Eqs. 3.12 and 3.18 can be combined to predict the change in the diffusion coefficient for molecular clusters aligned in a magnetic field. Defining β_f for a molecular cluster aligned in a magnetic field gives

$$\beta_f = (r_s + F\delta_0)/r_p \tag{3.18a}$$

where r_s and r_p are the radius of the solute and pore respectively and F is an empirical geometrical factor relating the molecular geometry to the magnetic anisotropy.

3.3 Theory of Interferometry

Interferometry provides a tool which will measure refractive index profiles in a transparent medium. Local refractive index changes in a diffusion process are due to variations in composition and concentration. Concentration profiles can be probed with light which permits a continuous observation of the profile with minimal disturbance to the diffusion process.

3.3.1 Refractive Index

The refractive index of a solution depends upon its composition and is defined as the ratio of the phase velocity of light in a vacuum c to that of light in the medium, v

$$n = \frac{c}{v} \tag{3.19}$$

The Lorentz-Lorenz law[96-98] for a pure substance is

$$RM = \frac{M}{\rho} \frac{(n^2 - 1)}{(n^2 + 2)} \tag{3.20}$$

which defines the molar refractivity RM as a function of molecular weight M, density ρ, and refractive index n. Equation 3.20 defines RM as a constant for any pure substance at isothermal conditions. For a

multicomponent, isothermal system with no chemical interactions, an average molar refractivity $\overline{RM}$ can be defined which is based upon the summation of the contribution from each individual component R:

$$\overline{RM} = \sum_i X_i \, RM_i \tag{3.21}$$

where X_i is the mole fraction of component i. If we similarly define an average molecular weight $\overline{M}$

$$\overline{M} = \sum_i X_i \, M_i \tag{3.22}$$

then Eq. 3.20 becomes for a mixture

$$\overline{RM}_i = \sum_i X_i \, RM_i = \frac{\sum_i X_i \, M_i \, (n^2 - 1)}{\rho \quad (n^2 + 2)} \tag{3.23}$$

Equation 3.23 predicts that the refractive index of a mixture will be a function of mole fraction and density for the system at a given wavelength of light. Since density is affected by temperature and pressure it is necessary for the system to be maintained at isothermal and isobaric conditions to determine n from concentration. For most solutions at low concentrations, n is a linear function of concentration c

$$n = ac + b_n \tag{3.24}$$

where a and b_n are empirical parameters.

Interferometry is a technique which measures local refractive index in a medium, therefore yielding local concentration of a diffusing molecule if a and b are known for the system.

3.2.2 Wave Nature of Light and Interference

Thomas Young first demonstrated that the light propagates as a wave, in 1802. Young performed an experiment securing light from two secondary sources through the use of two pinhole apertures as shown in Figure 4. A collimated light source illuminates a pinhole which diffracts a spherical wavefront to a second screen containing two additional pinholes. These two pinholes diffract two secondary phase-related spherical waves. When these two waves were observed on a screen Young saw a series of alternating bright and dark fringes. This phenomenon was accounted for by explaining the propagation of light as a wave phenomena.

Maxwell's equations of electromagnetic theory predict the propagation of visible light as two periodic transverse wave motions.[99] The waves are oscillating magnetic field and oscillating electric field vectors at 90° to each other. The other direction of propagation is shown in Figure 5. Such behavior can be described as simple harmonic motion

$$E(z,t) = A_E \cos(\omega t + \phi) \tag{3.25}$$

with A_E being the amplitude of the wave, t is time, ω is the angular speed and ϕ is the phase angle constant at $t = 0$. Expressing Eq. 3.25 in complex notation gives

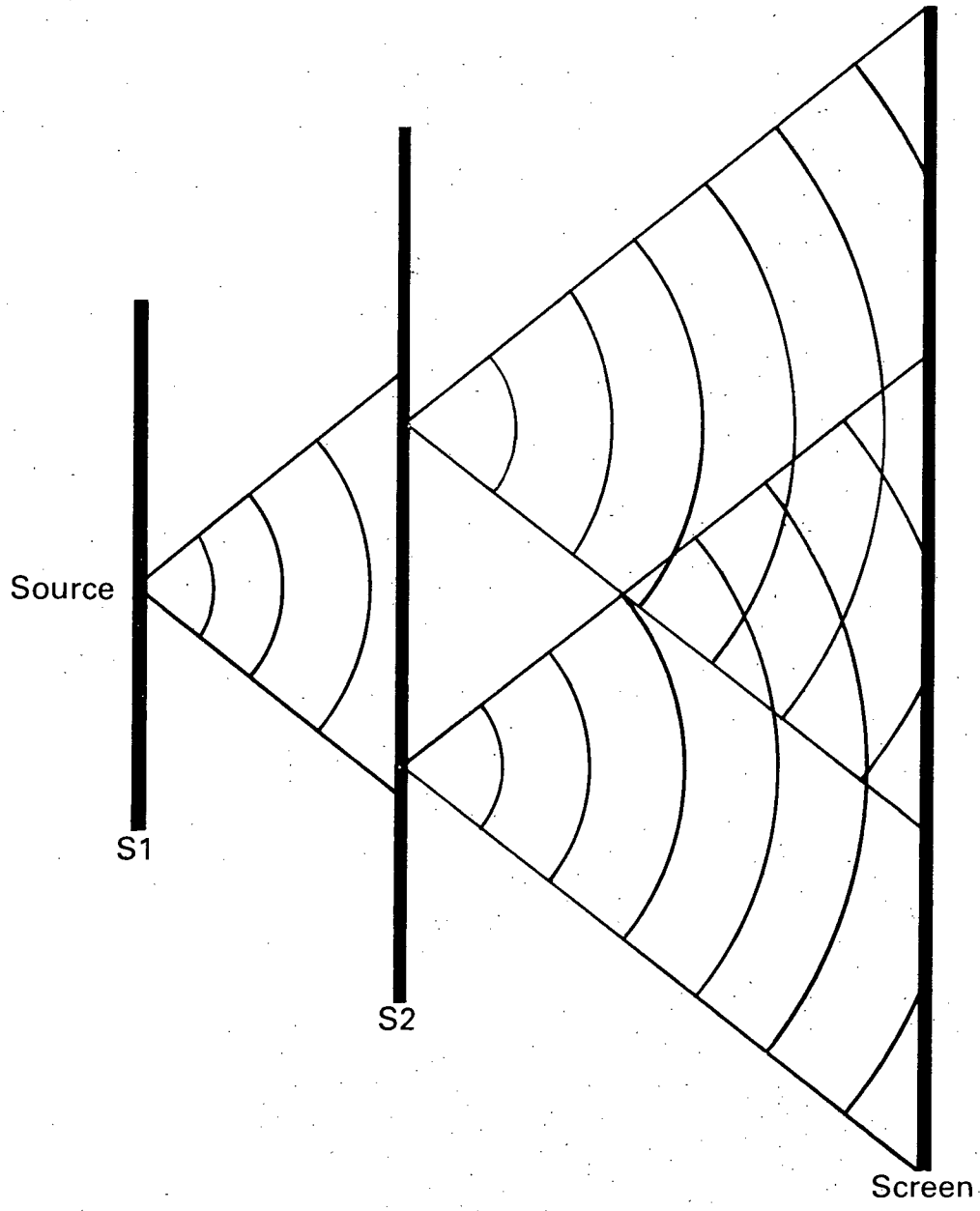

Fig. 4. Young's Double Slit Experiment

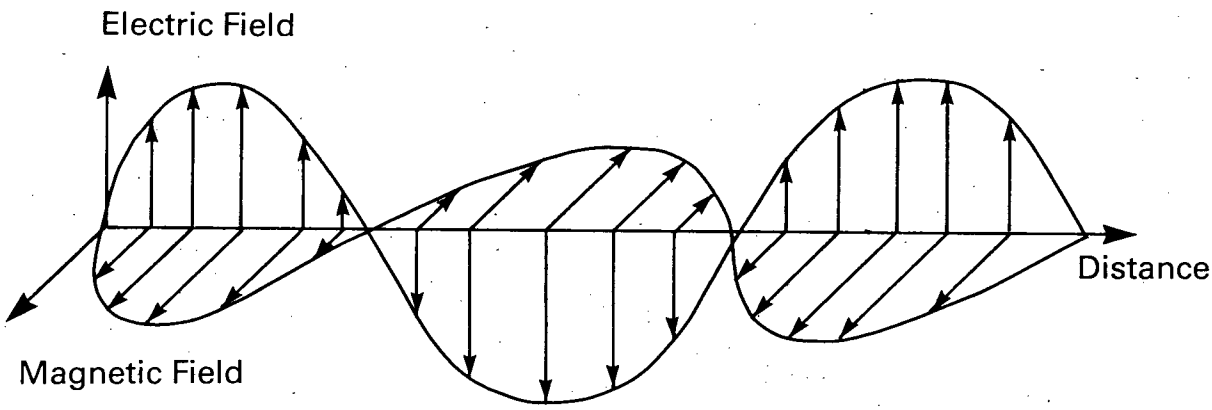

Fig. 5. Propagation of Light as an Electromagnetic Wave

$$E(Z,t) = \mathrm{Re}\left[Ze^{\,i(\omega t)}\right] \tag{3.26}$$

where $Z = Ae^{i\phi}$.

If two waves have the same amplitude, wavelength and general propagation direction and are superimposed upon each other, interference will result. If one wave is 180° out of phase with the other so the positive peaks of one wave coincide with the negative peaks of the other, destructive interference will occur and the amplitude of the two waves will be zero.

If a plane wavefront of light enters a medium with a locally variable refractive index, it will not remain plane, but the phase velocity of the front will be reduced as the refractive index increases. The resulting local variation in phase is proportional to the change in refractive index Δn and distance travelled by the wave. A quantity termed optical path length, L, is defined as

$$L = ns \tag{3.27}$$

A phase difference $\Delta\phi$ for the wave travelling through a constant geometrical distance and refractive index difference Δn is

$$\Delta\phi = \frac{\Delta ns}{\lambda_o} 2\pi \tag{3.28}$$

where λ is the wavelength of the light in a vacuum.

Figure 6 shows a plane wavefront of light passing through a

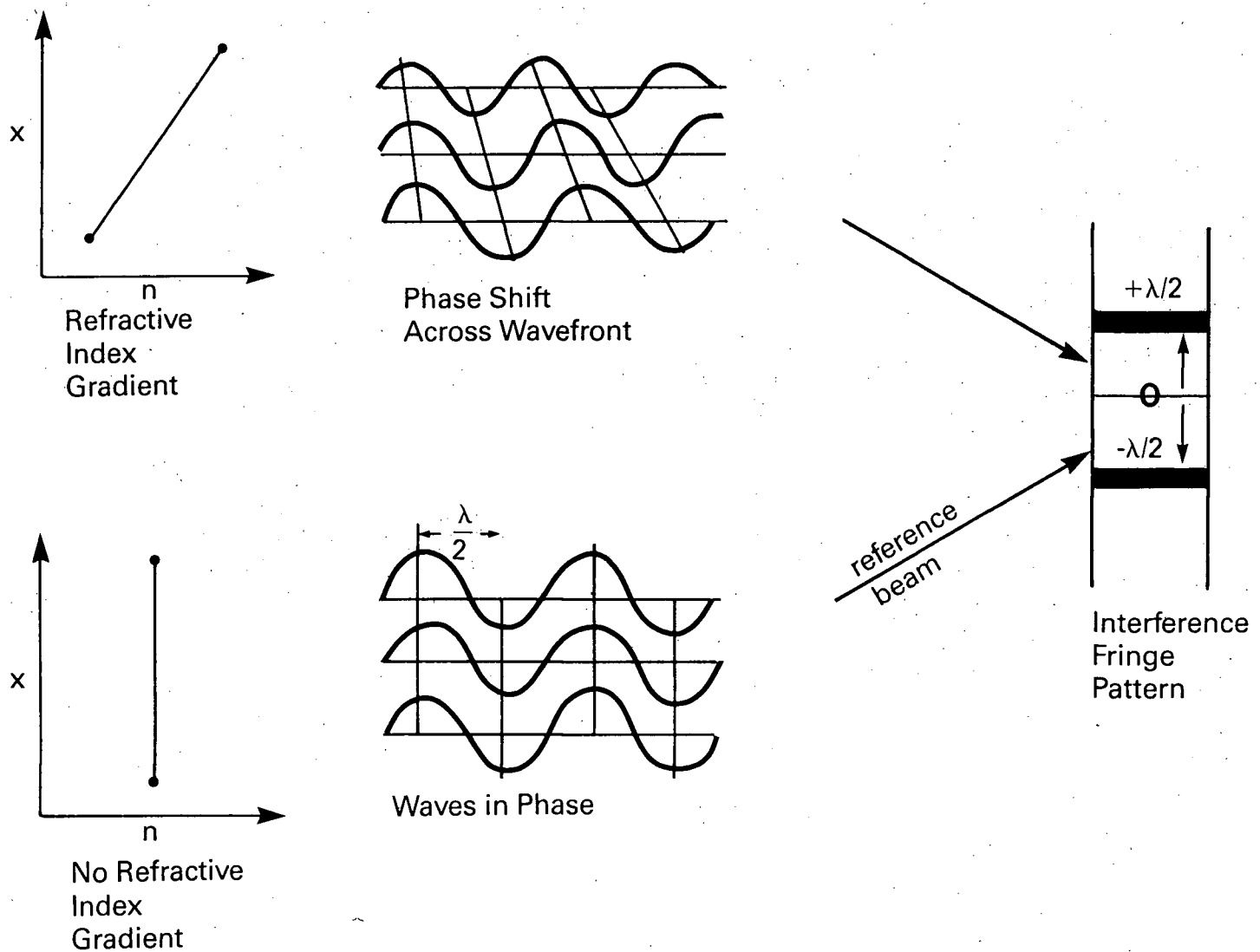

Fig 6. Principles of Double Beam Interferometry

medium of constant and variable refractive index field. The maximum change in optical path length between the edges of the refractive index gradient is one wavelength of light, λ. If the two wavefronts are superimposed an interference pattern would result with constructive interference occurring at the center and destructive interference occurring at the edges. From such an interference pattern it is possible to determine the phase relationship between the two wavefronts. This is the basis for double beam interferometry; two light beams are generated which have a known phase relationship in both time and space and are superimposed such that both the interference phenomenon and object are imaged. Phase differences between the two beams are then visible as interference fringes which can be evaluated to determine the local refractive index differences between the object and reference.

3.2.3 Double Beam Interferometry

This section will consider a quantitative description of the interference phenomenon observable in double beam interferometry and the necessary conditions for the observation and interpretation of interference fringes.

According to the definition of refractive index, Eq. 3.19, the ratio of distance z travelled by a wave of velocity v, is

$$\frac{z}{v} = \frac{nz}{c} \tag{3.29}$$

From the definition of optical path length, L, Eq. 3.27, z/v can be expressed as

$$\frac{z}{v} = \frac{L}{c} \tag{3.30}$$

The equation of motion for a wave describes the electric field vector in space and time. At some distance z from the source of light, the harmonic wave can be described by combining Eqs 3.25, and 3.30

$$E(z,t) = A \cos [\omega(t - \frac{L}{c}) + \emptyset]$$

or writing this equation in complex notation gives

$$E(Z,t) = \mathrm{Re}[Z \exp (i\omega t)] \tag{3.32}$$

where Z is the complex amplitude defined as

$$Z = \mathrm{Re}\{A \exp{-i[\omega L/c + \emptyset]}\} \tag{3.33}$$

Equations 3.31 or 3.32 state that at any given optical path length away from the source, E is a harmonic function of time only.

The wave described by Eq. 3.32 is an ideal single monochromatic wave. In reality such a light source does not exist. Even a laser produces light which is emitted by a number of individual atoms exceeding 10^{20}. Each atom is moving with some velocity due to the thermal energy of the atoms. In addition all atoms do not emit their radiation simultaneously but in bursts of some finite duration. The thermal motion of the atoms produces a Doppler shift in the frequency of light emitted by that atom.[99] The net result is that some point in space is illuminated by many wavetrains of different frequencies during the time of observation. In addition no optical detector (photographic

film, or the human eye) has a response time brief enough to observe individual waves of light. Rather the response of the detector is many orders of magnitude greater than the period of visible light (10^{-15} s). Therefore the detector measures a time-averaged intensity over many thousands of oscillations.

Real light sources can be represented as a superposition of terms like Eq. 3.32 using the Fourier integral[99] if the frequencies are strongly peaked about a certain frequency ω. The light is considered to be quasimonochromatic and the light source can be expressed as

$$E(t) = A(t) \cos [\omega t + \phi(t)] \tag{3.34}$$

where $A(t)$ and $\phi(t)$ are slowly varying functions compared with $\cos\omega t$; they change only slightly during one period $1/\omega$. Real quasimonochromatic light sources such as the laser have randomly varying functions $A(t)$ and $\phi(t)$. The period of oscillation for visible light $1/\omega$, is so short that two separate sources of quasimonochromatic radiation would drift out of phase with each other in 10^{-5} second or less, making it very difficult if not impossible to observe interference between the two sources.[99]

For this reason virtually all laboratory interferometers employ a single source of light. The term double beam interferometry refers to a class of interferometers which use a single source of quasimonochromatic light which is "divided" into two separate beams which are focused by a suitable lens system to superimpose the two beams producing an interference phenomenon. The Rayleigh interferometer used in this work

employs a double slit to produce two coherent sources from a single laser light source. The Rayleigh interferometer is depicted from above in Figure 7. A collimating lens expands the laser beam and produces a wavefront of light which is collimated and parallel across the entire area of the beam. This beam illuminates two vertical slits which divide the beam into two separate light sources exactly in phase with each other.These two beams then pass through separate compartments of the diffusion cell, each filled with a medium of different refractive index. The refractive index in one compartment of the diffusion cell is constant and known. The other compartment is filled with a medium of unknown refractive index and with a refractive index gradient in the vertical plane. Lens L1 is a plano-convex lens which focuses the two beams on a focal plane, FP. The beams are superimposed and since they are mutually coherent interference occurs at FP. Lens L2 is a cylinder lens which only focuses in one plane, in this case the vertical plane. It focuses an image of the diffusion cell vertically on FP, which gives an "image" of the interference pattern on FP. From this interference pattern it is possible to evaluate the local refractive index difference between the two compartments of the diffusion cell.

3.2.4 Interpretation of Interference Fringes

The spacing of the centers of adjacent interference fringes is determined by the wavelength of light used and the geometry of the optical system. Recall that the distance between each interference fringe represents a phase difference between the two beams equivalent to one wavelength of light. In this section simple geometrical principles

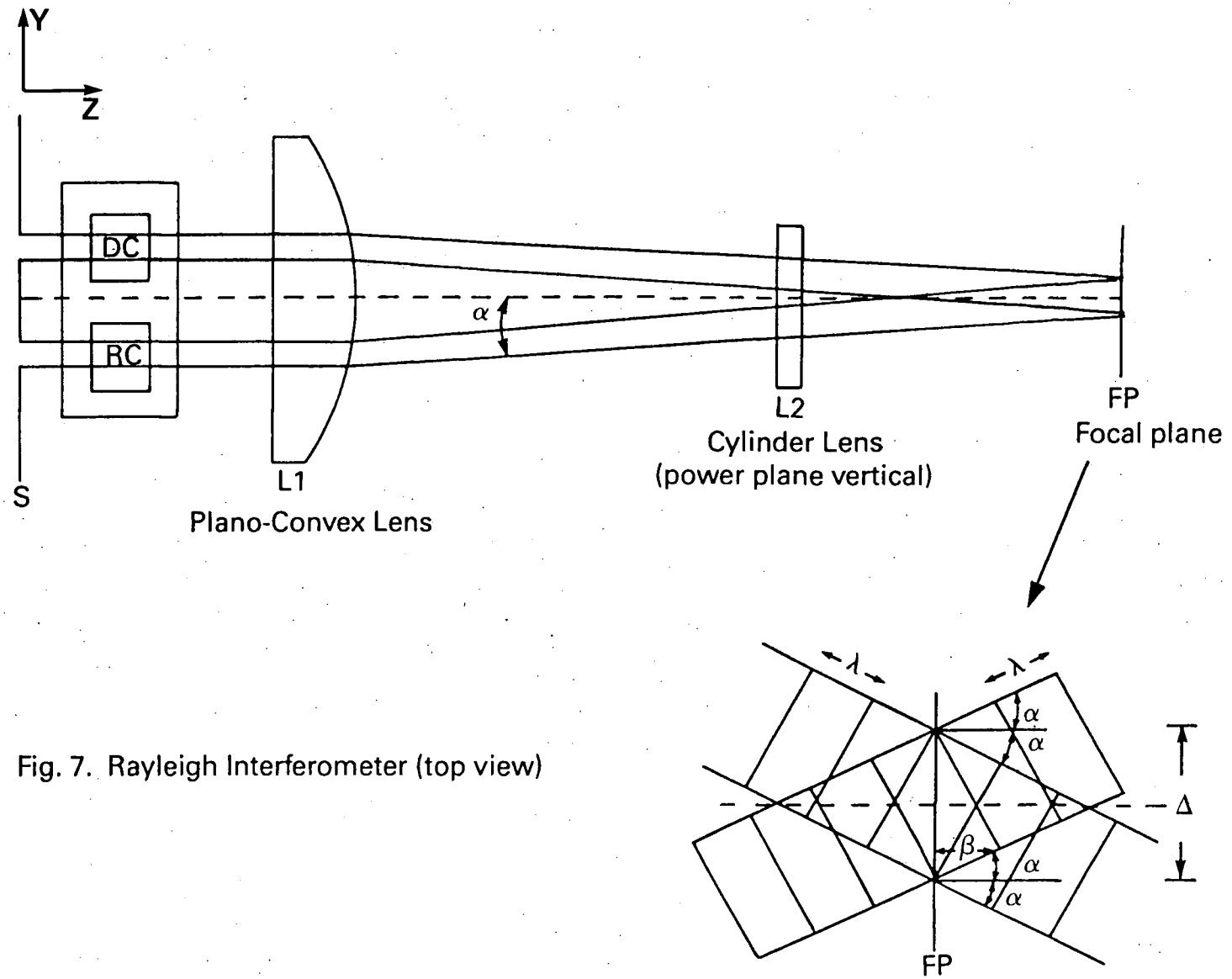

Fig. 7. Rayleigh Interferometer (top view)

will be used to derive a quantitative relationship between fringe spacing and refractive index changes in the diffusion cell.

Referring to Fig. 7 it can be seen that the angle α between the two beams is

$$\alpha = \tan^{-1} \frac{Y_s}{2z_{FP}} \tag{3.35}$$

The enlargement of the focal plane in Figure 7 shows the fringe spacing Δ which is a function of both α and λ, the wavelength of light in air. λ can be related to λ_o, the wavelength of light in a vacuum, through the refractive index relationship.

$$\lambda = \frac{\lambda_o}{n_a} \tag{3.36}$$

where n_a is the refractive index of air. The value B in Figure 7 is equal to

$$B = \frac{\lambda}{\cos\alpha} = \frac{\lambda_o}{n_a \cos\alpha} \tag{3.37}$$

By similar triangles, Δ is therefore

$$\Delta = \frac{B}{\tan \alpha} = \frac{\lambda_o}{n_a \cos\alpha \tan \alpha} = \frac{\lambda_o}{n_a \sin\alpha} \tag{3.38}$$

Therefore the fringe spacing for a Rayleigh interferometer may be determined at a given wavelength by the spacing of the masking slits and the focal length of L_1.

The phase difference between the two beams is equal to the difference in optical path lengths between the two beams. The optical path length for each half of the interferometer is a summation of optical path length contributions from the diffusion cell, quartz diffusion cell windows, transmission through the lenses and transmission of light through the air. The total optical path length for either the reference of diffusion side of the interferometer is then

$$L_T = \sum_i n_i z_i \tag{3.39}$$

where n_i and z_i are the refractive index and geometrical path length for medium i which would be either a lens, air, sucrose solution, or a quartz optical flat. Eq. 3.39 is valid if the refractive index is constant through each distance, z_i. A shift in the interference pattern equal to one fringe spacing, Δ, corresponds to a phase change between the reference and diffusion beams equal to one wavelength. This represents a difference in optical path length equal to λ. Since the geometrical distance is fixed, then a change in optical path length must result from a change in refractive index. The phase difference between the two beams $\Delta\phi$ corresponding to a fringe shift of Δ is

$$\Delta\phi = \frac{2\pi z}{\lambda} \Delta(n_2 - n_1) \tag{3.40}$$

In the Rayleigh interferometer the optical path length contribution from the lenses, air, and quartz optical components is identical between the

diffusion and reference sides. Therefore, any changes in optical path length must result from a change in refractive index in the diffusion compartment since the refractive index in the reference side is constant. The refractive index difference between the reference and diffusion sides of the diffusion cell producing one fringe shift is equal to an optical path length difference of λ.

$$\Delta(n_2 - n_1) = \frac{\lambda}{z_{DC}} \tag{3.41}$$

where z_{DC} is the geometrical distance through the diffusion cell.

The cylinder lens, L2, produces a vertical image of the diffusion cell on the focal plane. This has the effect of creating an infinite number of interferometers in the vertical plane (see Figure 7). Figure 8 shows a typical interference pattern produced by this interferometer. Starting at either end of the interference pattern the fringes are straight so a constant phase difference exists between the two sides of the diffusion cell. The refractive index is constant and known at each end of the diffusion cell, so the fringes are interpreted with respect to n_o, the known refractive index at each end of the cell. Moving towards the center of the interference pattern the fringes bend, resulting from a phase change between the two light rays passing through a given vertical position in the cell. At the location where the fringe pattern has shifted an amount equal to Δ, the phase change has been one wavelength of light between two consecutive fringes. From Eq. 3.41 the amount Δn can be calculated which is the difference in refractive index

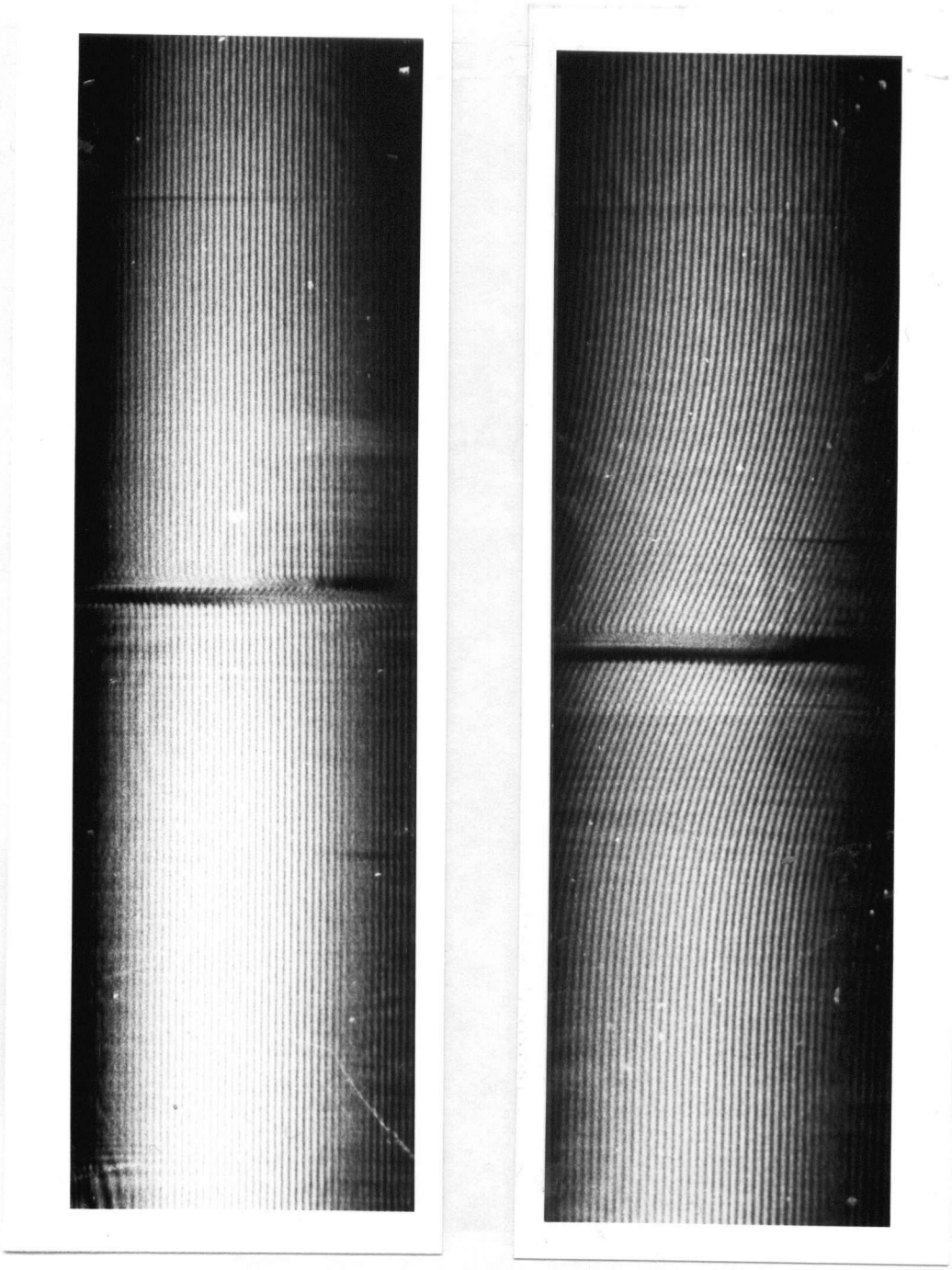

(a) (b)

Figure 8 - Typical Rayleigh Interference Patterns (a) No refractive index gradient in cell (b) Diffusion proceeding.

between the two vertical points. It is therefore possible to evaluate the refractive index difference at all locations in the cell simply by counting the number of fringe shifts and measuring the vertical location, x_i, at which a shift occurs. Therefore n(x), which is the refractive index at x_i corresponding to the i th fringe shift is:

$$n_i(x) = n_0 + \Sigma N_i \frac{\lambda}{z_{DC}} \tag{3.42}$$

x_i is measured from the boundary condition where $n(x_o) = n_o$ is known. This equation is valid if the refractive index in one of the diffusion cell compartments is constant, which is the case in these experiments since the reference compartment is filled with distilled water and is isothermal.

Equation 3.42 defines a refractive index profile for the diffusion cell. Since the membrane provides a discontinuity in the profile, Eq. 3.42 is applied to each end of the cell where the refractive index is known. Counting fringes towards the membrane yields a continuous profile on either side of the membrane. Applying Eq. 3.24 to the refractive index profile determines directly the concentration profile in the cell

$$C_i(x) = C_o + \sum_i \left. \frac{N_i \lambda a}{z_{DC}} \right|_t \tag{3.43}$$

where a is determined empirically from refractive index versus concentration data.

The mass flux at any point in the cell may be determined by the time rate of change of the integral of the concentration profile

$$J = \frac{\partial}{\partial t} \int_{x_o}^{x} C(x,t)dx \tag{3.44}$$

Concentration profiles are measured at several different times during the experiment and a numerical method is used to evaluate the integral and time derivatives in Eq. 3.44. The concentration gradient at a given time and position can be found by taking the derivative of the concentration profile with respect to x. With the mass flux and concentration gradient known, the diffusion coefficient D can be evaluated from Fick's first law

$$D = \frac{J}{\frac{dC(x,t)}{dx}} = \frac{\frac{\partial}{\partial t} \int_{x_o}^{x} C(x,t)dx}{\frac{dC(x,t)}{dx}} \tag{3.45}$$

Details concerning the numerical method used to evaluate the integral and derivative in Eq. (3.45) are included in Chapter 5.

CHAPTER 4

EXPERIMENTAL APPARATUS AND PROCEDURE

4.1 Experimental Apparatus

An optical interferometer measures small changes in the refractive index of a given medium, by detecting the phase change between two beams of coherent light. One wavefront forms a reference beam having been transmitted through a medium of known refractive index, while the comparison wavefront is transmitted through a medium of unknown refractive index. Recall from Chapter 3 that a phase change between the two beams equal to 1 wavelength of laser light (6.328×10^{-5} cm) will distort the interference fringe pattern by one fringe spacing. Therefore, any phase change between the two beams greater than a fraction of the wavelength will cause a distortion of the observed fringe pattern. This degree of sensitivity means that all optical components such as lenses and test cells must be designed and constructed to introduce a total wavefront aberration of less than a fraction of a wavelength into the transmitted laser beam. Details concerning these optical components and other components of the experimental setup are included in appropriate sections of this text. Figure 9 shows schematically the experimental setup. The following sections describe in detail the individual components of this setup.

4.1.1 Quartz Diffusion Cell

The fused silica diffusion cell was custom fabricated by Interoptics, LTD, of Ottawa, Ontario to state of the art optical tolerances. The cell is shown in Figure 10. It is constructed of three

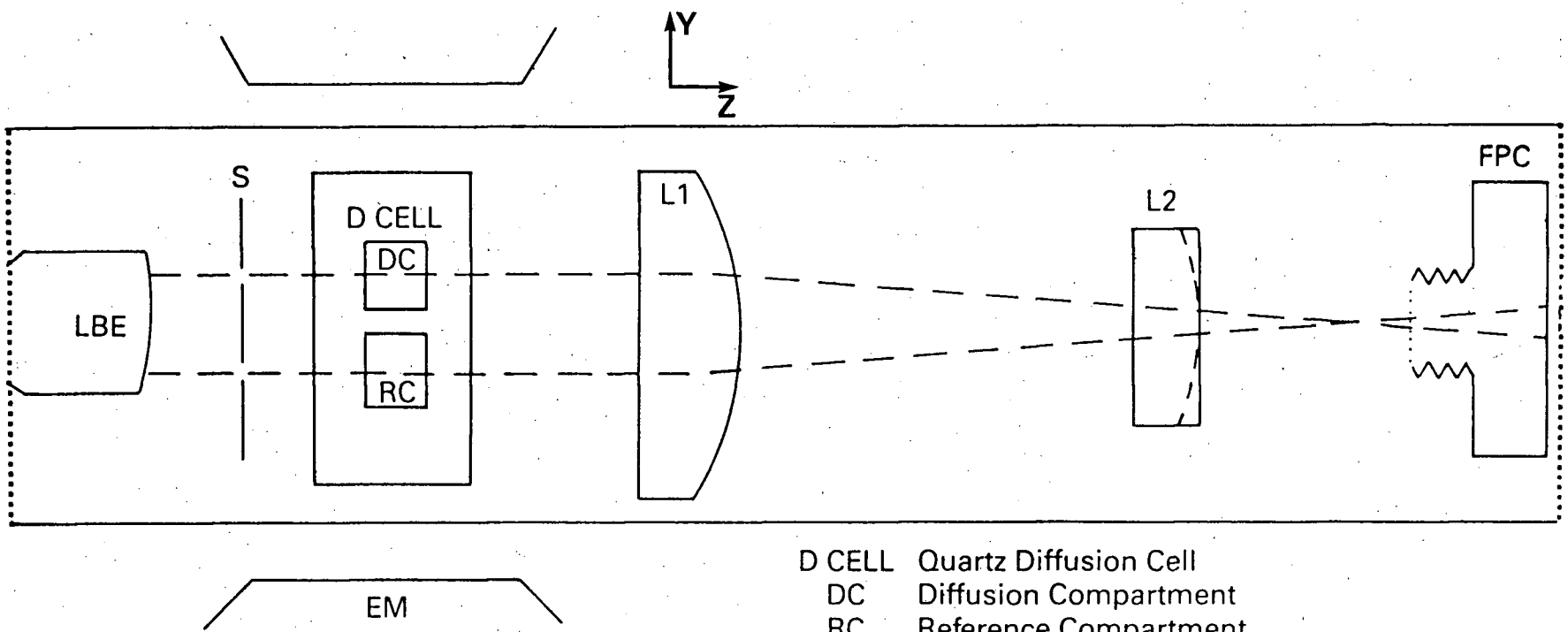

D CELL	Quartz Diffusion Cell
DC	Diffusion Compartment
RC	Reference Compartment
L1	Plano-convex lens
L2	Cylinder Lens
FPC	Focal plane camera
LBE	Laser and beam expander
EM	Electromagnet
S	Masking Slits

Fig. 9 Experimental Setup

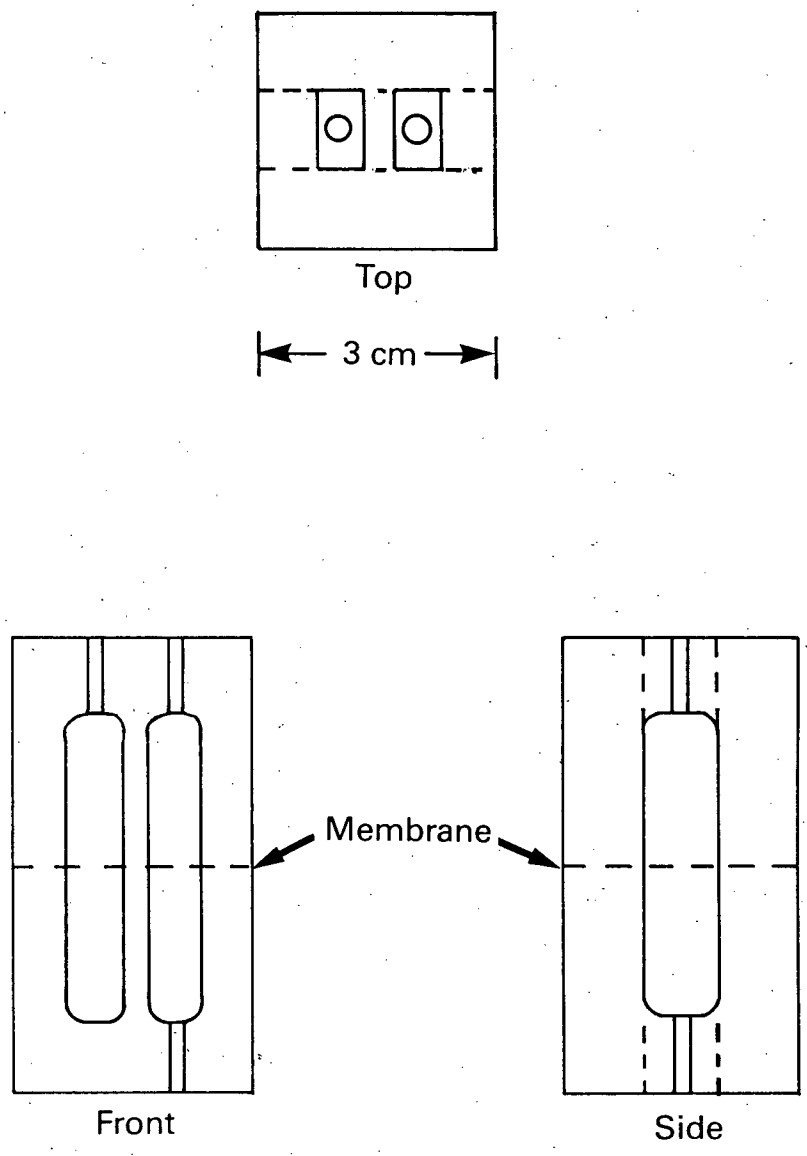

Fig. 10. Quartz Diffusion Cell

quartz optical flats cemented together with a special optical epoxy. The cell was cut in half to allow a membrane to be inserted at the mid-plane. Two parallel slots were drilled out of the center optical flat to provide the diffusion and reference compartments. The inside edges were chamfered so that any excess epoxy squeezed out during the assembly procedure would have a place to collect and not run out onto the interior windows, restricting the clear aperture. The flatness of all optical surfaces was maintained at $\lambda/20$ (λ = 6328 Å) and parallelism of all surfaces kept to at least one arc second.

The thickness of the reference and diffusion compartments was chosen as 1 cm. This value was selected to produce an optimum number of interference fringes for a sucrose concentration difference of 1% by weight. A 1% by weight change of sucrose concentration at 25°C corresponds to a refractive index change Δn, of approximately 0.0015.[40] For a $\Delta n = 0.0015$, the number of fringe shifts is given by Eq. 3.42 as

$$\Sigma N = \frac{\Delta n z_{DC}}{\lambda} \tag{4.1}$$

using $\lambda = 6.328 \times 10^{-5}$ cm (He-Ne laser light) and $z_{DC} = 1$ cm (cell thickness) yields a value of 24 fringes for ΣN. Therefore 24 is the number of fringes which must be measured manually with the microscope for a 1% by weight change in sucrose concentration. Therefore, a cell thickness of 1 cm will be convenient for ease of fabrication and structural rigidity and also to produce an optimum number of interference fringes for the range of sucrose concentration studied.

4.1.2 Plano-Convex Lens and Cylinder Lens

The plano-convex lens and cylinder lens are high quality singlets, custom made by Interoptics, LTD. They are fabricated from SF4 A grade high index glass with a refractive index of 1.74999 at a wavelength of 6.328×10^{-5} cm.[100] These lenses were made to state of the art tolerances for minimal spherical aberration. The total wavefront distortion for these lenses is diffraction limited to $\lambda/4$. The spherical lens has a focal length of 67.3 cm. The diameter of this lens is 10 cm and the thickness at the edge is 1 cm. The cylinder lens has a focal length of 15 cm. The length of the lens is 6 cm and the width is 3 cm in the power plane. The edge thickness of this lens is 0.935 cm.

The focal lengths of these lenses were selected to produce a clear, easily observable fringe pattern at the focal plane and also to meet the physical constraints introduced by the geometry of the magnet and laboratory space. The fringe spacing Δ is given by Eqs. 3.35 and 3.38 as a function of the plano-convex lens focal length f and slit width Y_s.

$$\Delta = \frac{f\lambda}{Y_s n_a} \tag{4.2}$$

where λ is the wavelength of laser light and n_a is the refractive index of the air. Y_s is equal to 1.0 cm which is determined by the spacing of the diffusion and reference compartments in the diffusion

cell. The focal length should be as large as practical to give an easily observable fringe spacing. However, simple physical limitations due to the geometry of the magnet and optical bench limit f to 1 meter or less. A value of 67.3 cm was selected because the tooling was readily available at Interoptics, LTD to manufacture this lens. This focal length produces a fringe spacing from Eq. 4.1 of $\Delta = 0.00426$ cm, which was easily observable through the 30 power measuring microscope.

The 15 cm focal length was selected for the cylinder lens to produce an image of the diffusion cell which would fill the frame of a 35 mm film. This lens produced an image of the test cell 0.9 cm long in the focal plane of the camera. The vertical magnification of this configuration was determined experimentally to be 0.32. Figure 19 summarizes all optical component parameters and dimensions.

4.1.3 Vertical Slit Assembly

Interference fringes are observable as the result of the phase difference between two different superimposed wavefronts of light. A double masking slit assembly divides the spatially coherent laser beam into two rectangular vertical beams which illuminate the reference and diffusion compartments of the diffusion cell and are in phase with each other prior to being transmitted through the diffusion cell. When a slit is illuminated with monochromatic and collimated light a diffraction phenomena occurs which is classified as Frauenhoffer diffraction.[99] This produces an "envelope" of coherent light, the width of which is determined by the width of the slit. The diffraction envelope width increases as the slit width decreases, while the

intensity of the envelope decreases with decreasing slit width. The selection of the optimum slit width is therefore a compromise between a width which gives adequate intensity of the diffraction envelope and yet is wide enough to easily observe the fringe pattern. The correct slit width was found by trial and error until a well-illuminated, clear interference pattern was observed on the focal plane of the camera. The final slit width was chosen as 0.05 cm ± 0.0001 cm. The distance between the dual slits is determined from the spacing of the diffusion and reference cell compartments and in this case is 1.0 ± 0.0001 cm.

Ordinary razor blades provide an inexpensive source of straight edges for slit construction. Four razor blades were used to make the double slit assembly. They were cemented onto a special frame under the 30 power measuring microscope. The microscope was used to observe their position during construction and establish adequate spacing, parallelism, and uniform width. The slit geometry was measured and verified to the limits of accuracy for the measuring microscope, ± 0.0001 cm. This assembly produced clear, well defined interference fringes and the cost is a fraction of the cost of commercially available masking slits. This is apparent from the photograph of a typical set of interference fringes shown in Figure 8.

4.1.4 Laser and Collimating Lens System

A Spectra-Physics model 124B helium-neon laser provides a coherent light source for the experiment. It is rated at 15 mW optical output at a wavelength of 6328 Å. It operates in the TEM_{oo} mode.[101]

A Spectra-Physics model 332 and 336 spatial filter and

collimating lens assembly are used to provide a collimated, spatially filtered beam.[102] The beam is first focused and passed through a pinhole aperture. This has the effect of removing any spatial noise in the beam and providing a smooth Gaussian intensity profile across the output beam. Spatial noise is produced from diffraction effects as the beam encounters small irregularities on the inside bore of the laser tube. To eliminate the scattered light from these diffraction effects the beam is focused and passed through an aperture 1.5 times the minimum focused spot diameter. This eliminates any noise and transmits about 99% of the Gaussian beam power. This spatially filtered beam is then passed through the beam expander lens and collimator which produces a beam 5.0 cm in diameter. Total wavefront deformation with this assembly is less than $\lambda/10$.

4.1.5 Optical Bench and Component Mounts

Since the objective of this work is to measure the effects of a homogeneous applied magnetic field on diffusion, it is imperative that no ferromagnetic material be placed in the field which would destroy the homogeneity. This criterion eliminated most commercially available optical benches and component mounts which usually contain some quantity of steel. Therefore, the optical bench and component mounts were custom made by the UBC chemical engineering workshop using only non-ferromagnetic materials; aluminum and nylon.

The optical bench consisted of a two meter long aluminum beam placed between the poles of the magnet. It rests upon two concrete and rubber vibration isolation platforms placed at each end of the magnet

which center the bench between the poles of the magnet, 70 cm above the floor. The beam is 10 cm wide and 5 cm thick. A strip of aluminum 4 cm wide by 0.5 cm thick is mounted on the optical bench along the entire length. The special mounting blocks slide along this strip and can be clamped in place by number 8 machine screws.

The aluminum diffusion cell holder is shown to scale in Figure 11. The cell fits in rectangular groove cut in a circular plate. Four vertical retaining posts keep it vertical and two nylon shim screws are used to align the two halves of the diffusion cell into the same plane. The cell is held in place by elastic retaining strips.

The plano-convex lens and mount are shown to scale in Figure 12. A threaded retaining ring holds it in the circular holder between Teflon washers.

The cylinder lens and mount are shown to scale in Figure 13. The lens slides in between two grooved retaining posts and is clamped in place by two nylon retaining screws.

All component mounts are placed in the clamping blocks by adjustable aluminum rods so the height can be adjusted. The axial position of the components can then be changed by moving the clamping block along the bench. A clamping block is depicted to scale in Figure 14.

4.1.6 Vibration Isolation

The configuration of the Rayleigh interferometer makes it relatively insensitive to vibrations. Vibrations could introduce errors into the measurements only if the optical path length between the two

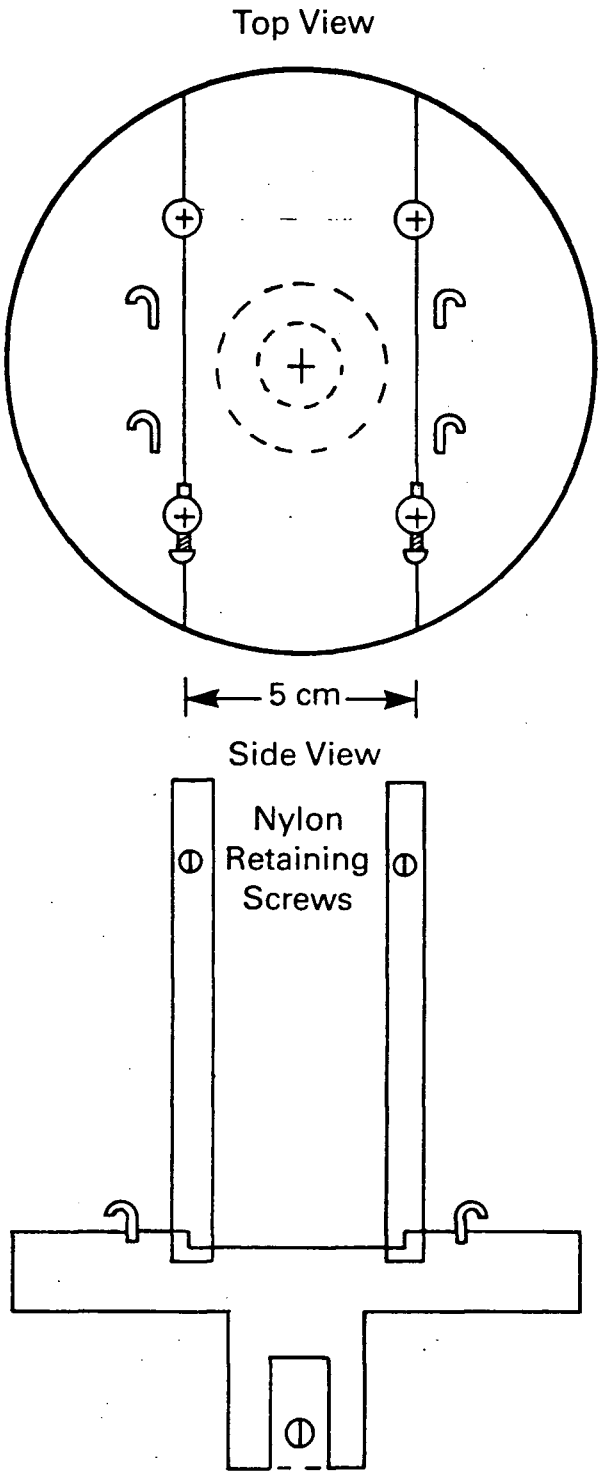

Fig. 11. Diffusion Cell Holder

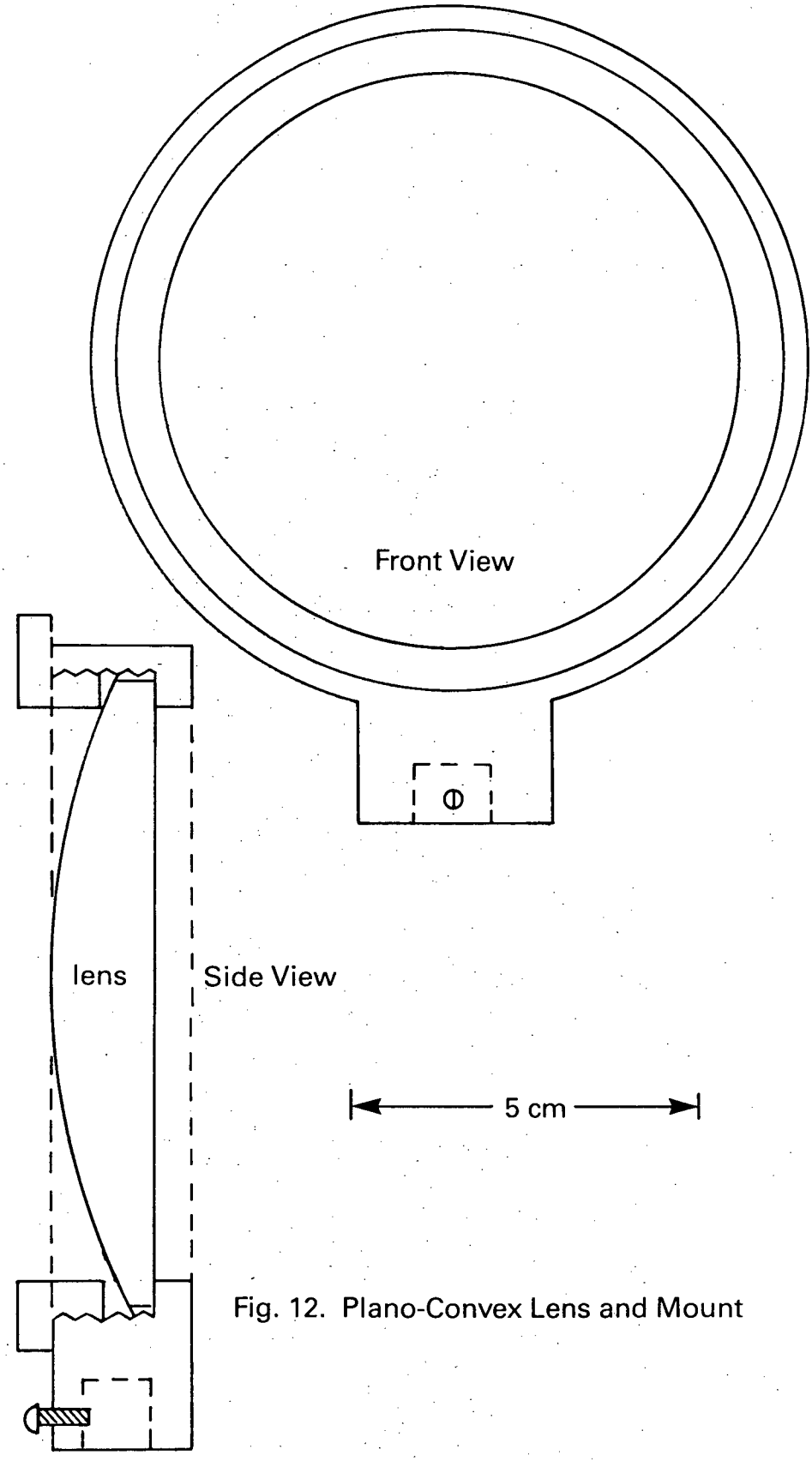

Fig. 12. Plano-Convex Lens and Mount

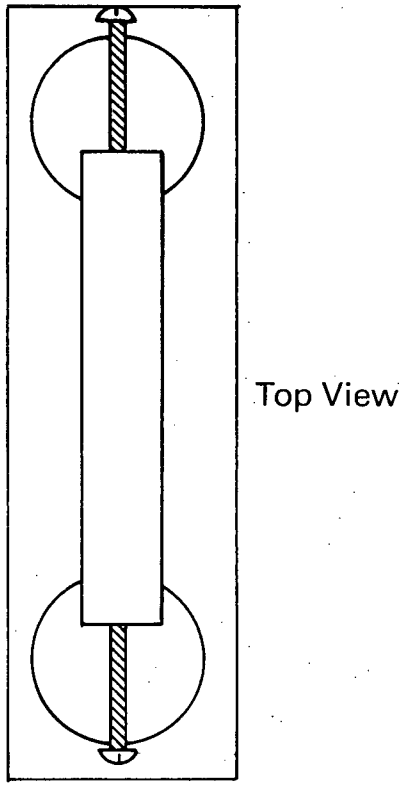

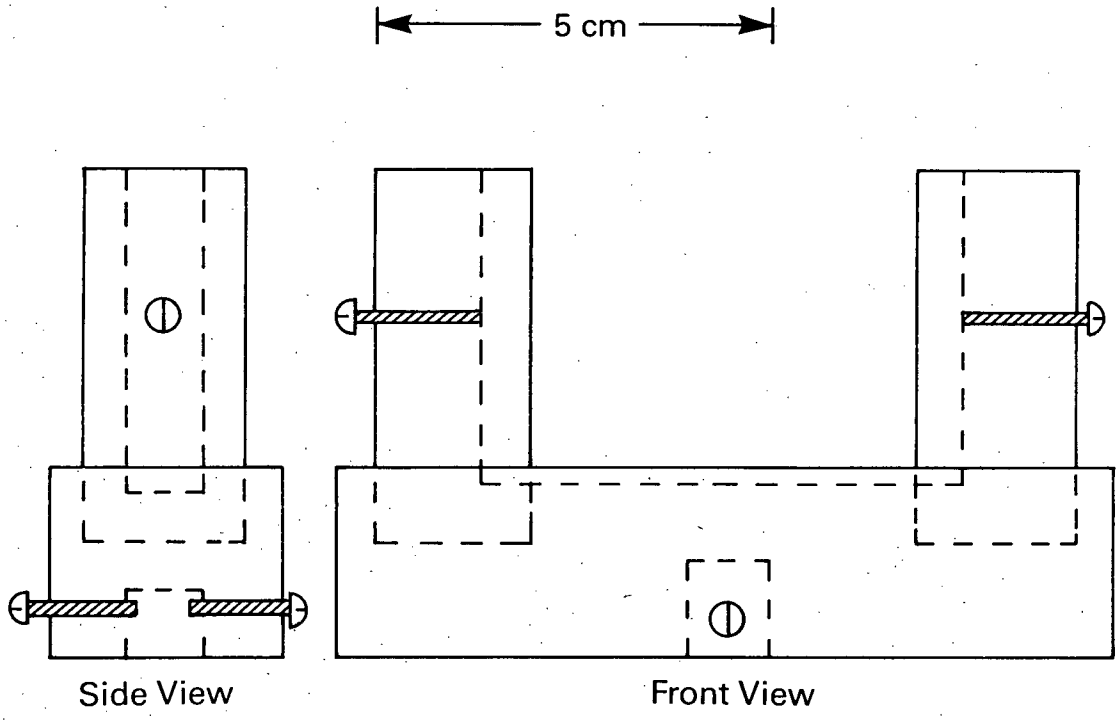

Fig. 13. Cylinder Lens and Mount

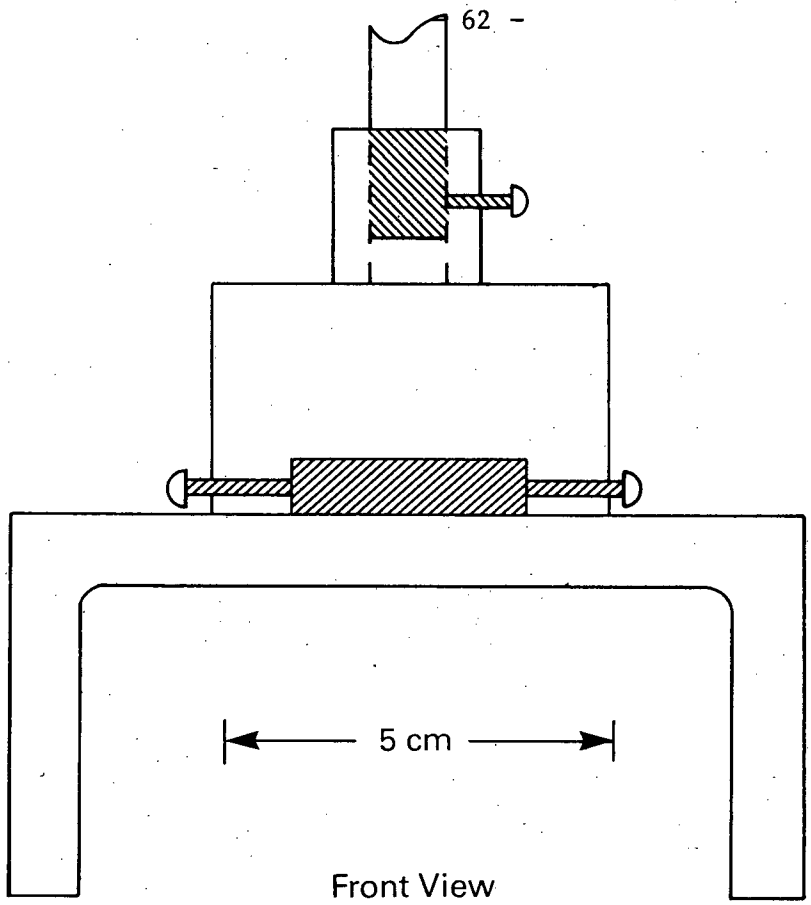

Front View

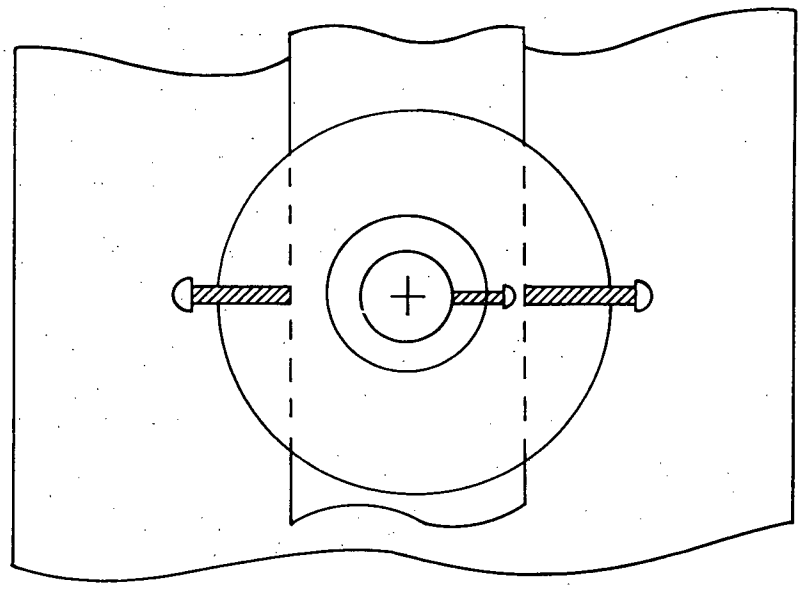

Top View

Fig. 14. Optical Bench and Mounting Block

interfering beams was changed. Because the diffusion cell is small (distance between reference and diffusion compartments is 1 cm) and rigidly constructed, any relative displacement between the two compartments is minimized, thereby reducing optical path length differences from vibrations.

The optical bench rests on two vibration isolated bases located on either side of the magnet. The base is constructed of concrete patio blocks sandwiched between high density foam rubber. Each base weighs approximately 500 kilograms. Figure 15 shows one of the vibration isolation platforms. The massive layered blocks and rubber combination acts as a spring mass system which provides sufficient dampening action to attenuate any vibration which might be transmitted through the floor.

The fringes were observed through the microscope to verify that any building vibrations would not cause any movement. When a building compressor in an adjacent room was switched on, no perceivable movement in the fringe pattern could be observed through the 30 power microscope.

4.1.7 Temperature Control

Maintaining a constant temperature in the diffusion cell is essential in order to eliminate an important independent variable in the diffusion process. The Einstein-Stokes equation (Eq. 3.8) for a liquid diffusion coefficient predicts that the diffusion coefficient is directly proportional to the absolute temperature of the system. Therefore any change in temperature will have a direct effect on the diffusion coefficient.

Temperature fluctuations in the air adjacent to the diffusion

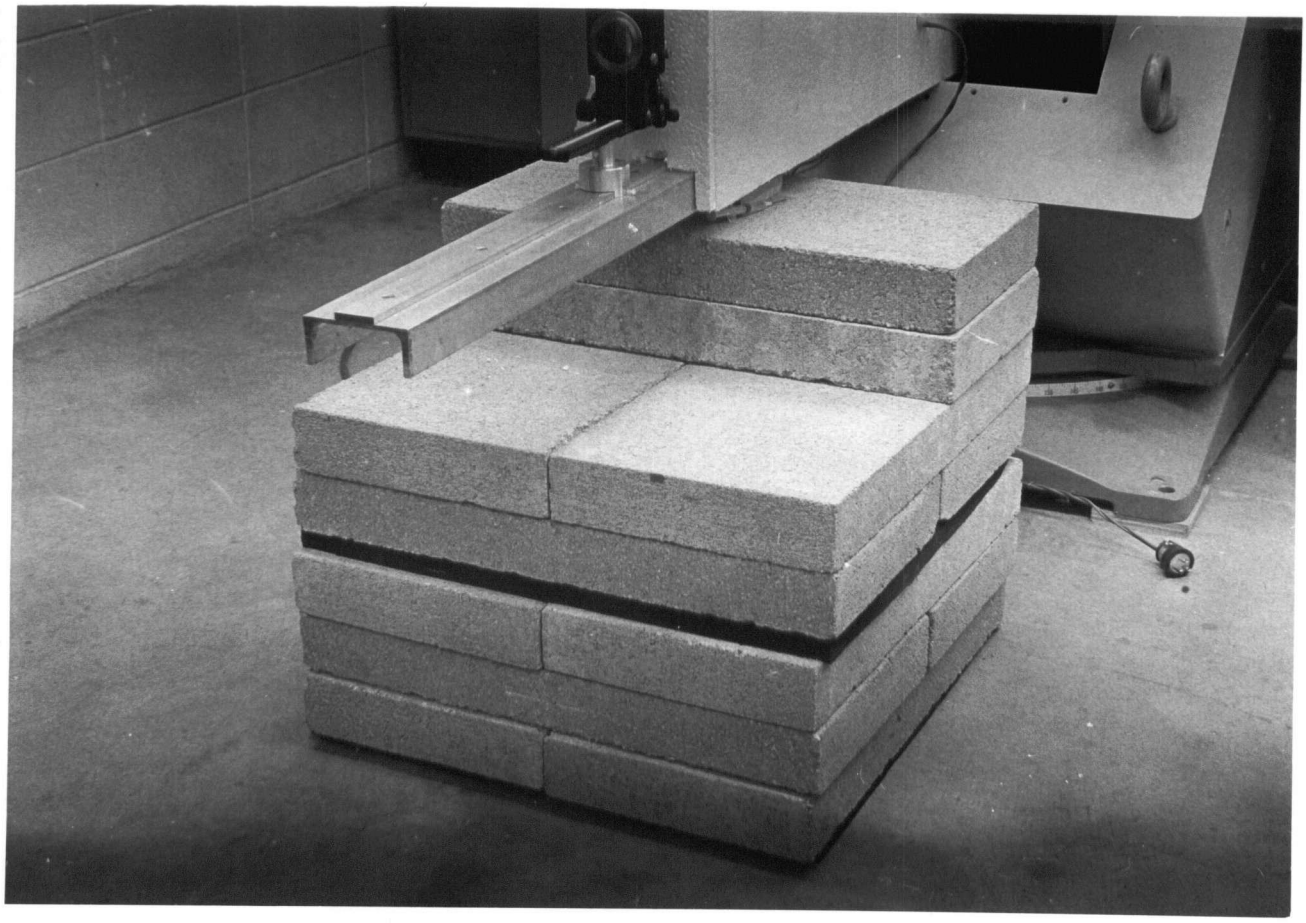

Figure 15 - Concrete and Rubber Vibration Isolation Platform.

cell are controlled to ± 0.1°C. This is achieved by a dual temperature control system. The ambient air temperature in the room was controlled to ± 1°C by a Koldwave model K16DF water-cooled air conditioner, rated at 4835 W. This was also used to remove the heat produced by the magnet and other electronic equipment.

The optical bench is enclosed in a 1 cm thick styrofoam box to provide thermal insulation. A 25 watt fan, the type used to cool electronic equipment, is mounted along the enclosure 30 cm from the diffusion cell. An electric resistance heater is mounted inside the enclosure across the output of the fan. It was constructed by wrapping nichrome wire around a 1.5 cm diameter glass tube. It is rated at 300 W at 115 VAC input.

The air temperature adjacent to the diffusion cell (4 cm away) is measured by an Omega model 100 R 30 platinum RTD, thermometer. The electric resistance of this thermometer is proportional to temperature. An Omega model 4201 proportional and on-off controller measures the resistance and therefore temperature of the thermometer. The sensitivity of the equipment is ± 0.05°C. This controller has an adjustable bandwidth between 0 and 5% of full scale. An error signal is generated by the controller which is proportional to the difference between the measured temperature and the setpoint temperature. This error signal in turn is used to drive a variable transformer which powers the electric heater. The bandwidth adjustment and voltage output of the variable transformer were adjusted simultaneously to provide a constant cycle time for the heater. This proved to be between 15 and 20

VAC with a cycle time of 10 to 15 seconds. The temperature fluctuations measured by the platinum thermometer and temperature controller combination were always within 0.1°C of the 25°C setpoint temperature. Turning on the magnet produced no change in the temperature indicated by the controller.

4.1.8 Membrane and Sucrose Solution

The membranes selected for this work are General Electric Nucleopore membranes.[103] They are made from a polycarbonate film which is bombarded by high speed sub-atomic particles from a nuclear reactor. The particles pass straight through the film, leaving tracks of molecular damage which can be etched preferentially in a chemical bath to round, linear pores of uniform diameter. The maximum pore diameter certified by the manufacturer varies no more than + 0% to -10% for each membrane. The surface is smooth and flat, maximum peak to valley distance on the membrane surfaces is less than 0.1 μm. The membrane dimensions used in this experiment are shown in Table I.

Table I Membrane Parameters for GE Nucleopore Membranes

Pore Size, μm	Pore Density pores/cm^2	Thickness, μm	Porosity cm^2/cm^2
8.0	1×10^5	50	.050
0.8	3×10^7	10	.151

The solution was made from AMCHEM reagent grade sucrose dissolved and diluted volumetrically with doubly distilled water at room temperature.

4.1.9 Electromagnet

A Varian Associates 30 cm Model V-7300 electromagnet was used to apply the magnetic field to the diffusion cell. The magnet was fitted with an 18 centimeter diameter pole piece with a 10 cm gap width. A Varian Associates Model V-7800 DC power supply and V-7872 heat exchanger were used to cool this magnet which could generate fields as high as 12.5 kG. Homogeneity of the field has been measured to better than 7 x 10^{-4} kG over the diameter of the pole piece at an applied field strength of 9.0 kG[21] The field strength homogeneity measurements are shown in Figure 16. The field strength was measured by a Hall-effect crystal probe mounted on one pole piece. The crystal is excited by an electronic oscillator and the output voltage from the crystal is proportional to the magnetic field. This signal is then used to control the current produced by the power supply. This configuration enables the magnetic field to be controlled to within 1PPM for a ± 10% change in line voltage or load resistance.[104] The power supply produces a continuously variable DC output between 5 amperes and 114 amperes. The magnet is cooled by a two loop water to water heat exchanger. Distilled water is continuously recirculated through the magnet and one side of the heat exchanger. Filtered city water flows through the other side, with waste heat being drained to the city sewer lines. A temperature sensor at the reservoir inlet controls a proportional flow control value in the raw water circuit, thus providing automatic temperature control of the magnet assembly water inlet temperature, maintained at less than 50°C.

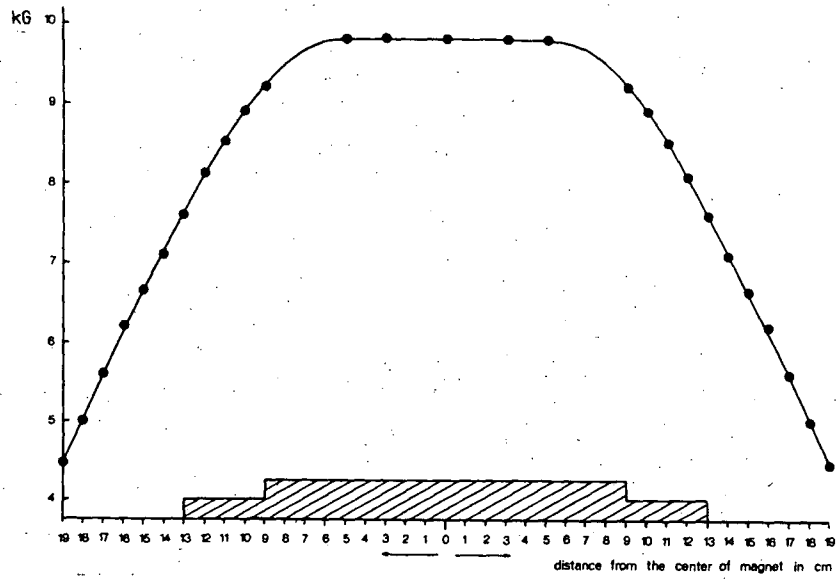

Figure 16 - Magnetic Field Homogeneity[21].
(used by permission).

An experiment was conducted to establish that the magnetic field did not affect the optical characteristics of the diffusion cell, laser, and optical components. The fringe pattern was examined through the 30 power measuring microscope when the magnet was brought up to full power (12.5 kG) and then switched off during a preliminary experiment with distilled water and 1% sucrose solution in the cell. No change in the fringe pattern could be seen through the microscope. Therefore, it was assumed that the magnetic field had no observable effects on the optical properties of this system.

4.1.10 Camera and Measuring Microscope

The interference fringes are photographed with a Contax model 139 Quartz 35mm single lens reflex camera. Kodak Panatonic-X film was used with Edwal FG-7 developer to provide a fine grain and high resolution medium for recording the fringe patterns. The Model 139 camera has an electronic automatic exposure control. However, the best exposure was found by trial and error to be 1/500 second, which was sufficiently short to give sharp photographs. The unfiltered laser beam was initially too intense to yield satisfactory exposure, even at the fastest shutter speed available. A Kodak Wratten No. 59 filter was used to attenuate the beam. This provided over 95% attenuation in the red-orange region of the spectrum which proved satisfactory for the 25 ASA film speed. Since the filter was placed less than 6 cm from the focal plane there was no noticeable distortion of the interference fringes.

A Contax Model S infrared controller set was used to provide

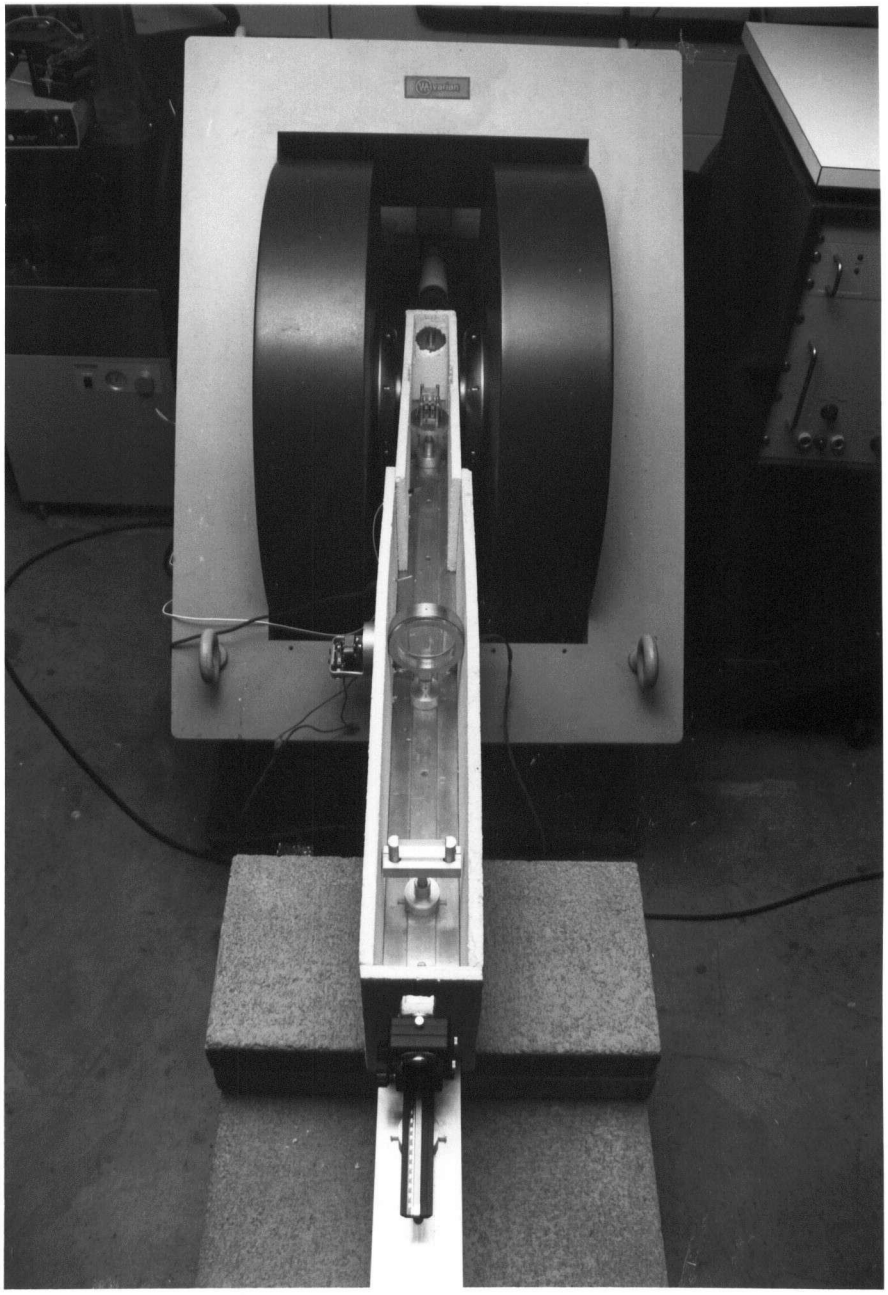

Figure 17 - Optical Bench and Magnet LBE) - Laser and Beam Expander, S1)-Masking Slits, DC)-Diffusion Cell, L1)-Plano-Convex Lens, L2) Cylinder Lens, EB) Extension Bellows.

remote control of the camera, thereby avoiding any vibration caused from a manual shutter release.

The camera was mounted on a Yashica Model F adjustable extension bellows providing a light-tight interface with the experimental enclosure and horizontal adjustment for proper focusing. The extension bellows was mounted on the optical bench using one of the aluminum mounting blocks.

Fringes were measured with a Gaertner model M-1160 measuring microscope. This consisted of a 32 power microscope mounted on a precision vernier stage capable of measuring ± 0.0001 cm distances. A 90° spider silk cross hair was used with the moveable stage to accurately measure fringe spacing. The precision lead screw has been calibrated to a standard scale, the accuracy of which is certified by the National Bureau of Standards.

A photograph of the optical bench assembly and magnet is shown in Figure 17.

4.2 Experimental Procedure

The complete procedure used to set up the interferometer and obtain interference fringe data is described below. Proper alignment of the interferometer involved four main steps: 1) Collimation and spatial filtering of the laser beam through focus and position adjustments on the collimating lens spatial filter assembly; 2) Proper height adjustment for all optical components; 3) Focusing the plano-convex lens L1; 4) and proper focus for the cylinder lens in order to focus on a plane in the center of the diffusion cell. When the interferometer

was satisfactorily aligned the membrane was mounted in the cell and an experiment began. Appropriate details are described in the following sections. Figure 9 shows the respective components described in the alignment procedure.

4.2.1 Aligning the Interferometer

(1) The spatial filter and collimating lens are adjusted to provide maximum beam intensity and good collimation. The X and Y motion adjustment screws on the pinhole aperture are first adjusted to center the aperture on the focused beam. The aperture is then adjusted axially to bring it into the focal plane of the beam, yielding maximum beam intensity with the most uniformly illuminated output. The collimating lens is then screwed on the spatial filter. To collimate the beam, it is directed to a screen placed across the room, approximately five meters away from the laser. The beam diameter is measured upon exit from the laser and the lens adjusted to produce an equivalent spot size on the screen. The beam is now considered collimated and filtered.

(2) The laser is placed on the optical bench. It is directed down the centerline of the bench. A calibrated ruler is used to check the height and verify that the beam is parallel with the optical bench centerline. Shims are placed under the laser head assembly to adjust the height and vertical angle of propagation of the beam.

(3) The cell holder and lenses are next placed on the optical bench. The clamping screws in the mounting block are kept loose and the lenses are placed in approximate position. The cell holder is centered between the pole pieces of the magnet. The height of each component is

adjusted to bring it into line with the beam center.

(4) Next the slit assembly is mounted over the opening to the insulated enclosure. A square is used to orient the slits orthogonal to the optical bench axis. The position is adjusted to center the slits in the 50 mm diameter laser beam.

(5) The bifocal lens system is then brought into focus. This is accomplished by placing a small screen in the focal plane of the camera body. A fine wire grid (1 mm spacing) is placed in the diffusion cell holder at a location corresponding to the correct focal plane for the diffusion cell. The cylinder lens, L2, is then removed from the mounting block. The plano-convex lens, L1, is moved axially along the optical bench until a spot was focused on the screen of the focal plane camera. The clamping screws are then tightened. The cylinder lens is placed back in the mounting block and its axial position on the optical bench adjusted until an image of the wire mesh is focused on the camera screen. The measuring microscope is then used to examine the image of the wire mesh and interference pattern to verify sharp focus and clear fringes.

(7) Finally the lenses are checked to verify that the surfaces are orthogonal to the propagation direction of the laser beam. They are rotated in the mounting blocks until the reflection from the masking slits is reflected back into the masking slits. The heights of the lenses are measured again before the clamping screws are tightened to verify no change during the alignment. The alignment of the interferometer is now complete. The wire mesh is removed from the

diffusion cell holder and the fringe pattern examined with the measuring microscope. The fringes should be straight since the refractive index is constant in the cell at this time.

4.2.2 Diffusion Cell and Membrane Preparation

(1) To remove dissolved gasses from the distilled water it is boiled for approximately 30 minutes. A 5 cc hypodermic syringe is filled with hot distilled water, before the water cools and air is re-dissolved in it. The remaining water is then cooled in an air tight sealed flask with no air space. 200 ml of this cooled water is then used to make a 1% by weight sucrose solution. This solution is then evacuated by a mechanical vacuum pump for approximately one hour to remove any gases which may have dissolved in the water during the mixing process. There may be a slight concentration change due to the evaporation of water during the gas removal. Therefore, the refractive index of this solution was measured with a Bausch and Lomb model 3L refractometer at 25°C to four decimal places before each experimental run. A 5 cc syringe is then filled with sucrose solution. The syringes filled with water and solution are placed in the insulated enclosure which has been set to the desired temperature. A minimum of four hours are allowed for the system to reach thermal equilibrium before an experiment is started.

(2) Next the diffusion cell and membrane are prepared. The membrane is boiled in distilled water for approximately thirty minutes before mounting to remove any unrelaxed stresses and entrapped air in the pores. This makes it easier to mount the membrane without any warps

or wrinkles. A new membrane is used for each run.

(3) The diffusion cell is cleaned with cotton Q-tips and soap. It is rinsed well with distilled water.

(4) A very thin coat of silicon vacuum grease is applied to both interfaces of the diffusion cell. The grease provides a water-tight seal between the membrane and glass and is not softened by water. If the coat is too thick excess grease will extrude, distorting the membrane shadow.

(5) The lower half of the cell is placed on a table top and the reference and diffusion side compartments filled with water and sucrose solution, respectively, from the hypodermic syringes. The compartments are filled until the meniscus is just over the top surface and then the membrane is removed from the boiling water and placed on the greased glass surface. The membrane is smoothed flat with a cotton Q-tip, expelling any extra water or solution. Great care must be taken to assure there are no warps or wrinkles in the membrane and it makes complete contact with the greased surface without any grease extruding onto the diffusion area of the membrane.

(6) The lower half of the diffusion cell is placed in the base of the cell mounting plate. The top half is then placed on the membrane, using care to assure no wrinkles are formed. The reflection of the laboratory fluorescent light tubes from the membrane surface will be undistorted if the membrane is smooth and no warps or wrinkles exist. The hypodermic syringe is then used to fill the reference side compartment with distilled water if these tests are satisfied. The top

half of the diffusion cell side is filled with 1% sucrose solution with the hypodermic syringe from the insulated enclosure. Rubber stoppers are placed in the openings to the diffusion cell. When the experiment is started, the sucrose solution in the upper half of the diffusion side compartment is removed and replaced with distilled water. The water, being of lower density than the sucrose solution, was placed in the top half of the cell to eliminate bulk flow effects which would result from the more dense liquid being above the lower density one.

(7) The diffusion cell holder is assembled and placed in the mounting blocks on the optical bench. The cell alignment is adjusted by turning on the laser and observing the reflection of the laser beam from the diffusion cell surfaces back into the masking slits. The two nylon shimming screws are adjusted to bring the two halfs of the cells into the same plane, making both surfaces orthogonal to the laser beam. When the reflections of the masking slit form vertical lines, both surfaces are flat and aligned in the same plane. The cell holder is then rotated in the mounting block until the slit reflection is directed exactly back into the masking slits. The height is checked again to verify the cell is centered in the laser beam. When all of these steps are completed the cell is then considered aligned and the experiment is ready to begin. The cover of the enclosure is replaced and at least two additional hours are allowed for the temperature to equilibrate.

The optical components are now in alignment and the experiment is ready to begin.

4.2.3 Beginning an Experiment

Initially the diffusion cell is completely filled with sucrose solution in the diffusion side compartment and the reference side is filled with distilled water until temperature equilibrium is reached. An experiment is initiated by removing the sucrose solution from the top half of the diffusion side compartment and replacing it with water.

(1) The sucrose solution in the top half of the diffusion cell side is carefully removed with a hypodermic syringe. It is essential that the membrane surface not be touched with the needle or else warping will occur and the run must be aborted. As much solution as possible is removed without actually touching the membrane. Only a slight meniscus in the corners of the cell remains with careful solution removal. It is estimated that the amount of solution remaining is less than one drop or 0.03 ml out of a total volume of the upper half of the compartment of 1.3 ml. The magnet is then turned on and water is inserted into the empty top half of the diffusion cell to replace the sucrose using another hypodermic syringe. All syringes have been kept inside the enclosure during the time the temperature is equilibrating so they are all at a constant temperature of 25°C. The stop watch is started after the water is injected. The rubber stopper is then replaced in the opening of the diffusion cell.

(2) The fringe pattern is observed through the measuring microscope, sighting the cross hairs onto a fringe near the membrane shadow. When that fringe has shifted by a distance approximately equal to two fringes, the camera is attached to the bellows and a photograph

taken using the remote control. The first photograph is not taken until 15 minutes have elapsed to allow any convection effects from the initial cell filling to dissipate. The rate of change of the fringe pattern is an exponential function, so initially the time intervals are quite close together (approximately 15 minutes), while at the end of the experiment the change is much more gradual so photographs are only taken every hour. A minimum of five photographs are taken for each experiment. If the fringes at either end of the cell have moved, the run is terminated since the boundary conditions have changed. The run was terminated after 3 hours.

CHAPTER 5

FRINGE PATTERNS AND DATA ANALYSIS

A typical interference fringe profile is shown in Figure 8. The pattern on the left is observed with a uniform sucrose concentration through the cell, and therefore a uniform refractive index in the cell. The phase difference between the reference and diffusion side beams is constant through the entire length of the diffusion cell, therefore the interference fringes are straight lines. However, in the presence of a refractive index gradient in one side of the diffusion cell, the phase difference is no longer equal between the two sides, but becomes a function of vertical position in the cell. This causes a bending of the fringe pattern as shown in the right half of Figure 8. The degree of bending in the pattern is directly proportional to the refractive index at that location in the diffusion cell. The equations used to determine refractive index, concentration, mass fluxes, and diffusivities from fringe data are described in detail in this section.

5.1 Assumptions

The following assumptions and simplifications are made in this analysis: 1) diffusion occurs only in one-dimension, 2) light rays are deflected as they are transmitted through a refractive index gradient, but travel through the cell in a straight line, 3) diffusion through the membrane is steady state at any given time, i.e., the mass fluxes are equal on both surfaces of the membrane, 4) the diffusion coefficient is independent of concentration at any given time in the diffusion process, 5) only binary diffusion is considered, i.e. sucrose and water, impurities being ignored.

5.1.1 One-dimensional Diffusion

The assumption of one-dimensional diffusion ignores any boundary layer effects occurring at the walls of the diffusion cell. The plane of focus is located near the center of the diffusion cell (approximately 5 mm from the wall). Initially the concentration gradient is only one-dimensional in the vertical direction. Viscous drag between the diffusing molecules and wall would cause a three dimensional concentration profile, however in the midplane of the cell the profile should be flat since boundary layers are no thicker than several molecular diameters (10.6 Å for sucrose). Therefore, diffusion near the cell midplane will remain essentially one-dimensional.

5.1.2 Light Ray Deflection

The path of a light ray through a refractive index gradient in the diffusion cell is shown in Figure 18. The path, L, is given by

$$L = \int_0^s n(x)ds \tag{5.1}$$

and the slope of the deflection is given by,[105-106]

$$\frac{dx}{ds} = \frac{1}{n(x)} \int_0^s \frac{dn}{dx} ds \tag{5.2}$$

This predicts that s will be an arc bending towards the direction of increasing refractive index. In these experiments with a dilute sucrose solution of 1% by weight the amount of deflection is small, so it will be assumed the ray is bent, but travels through the cell in a straight line as shown in Figure 18. Wavefront deflection is discussed in greater detail in Section 5.2.

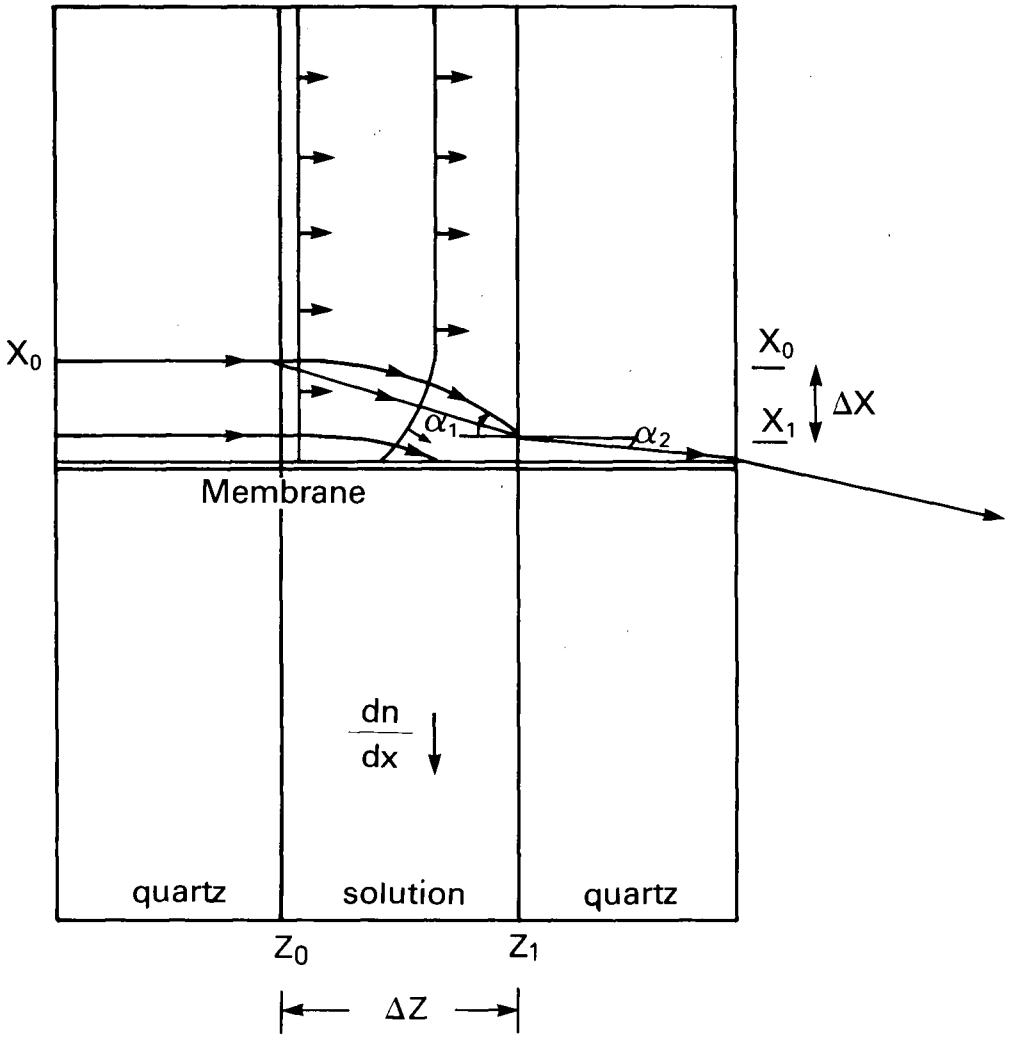

Fig 18. Wavefront Deflection Through Diffusion Cell and Refractive Index Gradient.

5.1.3 Steady State Membrane Diffusion

The Nucleopore membranes used in this experiment are thin (10 μm). Also, they are saturated with sucrose solution at the start of a run since the cell is filled with solution at least two hours prior to the start of an experiment. If there is no swelling or shrinkage of the membrane (easily observable during the duration of the run through the microscope by a change in the membrane shadow), then conservation of mass requires that the mass flux be equal at both membrane surfaces, i.e. there are no sources or sinks of sucrose within the membrane itself.

5.1.4 Constant Diffusivity

This assumption constitutes ideal Fickian diffusion. It is valid if the maximum concentration change in the diffusion cell is small, since the diffusion coefficient decreases with increasing concentration. The constant diffusivity condition is assumed for diffusion through the membrane at any given time interval during the run. The maximum difference in concentration during these experiments is 1% by weight between the two halves of the cell at zero time. The concentration change across the membrane is even smaller as the run proceeds since diffusion is not steady state and the concentration difference through the membrane decreases with time. This assumption has been verified experimentally by Bollenbeck for a 1% sucrose change.[40]

5.2 Calculating Refractive Index Profile

The obtained fringe pattern is traversed vertically with the measuring microscope. Figure 8 shows a typical interference pattern

during an experiment. The reference point for the measurements start at each end of the diffusion cell where the refractive index is constant and the fringes straight . The location where each fringe crosses the vertical axis of traverse is recorded with the corresponding fringe number. This is repeated with the other half of the cell. The final result is a set of fringe numbers and displacements counting from the ends of the cell towards the membrane. Each fringe shift represents a phase difference light. This phase difference $\Delta\emptyset$ is equal to the optical path length difference between the two beams

$$\Delta\emptyset = \lambda = \Delta ns \tag{5.3}$$

Since s is the geometrical distance the beam travels and is known from the geometry of the interferometer, Δn can be calculated from Equ. 5.3. Therefore, knowing the vertical locations in the cell which correspond to a phase shift of λ, from the interference fringes, it is possible to calculate a set of points giving n as a function of x_i, the vertical position in the cell corresponding to a fringe shift.

$$n(x_i) = n_\infty + \Delta n(x_i) \tag{5.4}$$

n_∞ is the known refractive index at each end of the cell equal to the initial refractive index at time = 0.

This simple analysis ignores the deflection of a light ray through a refractive index gradient normal to the direction of propagation, assuming the light ray travels in a straight horizontal

line through all locations in the diffusion cell. The physical reason for this deflection lies in the dependence of propagation velocity on refractive index. The different elements of a wavefront propagate through the medium at different times, causing the wavefront to tilt in the direction of increasing refractive index (see Figure 18). The downward deflection of the light ray introduces errors into the analysis because the vertical position of a ray on the focal plane do not correspond to the actual vertical position of the ray entering the diffusion cell.

If the original entry position of the ray and the optical path of the ray through the cell can be determined, then a corrected refractive index profile may also be derived for the one-dimensional diffusion process. A simple iterative scheme was used to derive the correct refractive index profile. The approximate refractive index profile was first determined from the observed fringe pattern data and Eq. 5.4. Snell's law* was then used to trace the ray through the optical system to the film plane. The calculated location of this light ray is compared with the actual location of the same ray observed on the film and the refractive index profile is modified. The entry position in the diffusion cell is modified by an amount proportional to the error between the same ray and corresponding position on the focal plane observed for this ray. This procedure is repeated until the "corrected"

---

*Snell's law states $n_1 \sin\alpha_1 = n_2 \sin\alpha_2$, where n_1 and n_2 are the refractive indices for two different mediums and α_1, α_2 are the angles of a light ray being transmitted through these respective media.

refractive index profile produces a fringe pattern corresponding to the one observed. The calculations are summarized below:

(1) Calculate refractive index profile from fringe data using Eq. 5.4 assuming no ray bending.

(2) Using profile determined from step 1, find a suitable correlation for n(x) (details concerning correlation are included in following section).

$$n(x) = f(x) \tag{5.5}$$

(3) From Eq. 5.5 evaluate dn/dx.

(4) If the arc of the ray passing through the diffusing fluid is represented by a straight line passing through a locally constant refractive index gradient then the refractive index along the path is given by

$$n(x) = n(x_o) + \left[\frac{dn}{dx}\right]_{x_o} (x_1 - x_0) \tag{5.6}$$

(5) The average refractive index, $\bar{n}$, along the line is then

$$\bar{n} = n(x_o) + 1/2 \left[\frac{dn}{dx}\right]_{x_o} (x_1 - x_0) \tag{5.7}$$

(6) The path of the ray is given by a modification of Eq. 5.2 as

$$\frac{dx}{ds} = \frac{1}{n(x)} \int_o^s \frac{dn}{dx}\, ds \tag{5.8}$$

(7) Integrating Eq. 5.8 with a constant refractive index gives

$$\frac{dx}{ds} = \frac{1}{n(x_i)} \left[\frac{dn}{dx} \right]_{x_{o,i}} s \tag{5.9}$$

(8) Substituting n(x) from Eq. 5.5 and integrating gives

$$(x_1 - x_0)_i = \frac{1}{2(\bar{n}_i)^3} \left[\frac{dn}{dx} \right]_{0,i} L_{01}{}'^2 \tag{5.10}$$

which is the vertical deflection through the cell thickness.

(9) Substituting the definition of optical path length for L_{01}, into Eq. 5.10 gives

$$L_{01} = \bar{n}\ s \tag{5.11}$$

therefore

$$(x_1 - x_0) = \frac{1}{2\bar{n}_i} \left[\frac{dn}{dx} \right]_{0,1} (z_1 - z_0)^2 \tag{5.12}$$

where $(z_1 - z_0)$ is the horizontal distance through the cell. We now have current estimates for $(x_1 - x_0)$, dx/ds, and dn/dx. According to the straight line approximation the path length through the cell can be found by Pythagorean's Thorem

$$s_i{}^2 = (x_1 - x_0)^2 + (z_1 - z_0)^2 \tag{5.13}$$

Knowing the arc length, average refractive index, and angle of deflection in the concentration gradient it is possible to trace the ray through the remaining optical system using Snell's law. Figure 19 lists all parameters used in the raytracing program for the various lenses and optical components.

The results of the raytracing program then give the position of this ray on the focal plane. It is compared with the position of the actual fringe pattern corresponding to the same ray observed on the film. Based upon the deviation between the two values, the x_o position of the original ray entering the cell is updated giving a new refractive index profile n(x). Steps 1 to 11 are then repeated until the calculated refractive index profile produces a hypothetical fringe pattern which corresponds to the observed one. This process takes four to five iterations to converge to a tolerance of 1×10^{-3} percent. The maximum deflections, refractive index gradients and percent errors for a typical run are given in Table II. A complete listing of the ray tracing computer prgram is given in Appendix C.

5.2.1 Mass Flux and Diffusivity Calculations

The fringe profiles were checked and corrected for deflection errors before molar fluxes and diffusivities were calculated. This required a suitable correlation function for the refractive index as a function of position, as was discussed in the previous section.

The profiles shown in Figure 20 indicate that the refractive index function has a sigmoid shape. The solution to Fick's second law with constant diffusivity (Eq. 3.2) predicts a sigmoid concentration

profile. If boundary conditions are such that the concentration profile is a step change from zero to C_o at x equal to zero and time equal to zero and constant diffusivity is assumed, then the solution to Eq. 3.2 is the complemented error function[107]

$$c(x,t) = 1/2\ C_o\ \mathrm{erfc}\ \frac{x}{2\sqrt{Dt}} \tag{5.14}$$

where x is the diffusion coordinate, t is time, and D the binary diffusion coefficient.

Since the membrane creates a discontinuity in concentration through the length of the cell, the data must be fitted to the correlation function separately on each side of the membrane.

Recall from Section 3.3.1 that the refractive index is a linear function of concentration for the dilute sucrose solution used in this work. Eq. 5.14 implies that the refractive index could be fitted to an error function on each side of the membrane as

$$n = m\ \mathrm{erf}\ (Ax) + b \tag{5.15}$$

where m, A, and b are constants, derived from the best fit of the refractive index data to Eq. 5.15.

The parameters in Eq. 5.15 were found by using a linear least-squares curve fitting routine[108] to find the values m and b which gave the best fit for the experimental data. m and b were correlated for the linear function:

$$n = mx_{lin} + b \tag{5.16}$$

where $x_{lin} = \mathrm{erf}(Ax)$. A value of A was first assumed, then m and b

Radius of Curvature r (cm)	Axial Distance Z (cm)		Refractive index n
	0.0		
	1.0		
	2.0		n_{quartz} = 1.45709
	3.0	DC Diffusion Cell	
∞			
99.29	58.2 59.2	L1 Plano-convex Lens	
∞			
22.4	110. 111.	L2 Cylinder Lens	n_{lens} = 1.7499
	126.6	FP Focal Plane	n_{air} = 1.000276

Fig. 19 Ray Tracing Parameters

found by a least squares method. The RMS error for the linearized function, Eq. 5.16, was calculated and a parameter search performed on A to give the minimum RMS error.

The RMS error for this function was less than 1×10^{-3} percent for most runs. Figure 20 shows a sample experimental run with the solid lines being the error function correlation for the experimental points. The fit of the experimental points to Eq. 5.15 error function correlation shows excellent agreement. This correlation function is then used for the wavefront bending calculations described in Section 5.1.

5.2.2 Mass Fluxes

To calculate the binary diffusivity it is necessary to know both the concentration gradient and mass flux at the membrane surface. The refractive index function will give the refractive index at the membrane surfaces and in turn the concentration from the relation

$$c = n\alpha_c + \beta_c \tag{5.17}$$

where α_c and β_c are determined experimentally. In this work the values used are

$$\alpha_c = 0.204014$$

$$\beta_c = -.0271606$$

which give c in units of gm-moles/ml. These parameters were measured by Bollenbeck[40] for a sucrose-distilled water system at 25°C and for a wavelength of 6330 Å using a Pulfrich refractometer and monochromatic light source. He used a linear regression analysis for data yielding

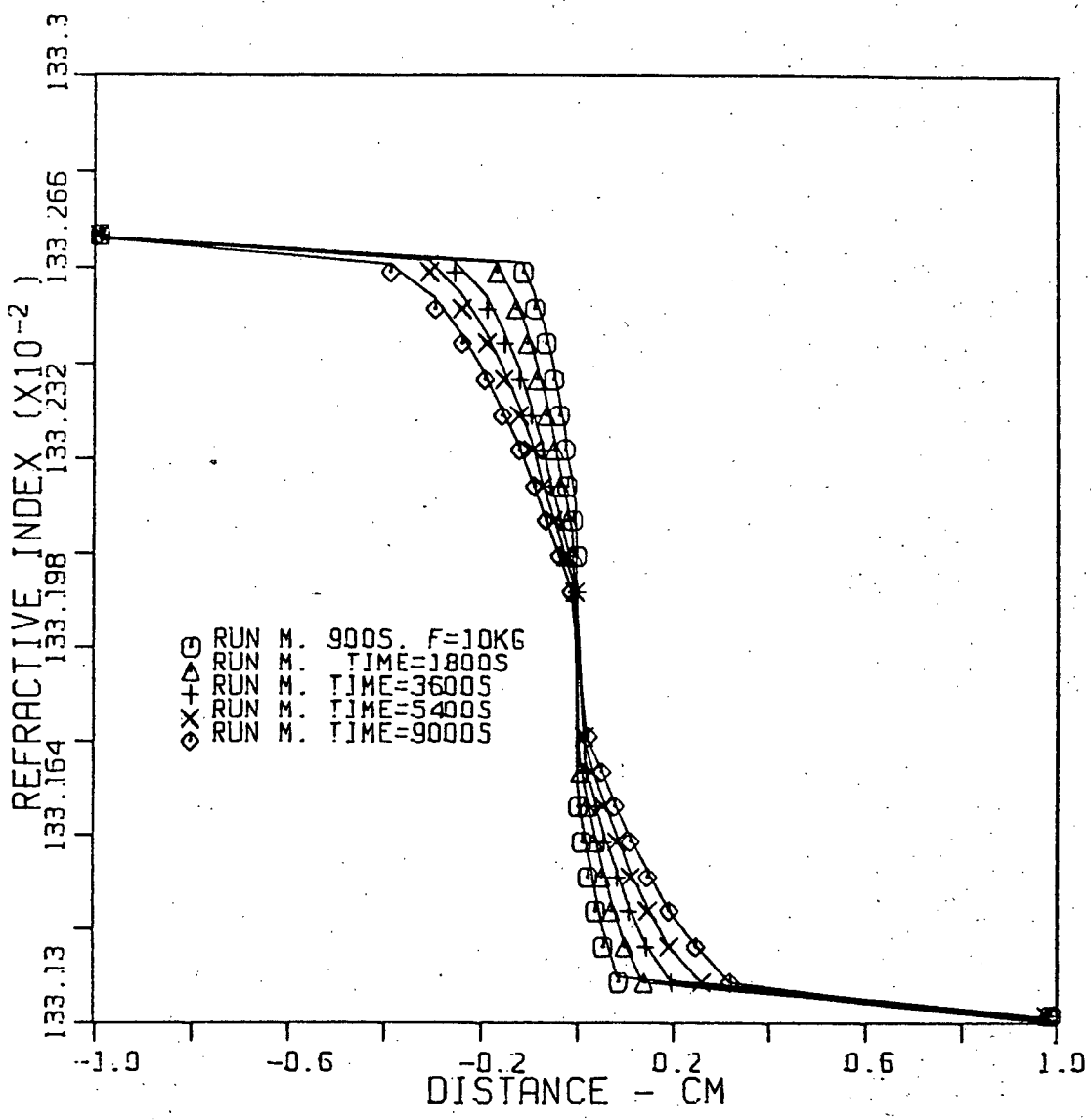

Figure 20 - Refractive Index Profiles for Typical Run.

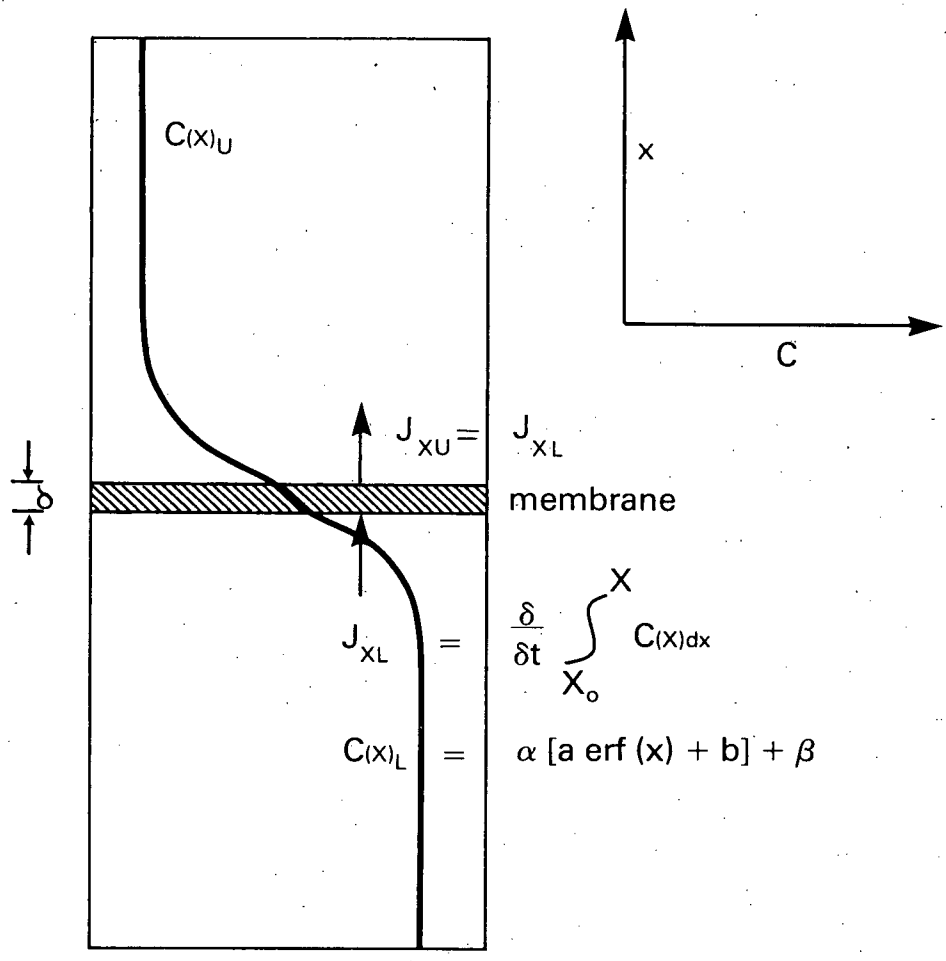

Fig. 21. Mass Flux and Concentration Profiles in Diffusion Cell

these values of α_c and β_c with a correlation coefficient of 0.9995. This equation is applicable from 0% to 5% by weight sucrose concentration.

Consider the mass flux of sucrose at the membrane surface in each half of the diffusion cell. Performing an unsteady state mass balance on this volume of cell between x_o and x in the vertical direction, along a uniform cross sectional area gives

$$J_{xo} = \frac{\partial}{\partial t} \int_{xo}^{x} C(x)dx \tag{5.18}$$

where J_{xo} is the mass flux at the membrane surface, x_o, and C(x) is the continuous concentration profile determined from Eqs. 5.15 and 5.17. The boundary conditions are taken at the surface of the membrane and the end of the diffusion cell. This assumes no sources or sinks between x_o and x. Finding the mass flux involves first integrating concentration profiles in the cell with respect to distance for several different times, then evaluating the concentration integrals with respect to time and differentiating. This analysis is only valid when the concentration at the ends of the cell is constant, i.e. no mass flux at either end of the cell. This condition is met during experiments when the experiment is terminated before the interference pattern changes at either end of the cell.

Combining Eqs. 5.17 and 5.18 gives for the mass flux

$$J_{xo} = \frac{-\partial}{\partial t} \alpha_c \int_{xo}^{x} n(x)dx + \beta_c(x_1 - x_0) \tag{5.19}$$

Using the error function correlation, Eq. 5.15, yields for the concentration integral

$$\int_{xo}^{x_1} C(x)dx = \alpha_c m\int_{xo}^{x_1} \mathrm{erf}(Ax)dx + \alpha_c b(x_1 - x_0) + \beta_c(x_1 - x_o) \qquad (5.20)$$

Integrating the error function in Eq. 5.20 gives[40]

$$\int_{xo}^{x} C(x)dx = \alpha_c \{\frac{m}{A} [Ax\mathrm{erf}(Ax) + \frac{1}{\sqrt{\pi}} e^{-(Ax)^2}]_{x_0}^{x_1} + b(x - x_0)\} + \beta_c(x - x_0) \qquad (5.21)$$

When a suitable number of concentration integrals at various times have been evaluated using Eq. 5.21 then the mass flux can be determined from Eq. 5.19. The time derivative in Eq. 5.19 may be evaluated by finite difference methods, graphical methods, or from a suitable correlation. A correlation method is preferred, since any irregularities in the data are smoothed. Based upon the error function solution to the diffusion equation, Bollenbeck[40] proposes a functional form of the concentration integral as a function of time

$$\int_{x}^{xo} C(x)dx = a_1 + a_2\mathrm{erf}\ (\frac{a_3}{t^{1/2}}) + a_4 t^{1/2} \exp \frac{-a_3^2}{t} \qquad (5.22)$$

The four constants in Eq. 5.22 can be determined from five different concentration profile integrals at different times. A UBC computer centre non-linear least-squares curve fitting routine[108] was used to

find the best fit for the constants in Eq. 5.22. This correlation function predicted the concentration profile integrals versus time with an RMS percent error better than 0.1 percent.

Eq. 5.22 can then be differentiated with respect to time to yield the mass flux in Eq. 5.19. The molar flux of sucrose at the membrane surface then becomes[40]

$$J_{xo} = \left[\frac{a_4}{2t^{1/2}} + \frac{a_4 a_3}{t^{3/2}} - \frac{1}{\sqrt{\pi}}\frac{a_2 a_3}{t^{3/2}}\right] \exp \frac{-a_3^2}{t} \tag{5.23}$$

The membrane diffusivity can now be calculated from Fick's first law since the molar flux and concentration gradient across the membrane are known. Equation 5.23 is only valid when the flux at the end of the cell is zero. This condition is met at the cell bottom as long as the concentration gradient is zero. Since the membrane is only 10 microns thick it can be assumed that a steady state condition exists through the membrane, i.e., the mass flux is equal on the top and bottom surfaces. The mass flux predicted by Eq. 5.23 is also the mass flux through the membrane, so Fick's first law can be applied to the membrane using this flux and knowing the sucrose concentration at each membrane surface

$$J_{xo} = D_M \frac{\Delta c}{\delta x} \tag{5.24}$$

where Δc is the concentration driving force or the concentration difference across the membrane, δx is the membrane thickness, and D_M is

the membrane diffusion coefficient. Δc can be evaluated from the interference fringe results.

Fick's law for binary diffusion can be written as

$$J_s = X_s(J_w + J_s) - cD_F \frac{\partial X_s}{\partial x} \tag{5.25}$$

where J_s is the molar flux of sucrose, J_w is the molar flux of water, D_F is the free diffusion coefficient, and X_s is the mole fraction of sucrose. For a binary system the concentration of sucrose c_s and concentration of water can be related,[40] assuming no chemical reactions between the water and sucrose

$$c_w = \gamma_1 c_s + \varepsilon_1 \tag{5.26}$$

the values of γ_1 and ε_1 are determined from the density as a function of composition by Bollenbeck[40] as

$$\gamma_1 = 11.68744 \tag{5.27}$$

$$\varepsilon_1 = 0.0553512 \tag{5.28}$$

If the concentration of water and sucrose are linearly related then the flux of sucrose can be related to the flux of water as

$$J_s = -\gamma_1 J_w \tag{5.29}$$

and Eq. 5.25 can be used to calculate D_F, at the free diffusion coefficient determined at the location x, in the cell.

CHAPTER 6

RESULTS

A total of twenty-three experiments were conducted for two different membrane pore sizes and conditions ranging from no magnetic field to an applied field strength of 12.5 kG. The only variables in these experiments were applied field strength and pore size. In all experiments the initial sucrose concentration difference across the membrane was 1% by weight of sucrose. The reference side of the diffusion cell was always filled with distilled water. The temperature of the enclosure was kept constant at 25°C ± .05 for all runs. Table III lists all experimental parameters and variables.

The raw data consisted of a set of fringe displacements taken at different times for each run. The fringe locations were measured with respect to a datum taken at 1.0 cm from the membrane at each end of the cell. The concentration of sucrose was constant at this location for all runs (0% in top half of cell and 1% by weight in lower half). Each distance measured by the microscope corresponded to a refractive index change equivalent to one fringe shift or one wavelength of laser light. These data were stored on permanent files for each run and were then used as input for the various data analysis computer programs.

The first program RAYTRACE took the raw data and converted it into refractive index profiles for each time interval using the equations derived in Chapter 5. These profiles were used to calculate the degree of raybending due to the refractive index gradient. A corrected refractive index profile was determined to account for the ray

bending. RAYTRACE then evaluated the constants A, b, and m for Eq. 5.15 to correlate the corrected refractive index gradient with the error function correlation. These parameters were stored on a permanent file for use by the mass flux and diffusivity calculation program. RAYTRACE is listed in Appendix C.

The program DIFFCALC used the correlation parameters A, b, and m to integrate the concentration profile in the cell. This integral was evaluated at each time interval and a partial derivative with respect to time was evaluated to determine the mass flux at the membrane surface for a given time. (see Section 5.2 for equations and derivations). The mass flux was evaluated for the lower half of the diffusion cell only and the flux through the membrane was assumed equal at both membrane surfaces. Ray deflection effects cause the rays entering the cell to be deflected downward towards the direction of increasing refractive index. This produces a thickening of the membrane shadow in the focal plane. Due to deflected light rays striking the upper surface of the membrane (see Figure 16) there is a loss of information near the upper surface of the membrane. Therefore, only mass fluxes in the lower half of the cell are used for diffusivity calculations. The concentration gradient producing the driving force for this mass flux is determined from the concentration difference at each membrane surface using the refractive index correlation evaluated by RAYTRACE. The diffusivity through the membrane is then calculated from Eq. 5.24 and free diffusion coefficient determined from Eq. 5.25. DIFFCALC is listed in Appendix D.

6.1 Raybending and Refractive Index Correlation

Figure 20 shows a typical refractive index profile for run M. The solid lines are the profiles corrected for raybending effects and correlated to the error function, Eq. 5.15. The points are the refractive index values calculated directly from the raw data, not accounting for wavefront deflection. As would be expected, the deflection is most noticeable near the membrane surface where the refractive index gradient is greatest. Near the end of the experiment, when diffusion has considerably reduced the magnitude of the refractive index gradient, wavefront deflection is much less, which is apparent from Figure 20 since the corrected profile and experimental profile are identical.

Table II lists the values of the corrected refractive index profile with the values of the uncorrected profile for each point in the run. Each x coordinate listed corresponds to one shift in the fringe pattern. Again it is apparent that the largest differences occur near the membrane, early in the experiment where refractive index gradients are largest.

The correlation parameters A, b and m for the refractive index profile correlation are listed in Appendix B for all runs.

6.2 Diffusivities

The diffusion coefficient through the membrane and free diffusion coefficient evaluated in the lower half of the diffusion cell for all runs are listed in Table III. These diffusion coefficients are calculated from the mass flux and concentration difference at the

Table II

Ray Bending Corrections of Data for Run L at 900 Seconds, Lower Half of Cell

n	$X_{observed}$	$X_{o,cell}$	Pass 1 ΔX	Pass 2 ΔX	Pass 3 ΔX	Pass 4 ΔX	Pass 5 ΔX	Pass 6 ΔX	$X_{o,cell}$
1.332146	-.0005	-.01485	.004567	-.000799	.000121	-1.8×10^{-5}	3×10^{-6}	$> 1 \times 10^{-6}$	.010019
1.33210	-.0030	-.008910	.004533	-.000707	.000106	-1.6×10^{-5}	2×10^{-6}	$> 1 \times 10^{-6}$	.002727
1.332273	-.0054	-.016038	.004448	-.000612	.000093	-1.4×10^{-5}	2×10^{-6}	$> 1 \times 10^{-6}$	-.004404
1.332336	-.0089	-.026433	.004241	-.000476	.000080	-1.1×10^{-5}	2×10^{-6}	$> 1 \times 10^{-6}$	-.015045
1.332400	-.0130	-.038610	.003892	-.000338	.000069	-9.0×10^{-6}	1×10^{-6}	$> 1 \times 10^{-6}$	-.027874
1.332463	-.0173	-.051381	.003435	-.000233	.000061	-7.0×10^{-6}	1×10^{-6}	$> 1 \times 10^{-6}$	-.041707
1.332526	-.0220	-.065340	.002878	-.000164	.000052	-5.0×10^{-6}	1×10^{-6}	$> 1 \times 10^{-6}$	-.057137
1.332589	-.0285	-.084644	.002108	-.000124	.000037	-4.0×10^{-6}	1×10^{-6}	$> 1 \times 10^{-6}$	-.078652
1.332653	-.0368	-.109295	.001274	-.000099	.000021	-3.0×10^{-6}	$>1 \times 10^{-6}$	$> 1 \times 10^{-6}$	-.105749
1.332716	-.333	-.989003	-.000001	$>- 1\times10^{-6}$	$>1\times10^{-6}$	$>-1.0 \times 10^{-6}$	$>1 \times 10^{-6}$	$> 1 \times 10^{-6}$	-.989006
		undeflected light rays							corrected for deflection

X observed = fringe location observed on film (cm)

X_0 cell = original entry position in cell for ray corresponding to X observed (cm)

ΔX = deviation between observed fringe and calculated fringe location (cm)

n = refractive index in cell at position X_0, cell

Table III

Membrane and Free Diffusion Coefficients

Pore diameter, d = 8.0 μm
Free area, A_F = 0.050 cm^2/cm^2

Run	Field Strength kG	D_M ($cm^2/s \times 10^6$)	D_F ($cm^2/s \times 10^6$)	$\frac{D_M}{D_F}$ ($\frac{cm^2}{cm^2}$) [a]
L	0.0	0.229	5.50	0.042
N	1.0	0.243	6.07	0.040
K	2.5	0.270	5.56	0.049
R	4.0	0.191	6.20	0.031
M	10.0	0.230	5.35	0.043
T	10.5	0.242	5.41	0.045
P	11.0	0.234	5.91	0.040
H	12.0	0.192	5.83	0.033

Pore diameter, = 0.8 μm
Free area, A_F = 0.151 cm^2/cm^2

A_2	0.0	0.889	5.22	0.170
E_2	2.5	0.436	5.17	0.084
C_2	5.0	0.897	5.04	0.178
D_2	10.0	0.414	4.98	0.083
B_2	12.5	1.246	5.25	0.237

[a]The ratio D_M/D_F is an indicator of experimental error, since it should be constant for a given membrane.

membrane surface. The concentration was extrapolated to x = 0 from the concentration correlation. The membrane coefficient given was time averaged for each run to smooth errors resulting from fringe pattern reading near the membrane surface. The free diffusion coefficient was taken at T = 3600s which was the third set of fringes out of a total of five different times to a time of 3 hours.

Faxen's equation predicting the ratio of the diffusion coefficient in a cylindrical pore to the bulk diffusion coefficient (Eq. 3.12) was used to calculate this ratio for the membrane-solution systems used in this work. For the 0.8 μm pore diameter the ratio D_P/D_F equals 0.9972 and for the 8.0 μm pore diameter it is 0.99972. Therefore, the membrane can be considered as a simple cross-sectional area reduction to diffusion, pore-solute interactions are negligible. The membrane diffusion coefficients measured in this work divided by the effective free area should yield the bulk diffusion coefficient. The effective free area can be calculated from the membrane manufacturer's specifications for pore size and surface porosity. For the 8.0 μm diameter pore size the free area for diffusion is 0.050 cm^2/cm^2. For the .8 μm diameter pore size the free area is 0.151 cm^2/cm^2. Table III lists the effective pore area calculated by dividing the experimental membrane diffusivity by the diffusional free area. Table IV lists the values of sucrose-water binary diffusion coefficients measured by other workers compared with the values determined in this work for the same temperature and concentration.

Figures 22 and 23 show the diffusion coefficients as a function of applied field strength for the 8.0 μm and 0.8 μm pore diameter

membranes. A linear regression analysis was performed on each data set. The straight line approximation is the best fit for the data predicted by the linear regression analysis. Table V lists the slope, y-intercept, and correlation coefficient for each data set. A correlation coefficient equal to zero indicates no correlation between the data and straight line and a value of 1.0 indicates all points are equal to the correlated values.

Table IV

Comparison of Aqueous Sucrose Solution Binary Diffusion Coefficients Measured by Interferometric Methods

D_F ($cm^2/s \times 10^6$)	Researchers	Comments	Estimated Accuracy (%)
5.215	Gosting et al.[51]	Gouy interf., free diff., vapor light source	0.2%
5.21[a]	Duda et al.[57]	Wedge interf., free diff.	3%
5.262	Bollenbeck[40]	Rayleigh interf., memb. diff.	3%
5.56	Gableman-Gray[64]	Holography, free diff.	2%
5.36[b]	This work	Rayleigh interf., memb. diff.	3%[c]

-All values measured at 25°C and 0.5% weight fraction sucrose.

[a]Value extrapolated to 0.5% weight fraction sucrose.

[b]Average value measured for no field conditions.

[c]Values measured agree with accepted values measured at similar conditions to within ± 3%.

Table V

Results of Linear Regression Analysis for Sucrose Diffusion Coefficients in Applied Magnetic Field.

Data Set	Slope	Y-intercept	Correlation Coefficient
8.0 μm pore, D_F	-0.0122	5.808×10^{-6}	0.191
8.0 μm pore, D_M	-0.0016	0.239×10^{-7}	0.296
0.8 μm pore, D_F	-0.0038	5.155×10^{-6}	0.169
0.8 μm pore, D_M	0.0186	0.665×10^{-6}	0.274
0.8 μm pore, D_F*	-0.025	5.212×10^{-6}	0.959
0.8 μm pore, D_M*	-0.0332	0.804×10^{-6}	0.525

*Data set evaluated with point at 12.5 kG removed (see text for justification).

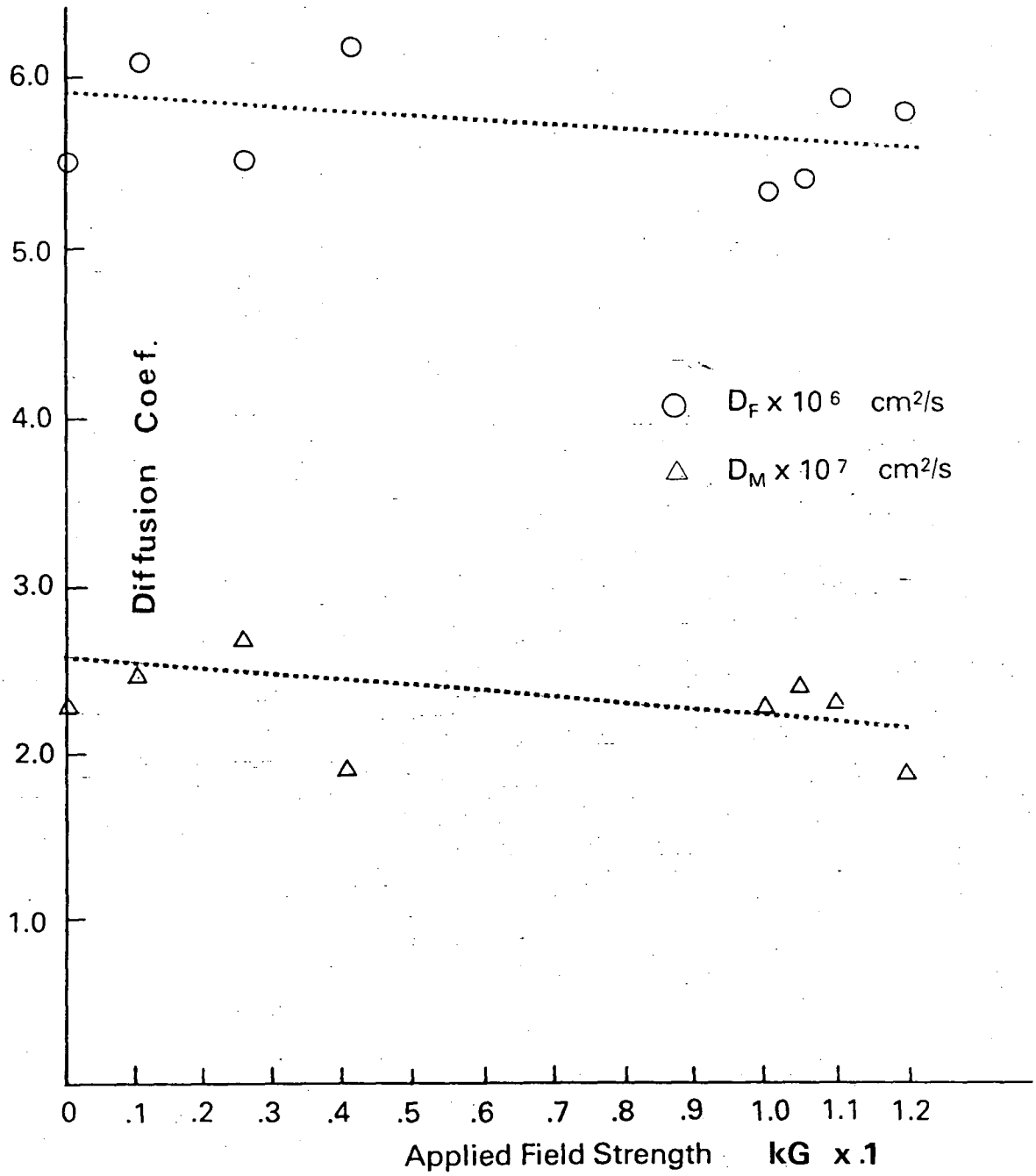

Fig. 22. Diffusion Coeffients vs Field Strength for 8.0 μm Pore Diameter

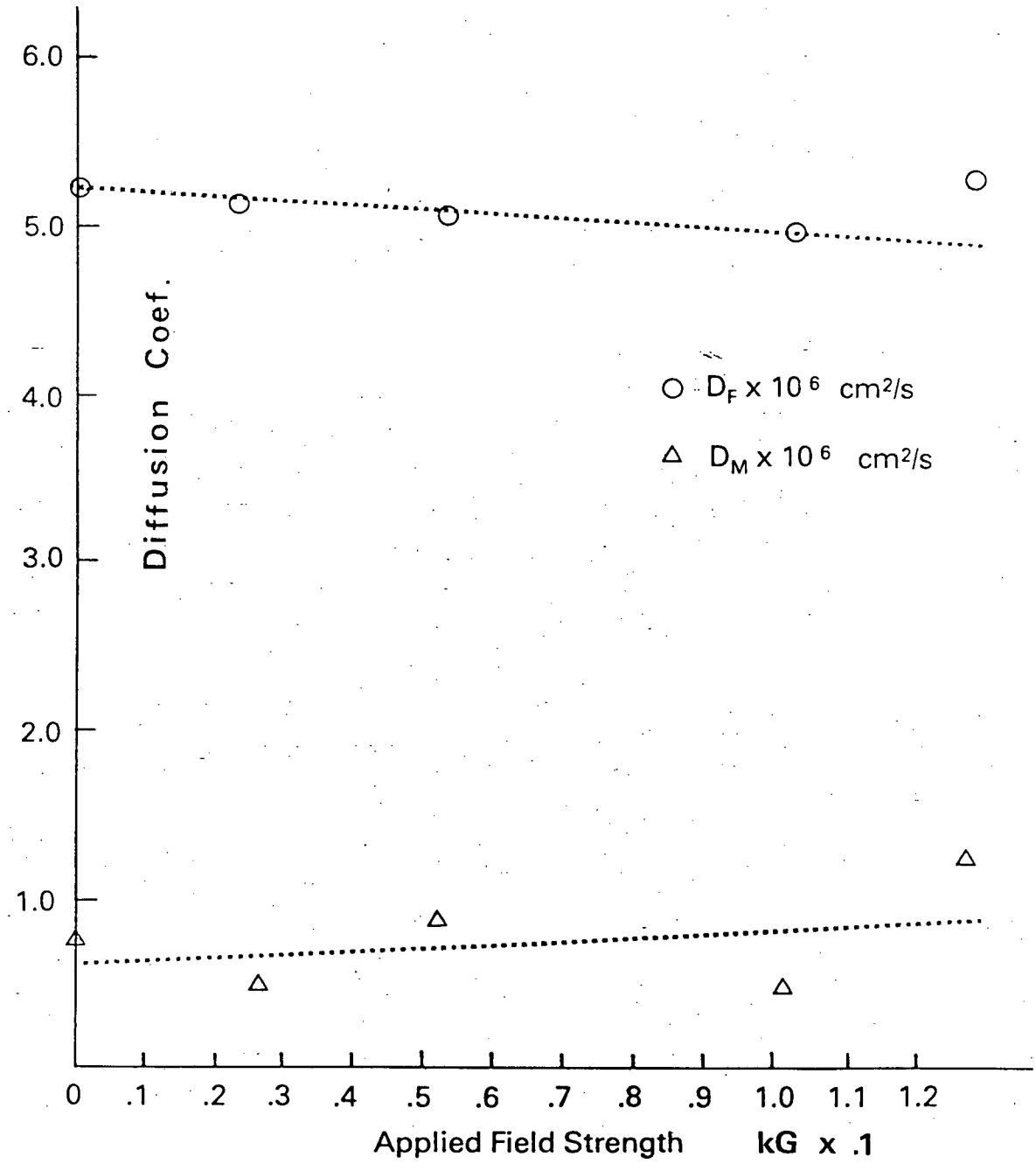

Fig. 23. Diffusion Coefficients vs Field Strength for 0.8μm Pore Diameter

CHAPTER 7

CONCLUSIONS AND RECOMMENDATIONS FOR FURTHER RESEARCH

7.1 Discussion

A Rayleigh interferometer was designed and constructed to measure molecular diffusion coefficients for an aqueous sucrose solution through a porous membrane in an applied magnetic field. The interferometer was constructed to satisfy the design constraints requiring to fit betweeen the 10 cm gap of an electromagnet without disturbing the homogeneity of the magnetic field. The interferometer produced an image of the refractive index profile in the diffusion test cell which was evaluated as a function of time to yield concentration profiles, mass fluxes and diffusivities for the diffusing molecules at a constant temperature and different applied magnetic field strengths.

A computer program was written to reduce the interference fringes to refractive index and concentration profiles, mass fluxes, and diffusion coefficients. Optical errors introduced by wavefront deflection through a refractive index gradient were considered and a computer program was written to correct the refractive index profiles for this effect.

This equipment was used to study the diffusion of an aqueous sucrose solution through a General Electric Nucleopore membrane in magnetic field strengths from 0 to 12.5 kG. A 1% by weight solution of sucrose was allowed to diffuse through membranes with pore diameters 0.8 μm and 8.0 μm at a temperature of 25 ± .05°C.

Any molecular magnetic anisotropies will cause a partial or

complete alignment of the molecule in a magnetic field. This would be observable as a change in the molecular diffusion coefficient through the porous membrane. The results of the linear regression analysis indicate a slight decrease (1 to 2%) for three sets of diffusion coefficients as the applied magnetic field increases to 12.5 kG. While the limited number of data points and relatively large amount of data scatter prevent a definite correlation from being made between the diffusivity and field strength, the results clearly indicate a trend. The correlation coefficient from 0.19 to 0.9 indicates that this trend is more than just random experimental error. The fact that a new membrane was used for each run may account for some of the data scatter. Therefore, some degree of alignment of the sucrose-water clusters appears to be taking place in the magnetic field. The membrane diffusivities measured for the 0.8 μm pore size do not show a decrease in the magnetic field as the other three sets of data do. If the value measured at 12.5 kG is weighted less than the other four points, the linear regression analysis would show a slight decrease in the diffusion coefficients in an applied magnetic field. The values of free diffusion area, A_F, tabulated in Table III would justify a lower level of confidence in this point. The calculated value of A_F, the ratio of membrane to free diffusivities, should be a constant for each membrane. The value calculated for this point is much higher than the ones corresponding to the other experimental points which would indicate some unknown experimental error in the diffusivity measured for 12.5 kG field strength. The correlation coefficients evaluated for D_F and D_M with this point removed indicate a better fit than with the point included (see Table V).

An aqueous sucrose solution was selected for this initial work because accurate, widely accepted diffusion data over a concentration range are available for comparison. The bulk binary diffusion coefficient measured in these experiments for no field conditions at 25°C agree with the values measured at the same temperature and concentration by Gosting and Morris[51] within 3%.

7.2 Recommendations

Based upon the results obtained in these experiments, two further areas of research and development can be recommended; 1) improving the accuracy and sensitivity of the interferometer and, 2) examining diffusion of molecules exhibiting a higher degree of anisotropy than sucrose.

Temperature variations were not felt to be a major source of experimental error. The maximum temperature change of the air surrounding the diffusion cell was 0.1°C during a run. The Stokes-Einstein equation (Eq. 3.8) predicts the diffusion coefficient to be a linear function of absolute temperature, the Boltzman constant being the constant of proportionality. For a maximum temperature change of 0.1°C at 25°C, the diffusion coefficient would change by .03%, clearly less than the data scatter in this work.

From the experience gained in this work, it is felt that a major source of error lies in accurately measuring the fringe patterns near the membrane surface. The refractive index gradient is greatest immediately adjacent to the membrane surface, so therefore the wavefront deflection is also greatest at that location. Wavefront deflection is

observable as a thickening of the membrane shadow and a downward displacement of that shadow on the film focal plane. The membrane surface shadow provides a fiduciary point to reference the interference fringe locations in each half of the cell. The edges of the membrane shadow tend to be blurred in the image of the interference pattern on the film when viewed through the measuring microscope. It is felt that the membrane shadow is not the best fiduciary point for referencing interference fringe locations. Therefore, it is recommended that the diffusion cell be modified to produce a more definite fiduciary mark on the interference pattern. This could be accomplished by constructing a wire scale which could be placed inside the diffusion compartment. The wire grid would produce a shadow in the focal plane providing reference locations on the fringe pattern thereby eliminating the need to clearly define the membrane shadow boundaries. This may introduce some problems in the analysis if the one-dimensional nature of the diffusion is interrupted by the wire grid.

In addition to improving the accuracy of the equipment and experimental procedure efforts could be made to reduce the time required to measure fringes and input fringe data to the computer. Measuring fringes through the microscope and recording several hundred data points is a very tedious and time consuming process. The total elapsed time required to set up an experiment and obtain diffusivities is approximately one week. Any magnetic field effect on diffusion is small, so it is essential that a large number of experiments be performed to give statistical significance to any observed change in

diffusion rate. Therefore, a more efficient data evaluation system is desirable to minimize the time required to conduct an experiment. Renner and Lyons[63] report on a computer recorded automated interferometric system. They utilize a photomultiplier tube correlated with a motor driven measuring microscope to automatically measure the interference fringes and provide input to a numerical method computer program. Adams[109] et. al and Watkins[110] et. al discuss similar methods using electronic light sensing elements to provide an automated data acquisition system. An electronic data acquisition system would considerably reduce the time required to measure and evaluate data enabling one to conduct a greater number of experiments for a given amount of time.

The next logical extension of this work is to study diffusion of strongly anisotropic molecules in a magnetic field. Partial or complete alignment in a magnetic field has been observed for several macromolecules and molecular clusters by measuring the magnetically induced birefringence (Cotton-Mouton effect; discussed in Chapter 3). Any molecular system exhibiting a Cotton-Mouton effect should also show a change in diffusion rate in a porous membrane. A Cotton-Mouton effect has been observed for polypeptides (Poly (Try-Glu)), nucleic acid fragments,[84] rodlike viruses,[84] DNA,[84] liquid crystals,[78-82] chloroplasts,[84] retinal rods,[84] and micellar aqueous soap solutions.[83]

Interferometric measurement of macromolecular diffusion presents several problems which must be addressed. The size of these molecules range from a few Angstroms to several thousand Angstroms. In this size

range optical dispersion of the helium-neon laser light (wavelength equals 6382 Å) may be significant enough to destroy the spatial coherence of the transmitted laser beam. In addition, these systems are strongly absorbing in the visible light spectrum being used. This absorption may introduce heating and convection effects into the diffusing system. Hall[111] et. al discuss these effects in optical absorption by hemoglobin using laser light. Macromolecular diffusion coefficients tend to be highly concentration dependent, so the simplifying assumptions of constant diffusivity would not be applicable.

The method developed in this work has been applied to binary diffusion. However, most proteins and organic macromolecules require a buffer solution to prevent denaturation, so diffusion is no longer binary, but multicomponent. This introduces another independent variable into the analysis since the diffusion rate of the buffer and its coupling to the macromolecule must be evaluated.

7.3 Conclusions

A physical model is developed describing the effect of an applied magnetic field on the diffusion rate of anisotropic molecules through a porous membrane. The model predicts a decrease in the diffusion rate of a molecular system diffusing through a porous membrane in a magnetic field applied transverse to the pore direction. Rayleigh interferometry has been applied to measure the local diffusion coefficient in a specially designed diffusion cell for an aqueous sucrose system diffusing through a GE Nucleopore membrane in an applied magnetic field. A slight decrease (1 to 2%) in the measured diffusion

coefficient was observed in applied field strengths up to 12.5 kG as was predicted by the model developed in this work. Therefore, optical interferometry has been demonstrated to be a useful technique to elucidate certain aspects of molecular-magnetic interactions and their effects on molecular transport properties. Free diffusion coefficients for a dilute aqueous sucrose solution compare with accepted value to within ± 3%. However, the difficulty in clearly defining the membrane surface boundary in the image of the diffusion cell limits the experimental accuracy to a magnitude comparable to expected change in sucrose diffusion rate in a magnetic field. It is therefore, recommended that modifications be made to the diffusion cell to eliminate the need to use the membrane shadow as a fiduciary point for the data analysis and improve the accuracy of the interferometer. To further verify the proposed model developed in this work it is also recommended that further work be done, using molecules with a higher degree of anisotroy than sucrose, which would be expected to exhibit a larger magnetic field effect on their diffusion rate.

NOMENCLATURE

$a_{1...4}$	Constants in Eq. 5.22
a	Constant in Eq 3.24
A_F	Cross-sectional area for free diffusion
A	Constant in Eq. 5.15
A_E	Amplitude of light wave
$\vec{B}$	Magnetic induction vector
b_n	Constant in Eq. 3.24
b	Constant in Eq. 5.15
c	Velocity of light in a vacuum
C	Concentration
C_M	Cotton-Mouton constant
D	Diffusion coefficient
d	Diameter
E	Harmonic motion of light wave
F	Geometrical factor in Eq. 3.18a
f^M	Maxwellian distribution function in Eq. 2.1
f	Stoke's frictional coefficient
H	Magnetic field strength
J	Molar flux
K	Boltzman's constant
L	Optical path length defined in Eq. 3.27
M	Molecular weight
$\vec{M}$	Intensity of induced magnetization vector

mv^2	Momentum
m	Constant in Eq. 5.15
n	Refractive index
q	Heat flow
r	Radius
R	Gas constant
RM	Molar refractivity
s	Geometrical path length of a light ray
t	Time
T	Temperature
$\vec{V}$	Velocity vector
$\bar{v}$	Mean square transit velocity for molecular motion
V	Velocity of light through a given medium
x	Distance
Y_s	Masking slit spacing
z	Distance
Z	Complex amplitude of a light wave
Z_k	Electric charge on diffusing ion

Greek Symbols

α	Molecular optical polarisabilities
α_c	Constant in Eq. 5.17
β	Ratio of solute to pore radii in Eqs. 3.11, 3.12, and 3.18a
β_c	Constant in Eq. 5.17
$\bar{\delta}_x$	Mean square Brownian displacement

δ_o	Degree of orientation for a molecule aligned in magnetic field
δx	Membrane thickness
Δ	Difference
ε_1	Constant in Eq. 5.26
γ	Ratio of solvent to pore radii in Eq. 3.11
γ_1	Constant in Eq. 5.26
λ	Wavelength of light
η	Viscosity
μ	Chemical potential
π	Osmotic pressure
ρ	Density
σ	Staverman's reflection coefficient
ϕ	Phase angle of light wave at time = 0
χ	Magnetic susceptibility tensor
ω	Angular speed of light wave

Subscripts

a	Air
b	Bulk
DC	Diffusion cell
f	Magnetic field
F	Free diffusion
FP	Focal plane of interferometer
lin	Linearized
M	Membrane
P	Pore

s	Solute
w	Water
$\parallel$	Denotes value parallel to applied magnetic field
$\perp$	Denotes value perpendicular to applied magnetic field
x	Value along principal x-axis
y	Value along principal y-axis
z	Value along principal z-axis

Superscripts

H	With applied magnetic field
o	Without applied magnetic field

REFERENCES

1. Busby, D.E., "Biomagnetics - Considerations Relevent to Manned Space Flight", NASA CR-889 (Sept. 1967).

2. Barnothy, J.M., and Barnothy, M.F., and Boszormenyi-Nagey, J., "Influence of a Magnetic Field Upon the Leucocyte of a Mouse", Nature, 177, 577 (1956).

3. Barnothy, M.F., and Barnothy, J.M., "Biological Effect of a Magnetic Field and the Radiation Syndrome", Nature, 181, 1785 (1958).

4. Lechner, F., "Influencing of Bone Formation Through Electromagnetic Potentials", Langenbecks Arch. Chir. 631 (1974).

5. Ketchen, E.E., Porter, W.E., Bolton, N.E., "Biological Effects of Magnetic Fields on Man", Am. Indst. Hygiene Assoc. J., 39, 1 (1978).

6. Lechner, F., Kraus, W., "Influencing of Disturbed Fracture Healing Through Electromagnetic Fields", Hefte Zur Unfallheilkunde, 114, 325 (1973).

7. Freedman, A.P. "Medical Significance of the Magnetic Activities of the Human Body", Biomagnetism, Walter de Gruyter and Co., Berlin (1981).

8. Personal communication with C. Smith, U.B.C. Sports Medicine, May (1982).

9. Barnothy, M.F., Biological Effects of Magnetic Fields, Plenum Press, N.Y., Vol. 1 (1964), VII (1969).

10. Bhatnagar, S.S., Mathur, K.N., Physical Principles and Applications of Magnetochemistry, Macmillan and Co., London (1935).

11. Gross, L., Biological Effects of Magnetic Fields, Ph.D. Thesis, New York University (1963).

12. Liboff, R.L., "A Biomagnetic Hypothesis", Biophysical J., 5, 845 (1965).

13. Lielmezs, J., Aleman, H., "Weak Transverse Magnetic Field Effect on the Viscosity of $Mn(NO_3)_2$ - H_2O Solution at Several Temperatures", Thermochim. Acta, 20, 219 (1977).

14. Lielmezs, J., Aleman, H., "Weak Transverse Magnetic Field Effect on the Viscosity of $Ni(NO_3)_2$ - H_2O Solution", Thermochim. Acta, 21, 233 (1977).

15. Lielmezs, J., Aleman, H. "External Transverse Magnetic Field Effect on Electrolyte Diffusion in HCl-H_2O Solution", Electrochim. Acta, 21, 273 (1976).

16. Lielmezs, J., Aleman, H., "Weak Transverse Magnetic Field Effect on the Viscosity of KCl-H_2O Solution", Thermochim. Acta, 18, 315 (1977).

17. Lielmezs, J., Aleman, H., Musbally, G.M., "External Transverse Magnetic Field Effect on Electrolyte Diffusion in KCl-H_2O Solution", Z. Phys. Chem. Neue Folge, 90, 8 (1974).

18. Lielmezs, J., Aleman, H., "External Transverse Magnetic Field Effect on Electrolyte Diffusion in NaCl-H_2O Solution", Thermochim. Acta, 9, 247 (1974).

19. Lielmezs, J., Aleman, H., "External Transverse Magnetic Field Effect on Electrolyte Diffusion in LiCl-H_2O Solutions", Bioelectrochem. and Bioenerg., 5, 285 (1978).

20. Lielmezs, J., Aleman, H., "External Transverse Magnetic Field Effect on Electrolyte Diffusion in CuCl-H_2O Solution", Thermochim. Acta, 15, 63 (1976).

21. Lielmezs, J. Aleman, H., "External Magnetic Field Effect on Viscometer Efflux Times of Calf Thymus DNA in 0.0172 M KCl Solution During the Thermal Denaturation Process", Thermochim. Acta, 43, 9 (1981).

22. Thysse, B.J., Van Ditghuyzen, P.G., Hermans, L.J.F., Knaap, H.F.P., "The Influence of a Magnetic Field on the Transport Properties of Symmetric Top Molecules", Proc. 7th Symp. Thermophys. Prop. 638 (1978).

23. Beenakker, J.J.M., Hermans, L.J.F., Hulsman, H., Knaap, H.F.P., Korving, J. "The Influence of an External Field as a Tool in the Study of Transport Properties of Rotating Molecules", Proc. 5th Symp. Thermophys. Prop. 168 (1970).

24. McCourt, F.R., Knaap, H.F.P., Moraal, H., "The Senfteben-Beenakker Effects for a Gas of Rough Sperical Molecules", Physica, 43, 485 (1969).

25. Tip, A., "On the Senfteben-Beenakker Effect in Mixture", Physica, 37, 411 (1967).

26. Beenakker, J.J.M., Hulsman, H., Knaap, H.F.P., Korving, J., and Scoles, G., "The Influence of a Magnetic Field on the Viscosity and Other Transport Properties of Gaseous Diatomic Molecules", Adv. in Therophys. Prop. at Extreme Temp. and Press., ASME, 216 (1965).

27. Mehaffey, J.R., Garisto, F., Kapral, R., Desai, R.C., "Magnetic Field Dependence of Thermal Correlations in Molecular Gases", J. Chem. Phys., 58, No. 10, 4084 (1973).

28. Moraal, H., McCourt, F.R., "The Senftleben Effects for a Gas of $^2\Sigma$ Molecules", Physica, 46, 367 (1970).

29. Hermans, L.J.F., Schutte, A., Knaap, H.F.P., Beenakker, J.J.M., "Transverse Heat Transport in Polyatomic Gases Under the Influence of a Magnetic Field", Physica, 46, 491 (1970).

30. Beenakker, J.J.M., "The Influences of Electric and Magnetic Fields on the Transport Properties of Polyatomic Dilute Gases", Festkörperproblems, 8, 276 (1968).

31. Udayan De, Bhanja, S., Barua, A.K., "The Effect of Magnetic Field on the Heat Conductivity of O_2-N_2 and O_2-H_2 Gas Mixtures", J. Chem. Phys., 68, n7, 3226 (1978).

32. Hulsman, H., Van Kuik, F.G., Walstra, K.W., Knaap, H.F.P., Beenakker, J.J.M., "The Viscosity of Polyatomic Gases in a Magnetic Field", Physica, 57, 501 (1972).

33. Korving, J., "Viscosity of NH_3 in High Magnetic Fields", Physica, 46, 619 (1970).

34. Eggermont, G.E.J., Oudeman, P., Hermans, L.J.F., "Experiments on the Influence of a Magnetic Field on the Thermal Diffusion in Polyatomic Gases", Physics Ltrs., 50A, N3, 173 (1974).

35. Vugts, H.F., Tip, A., Los, J., "The Senftleben Effect on Diffusion", Physica, 38, 579 (1968).

36. Burgmans, A.L.J., van Ditzhuyzen, P.G., Knaap, H.F.P., "The Viscomagnetic Effect in Mixtures", Z. Naturflorsch., 28a, 849 (1973).

37. Burgmans, A.L.J., van Ditzhuyzen, P.G., Knaap, H.F.P., Beenakker, J.J.M., "The Temperature Dependence of the Viscomagnetic Effect", Z. Naturforsch., 28a, 835 (1973).

38. Vevai, J.E., Elliot, D.G., Honeywell, W.I., "Senfleben-Beenakker Thermal Conductivity Effect Apparatus", Rev. Sci. Inst. 49, N8, 1116 (1978).

39. Beenakker, J.J.M., McCourt, F.R., "Magnetic and Electric Effects on Transport Properties", Am. Rev. Phys. Chem., 21, 47 (1970).

40. Bollenbeck, P., A Modified Rayleigh Interferometer for Membrane Transport Studies", Ph.D. Dissertation, University of Colorado (1972).

41. Senfteben, H., "Magnetische Beeinflussing des Warmeleitvertische Paramagnetischer Gase", Physik Z., 31, 961 (1930).

42. Iberall, A., Schindler, A. Physics of Membrane Transport, General Technical Services, Inc., Upper Darby, Pa. (1973).

42a. Brenner, H., "Rheology of a Dilute Suspension Dipolar Spherical Particles in an External Field", J. Colloid and Interface Sci., 32, N1,141 (1970).

43. Lielmezs, J., Musbally, G.M., "Effect of External Magnetic Field on Diffusion of Electrolytes in Solution", Electrochim. Acta, 17, 1609 (1972).

44. Camp, F.W., Johnson, E.F., "Magnetic Effects in Certain Systems of Chemical Engineering Interest", I & EC Fundamentals, 4, N2, 145 (1965).

45. O'Brien, R.N., Santhanam, K.S.V., "Magnetic Field Effects on the Diffusion Layer at Vertical Electrodes During Electrodeposition", J. Electrochem. Soc., 129, N6, 1266 (1982).

46. Lielmezs, J., Aleman, H., Fish, L.W., "Weak Transverse Magnetic Field Effect on the Viscosity of Water", Z. fur Physik., Chem. Neue Folge, 99, 117 (1976).

47. Lielmezs, J., Aleman, H., "Weak Transverse Magnetic Field Effect on the Viscosity of Water at Several Temperatures", Thermochim. Acta, 21, 225 (1977).

48. Philpot, J. St. L., Cooke, C.H., "A Self-Plotting Interferometric Technique for the Ultracentrifuge", Research, 1, 234 (1947).

49. Longsworth, L.G., "Experimental Tests of an Interference Method for the Study of Diffusion", J. Am. Chem. Soc., 69, 2510 (1947).

50. Ogston, A.G., "The Gouy Diffusiometer, Further Calibration", Proc. Roy. Soc. (London), A196, 272 (1949).

51. Gosting, L.J., Moris, M.S., "Diffusion Studies on Dilute Aqueous Sucrose Solutions at 1 and 25° with the Guoy Interference Method", Am. Chem. Soc. J., 71, 1521 (1949).

52. Gosting, L.E., Akeley, D.F., "A Study of the Diffusion of Urea in Water at 25° with the Gouy Interference Method", Am. Chem. Soc. J., 74, 1113 (1952).

53. Svensson, H., "On the Use of Rayleigh-Philpot-Cook Intereference Fringes for the Measurement of Diffusion Coefficients", Acta Chemica Scand., 5, 72 (1951).

54. Longsworth, L.G., "Tests of Flowing Junction Diffusion Cells with Interference Methods", Rev. Sci. Inst., 21, N6, 524 (1950).

55. O'Brien, R.N., "Interferometer for Electrochemical Investigations", Rev. Sci. Inst., 35, N7, 803 (1964).

56. O'Brien, R.N., Yakymyshyn, W.F., Leja, J., "Interferometric Study of Zb/$ZnSO_4$/Zn System", J. Electrochem. Soc., 110, 820 (1963).

57. Duda, J.L., Sigelko, W.L., Ventras, J.S., "Binary Diffusion Studies with a Wedge Interferometer", J. Phys. Chem., 73, N1, 141 (1969).

58. O'Brien, R.N., Hyslop, W.F., "A Laser Interferometric Study of the Diffusion of O_2, N_2, H_2 and Ar into Water", Can. J. Chem., 55, 1415 (1977).

59. Rard, J.A., Miller, D.G., "The Mutual Diffusion Coefficients of NaCl-H_2O and CaCl-H_2O at 25°C from Rayleigh Interferometry", J. Solution Chem., 8, N10, 701 (1979).

60. Rard, J.A., Miller, D.G., "Mutual Diffusion Coefficients of $SrCl_2$-H_2O and CsCl-H_2O at 25°C from Rayleigh Interferometry", J. Chem. Soc., Faraday Trans., 1, 78, 887 (1982).

61. Rard, J.A., Miller, D.G., "Mutual Diffusion Coefficients of $BaCl_2$ - H_2O and KCl-H_2O at 25°C from Rayleigh Interferometry", J. Chem. Eng. Data, 25, 211 (1980).

62. Sorell, L.S., Myerson, A.S., "Diffusivity of Urea in Saturated and Supersaturated Solutions", AIChE J., 28, N5, 772 (1982).

63. Renner, T.A., Lyons, P.A, "Computer-Recorded Gouy Interferometric Diffusion and the Onsager-Gosting Theory", J. Phys. Chem., 78, 2050 (1974).

64. Gableman-Gray, L., Fenichel, H., "Holographic Interferometric Study of Liquid Diffusion", Applied Optics, 18, N3, 343 (1979).

65. O'Brien, R.N., Langlais, A.J., Seufert, W.D., "Diffusion Coefficients of Respiratory Gases in a Perfluorocarbon Liquid", Science, 217, 153 (1982).

66. Bollenbeck, P.H., Ramirez, W.F., "Use of a Rayleigh Interferometer for Membrane Transport Studies", I&EC Fund., 13, N4, 385 (1974).

67. Min, S., Duda, J.L., Nother, R.H., Vrentas, J.S., "An Interferometric Technique for the Study of Steady State Membrane Transport", AIChE J., 22, N1, 175 (1976).

68. Forgacs, C., Liebovitz, J., O'Brien, R.N., Spiegler, K.S., "Interferometric Study of Concentration Profiles in Solutions Near Membrane Interfaces", Electrochim, Acta, 20, 555 (1975).

69. Einstein, A., Investigations on the Theory of Brownian Movement, Dover, New York (1956).

70. Stokes, G.G., Trans. Cambridge Phil. Soc., 9, Part II, 8 (1851).

71. Staverman, A.J., "Non-Equilibrium Thermodynamics of Membrane Processes", Rev. Trav. Chim., 70, 344 (1951).

72. Renkin, E.M., "Filtration, Diffusion and Molecular Sieving Through Porous Cellulose Membranes", J. Gen. Physiol., 38, 225 (1954).

73. Dawson, H., Textbook of General Physiology, 4th Ed., J & A Churchill, London (1970), p. 414.

74. Faxen, H., "Movement of a Rigid Sphere Along the Axis of a Pipe Filled with a Viscous Fluid", Ark, Mat., Astron. och Fysik, 17, 27 (1922).

75. Williamsen, B.G., Geankopolis, C.J., "Diffusion of Sucrose in Protein Solutions with Pore Restriction Effects Present", J. Chem. Eng. Data, 26, 368 (1981).

76. Bueche, F., Introduction to Physics for Scientists and Engineers, 3rd Ed., McGraw-Hill, New York (1980).

77. Schmalz, T.G., Norris, C.L., Flygare, W.H., "Localized Magnetic Susceptibility Anisotropics", J. Am. Chem. Soc., 95, N24 (1973).

78. Fujuwara, F.Y., Reeves, L.W., "Liquid Crystal/Glass Interface Effects on the Orientation of Lyotropic Liquid Crystals in Magnetic Fields", Can. J. Chem., 56, 2178 (1978).

79. Ratna, B.R., "Magnetic an Electric Birefringence in the Isotropic Phase of a Nematic of Large Positive Dielectric Anisotropy", Mol. Cryst. Liq. Cryst., 58, 205 (1980).

80. Buckingham, A.D., "Experiments with Oriented Molecules", Chem. in Britian, 54, (Feb, 1965).

81. Lizuka, E., Kondo, Y., "Magnetic-Field Orientation of the Liquid Crystals of Polyribonucleotide Complexes", Mol. Cryst. Liq. Cryst., 57, 285 (1979).

82. Muta, K., Takezoe, H., Fukados, A., Kuze, E., "Mixing Effects on the Cotton-Mouton Constant of 30CB and 50CB in Isotropic Phase", Jap. J. Appl. Phys., 20, N3 (1981).

83. Porte, G., Poggi, Y., "Behavior of Micellar Aqueous Solutions in High Magnetic Field", Phys. Rev. Ltrs., 41, N21 (1978).

84. Maret, G., Dransfeld, K., "Macromolecules and Membranes in High Magnetic Fields", Physica, 86-88B, 1077 (1977).

85. Fessenden, R.J., Fessenden, J.S., Organic Chemistry, 2nd Ed., Prindle, Weber & Schmidt Publishers, Boston (1982).

86. Harvey, J.M., Symons, M.G.R., "The Hydration of Monosaccharides - an NMR Study", J. Solution Chem., 7, N8, 57 (1978).

87. James, D.W., Frost, R.L., "Structure of Aqueous Solutions, Structure Making and Structure Breaking of Sucrose and Urea", J. Phys. Chem., 78, N17, 1754 (1974).

88. Mathlouthi, M., "X-Ray Diffraction Study of the Molecular Association in Aqueous Solutions of D-Fructose, D-Glucose, and Sucrose", Carbohydrate Res., 91, 113 (1981).

89. Jeffry, G.A., "Intramolecular Hydrogen-Bonding in Carbohydrate Crystalate Structures", Carbohydrate Res., 28, 233 (1973).

90. Hanson, J.C., Sieker, L.C., Jensen, L.H., "Sucrose: X-Ray Refinement and Comparison with Neutron Refinement", Acta Cryst., B29, 797 (1973).

91. Brown, G.M., Levy, H.A., "Further Refinement of the Structure of Sucrose Based on Neutron-Diffraction Data", Acta Cryst, B29, 790 (1973).

92. Mulay, L.N., Boudreaux, E.A., Theory and Applications of Molecular Diamagnetism, John Wiley & Sons, New York (1976).

93. Shporer, M., Vega, A.J., Frommer, M.A., "Diamagnetic Susceptibility Effects in NMR Measurements of the Properties of Water in Polymeric Membranes", J. Polymer Sci., 12, 645 (1974).

94. Packer, K.J., "Nuclear Spin Relaxation Studies of Molecules Adsorbed on Surfaces", Progr. Nucl. Magnetic Resonance Spectroscopy, 3, 87 (1968).

95. Resing, H.A., "Nuclear Magnetic Resonance Relaxation of Molecules Adsorbed on Surfaces", Adv. Mol. Relaxtion Processes, 1, 109 (1967-1968).

96. Beysens, D., Calmettes, P., "Temperature Dependence of the Refractive Indices of Liquids: Deviation from the Lorentz-Lorenz Formula", J. Chem. Phys., N2 (1977).

97. Reisler, E., Eisenberg, H., Minton, A.P., "Temperature and Density Dependence of the Refractive Index of Pure Liquids", J. Chem. Soc., Faraday Trans., II, 68, 1001 (1972).

98. Lin, C.T., Marques, A.D.S., Pessine, F.B.T., Guimaraes, W.V.N., "The Shape of the Refractive Index Versus Composition Curves for Hydrogen-Bonded Liquid Mixtures", J. Molecular Structure, 73, 159 (1981).

99. Klein, M.V., Optics, John Wiley & Sons, New York, 1970.

100. Driscoll, W.G., and Vaughn, W., Handbook of Optics-Optical Society of America, McGraw-Hill Co., New York (1978).

101. Model 124B Nelium-Neon Laser, Spectra Physics Mountain View Calif., G/124B (1979).

102. Models 332, 336, and 338 Telescopes and Spatial Filters - Spectra-Physics, Mountain View, Calif., B/332-338 (1977).

103. Rickles, R.N., Membranes; Technology and Economics, Noyes Development Corp. (1967).

104. V-7560 Fieldial Regulator Mark I, Varian Associates Publication, 87-170-406 Rev., A1171 (1971).

105. Beach, K.W., Muller, R.H., Tobias, C.W., "Light Deflection Effects in the Interferometry of One-Dimensional Refractive-Index Fields", J. of Optical Soc., of Am., 63, N5, 559 (1973).

106. Clifton, M., Sanchez, V., "Optical Errors Encountered in Using Holographic Interferometry to Observe Liquid Boundary Layers in Electrochemical Cells", Electrochim. Acta, 24, 445 (1979).

107. Carrier, G., Pearson, C.E., Partial Differential Equations, Academic Press, New York (1976).

108. UBC Curve, Curve Fitting Routines, University of British Columbia Computing Centre, 1981.

109. Adams, W.A., Davis, A.R., Seabrook, G., Ferguson, W.R., "A Digitized Laser Interferometer for High Pressure Refractive Index Studies of Liquids", Can. J. of Spectroscopy, 21, N2, 40 (1976).

110. Watkins, L.S., Tvarusko, A., "Lloyd Mirror Laser Interferometer for Diffusion Layer Studies", Rev. Sci. Inst., 41, N12, 1860 (1970).

111. Hall, R.S., Young, S.O., Johnson, C.S., "Photon Correlation Spectroscopy in Strongly Absorbing and Concentrated Samples with Applications to Unliganded Hemoglobin", J. Phys. Chem. 84, N7, 756 (1980).

APPENDIX A

Interference Fringe Data

This appendix contains all experimental data points. The points are tabulated for each run in columns corresponding to each time, given in seconds. Each point is the location in centimeters where an interference fringe "bends" by an amount equal to one fringe spacing. Fringes are measured from each end of the diffusion cell where they are straight, i.e., no refractive index gradient. Negative values denote fringes measured in lower half of cell. The membrane surface in each half of cell is located at 0.0 cm.

RUNL, FIELD=0.0 , PORE D=8.0 MICRON

****

900.0	1800.0	3600.0	5400.0	7200.0
0.3330	0.3300	0.3300	0.3300	0.3330
0.0231	0.0386	0.0575	0.0837	0.1050
0.0167	0.0278	0.0450	0.0643	0.0823
0.0110	0.0205	0.0344	0.0502	0.0635
0.0065	0.0147	0.0260	0.0413	0.0507
0.0033	0.0090	0.0183	0.0303	0.0398
0.0002	0.0045	0.0126	0.0225	0.0305
-.0005	0.0007	0.0070	0.0151	0.0215
-.0030	-.0026	0.0010	0.0081	0.0129
-.0054	-.0064	-.0009	0.0015	0.0050
-.0089	-.0108	-.0059	-.0020	-.0023
-.0130	-.0150	-.0118	-.0087	-.0095
-.0173	-.0199	-.0169	-.0157	-.0177
-.0220	-.0257	-.0225	-.0224	-.0257
-.0285	-.0320	-.0300	-.0297	-.0349
-.0368	-.0400	-.0376	-.0388	-.0438
-.3330	-.0525	-.0466	-.0470	-.0542
	-.3330	-.0588	-.0585	-.0671
		-.0768	-.0730	-.0837
		-.3330	-.0935	-.1086
			-.3330	-.3330

****

RUN N, FIELD= 1.0kG, PORE D=8.0 MICRON

900.0	1800.0	3600.0	5400.0	9000.0
0.3330	0.3300	0.3300	0.3300	0.3330
0.0279	0.0450	0.0650	0.0931	0.1245
0.0193	0.0335	0.0492	0.0700	0.0926
0.0136	0.0252	0.0383	0.0549	0.0737
0.0096	0.0184	0.0300	0.0429	0.0602
0.0053	0.0128	0.0228	0.0336	0.0471
0.0013	0.0084	0.0152	0.0249	0.0360
-.0028	0.0036	0.0095	0.0172	0.0259
-.0061	0.0001	0.0036	0.0100	0.0171
-.0090	-.0032	-.0002	0.0031	0.0081
-.0127	-.0071	-.0055	-.0071	0.0001
-.0166	-.0108	-.0120	-.0125	-.0058
-.0204	-.0155	-.0170	-.0198	-.0134
-.0263	-.0200	-.0230	-.0276	-.0220
-.0350	-.0257	-.0302	-.0360	-.0310
-.3330	-.0317	-.0378	-.0457	-.0414
	-.0406	-.0470	-.0561	-.0520
	-.0520	-.0590	-.0692	-.0645
	-.3330	-.0765	-.0914	-.0793
		-.3330	-.3330	-.0970
				-.1255
				-.3330

RUN K, FIELD=2.5 kG, PORE D=8.0 MICRON

900.0	1800.0	3600.0	5400.0	9000.0
0.3330	0.3300	0.3300	0.3300	0.3300
0.0256	0.0437	0.0670	0.0828	0.1094
0.0177	0.0311	0.0499	0.0628	0.0842
0.0118	0.0225	0.0376	0.0495	0.0671
0.0079	0.0164	0.0287	0.0380	0.0521
0.0036	0.0116	0.0205	0.0287	0.0395
0.0010	0.0066	0.0138	0.0200	0.0300
-.0013	0.0016	0.0079	0.0124	0.0194
-.0045	-.0035	0.0022	0.0056	0.0106
-.0074	-.0083	-.0046	-.0053	0.0025
-.0107	-.0124	-.0097	-.0118	-.0006
-.0139	-.0161	-.0152	-.0189	-.0090
-.0176	-.0218	-.0209	-.0258	-.0172
-.0225	-.0272	-.0271	-.0338	-.0264
-.0280	-.0327	-.0347	-.0427	-.0358
-.0370	-.0404	-.0431	-.0529	-.0462
-.3330	-.0505	-.0525	-.0645	-.0584
	-.3330	-.0650	-.0793	-.0708
		-.0868	-.1031	-.0857
		-.3330	-.3330	-.1063
				-.1378
				-.3330

RUN R, FIELD = 4.0 kG, PORE D= 8.0 MICRON

****

900.0	1800.0	3600.0	5400.0	9000.0
0.3330	0.3300	0.3300	0.3300	0.3330
0.0278	0.0411	0.0645	0.0930	0.1182
0.0188	0.0300	0.0484	0.0653	0.0884
0.0131	0.0217	0.0378	0.0508	0.0704
0.0081	0.0155	0.0289	0.0393	0.0547
0.0050	0.0110	0.0211	0.0302	0.0429
0.0014	0.0062	0.0150	0.0221	0.0274
-.0016	0.0015	0.0084	0.0143	0.0219
-.0041	-.0001	0.0016	0.0074	0.0133
-.0076	-.0044	-.0033	0.0001	0.0051
-.0111	-.0083	-.0087	-.0003	-.0009
-.0151	-.0126	-.0146	-.0066	-.0093
-.0190	-.0178	-.0201	-.0131	-.0170
-.0251	-.0227	-.0272	-.0201	-.0265
-.0337	-.0292	-.0348	-.0273	-.0373
-.3330	-.0371	-.0433	-.0353	-.0484
	-.0494	-.0553	-.0455	-.0587
	-.3330	-.0728	-.0571	-.0745
		-.3330	-.0711	-.0918
			-.0928	-.1186
			-.3330	-.3330

****

RUN M, FIELD=10.0 kG PORE D=8.0 MICRON

900.0	1800.0	3600.0	5400.0	9000.0
0.3330	0.3300	0.3300	0.3300	0.3330
0.0298	0.0476	0.0656	0.0870	0.1083
0.0192	0.0336	0.0489	0.0651	0.0829
0.0134	0.0246	0.0368	0.0493	0.0650
0.0082	0.0180	0.0280	0.0380	0.0499
0.0045	0.0124	0.0194	0.0280	0.0378
0.0009	0.0072	0.0129	0.0195	0.0272
-.0003	0.0024	0.0062	0.0114	0.0170
-.0031	-.0027	-.0003	0.0048	0.0083
-.0061	-.0070	-.0061	-.0018	-.0037
-.0087	-.0117	-.0121	-.0086	-.0115
-.0126	-.0162	-.0182	-.0160	-.0210
-.0167	-.0218	-.0245	-.0238	-.0300
-.0219	-.0278	-.0322	-.0315	-.0410
-.0291	-.0349	-.0408	-.0410	-.0520
-.0378	-.0425	-.0509	-.0509	-.0651
-.3330	-.0564	-.0636	-.0630	-.0809
	-.3330	-.0856	-.0805	-.1004
		-.3330	-.1043	-.1301
			-.3330	-.3330

RUN T, FIELD = 10.5 kG, PORE D = 8.0 MICRON

960.0	1800.0	3600.0	5400.0	9120.0
0.3330	0.3300	0.3300	0.3300	0.3330
0.0280	0.0376	0.0686	0.0875	0.1142
0.0183	0.0274	0.0482	0.0642	0.0847
0.0126	0.0193	0.0356	0.0487	0.0673
0.0078	0.0134	0.0264	0.0368	0.0514
0.0044	0.0079	0.0186	0.0275	0.0401
0.0003	0.0037	0.0124	0.0192	0.0290
-.0014	0.0001	0.0066	0.0115	0.0193
-.0039	-.0003	0.0006	0.0048	0.0102
-.0070	-.0047	-.0036	-.0001	0.0025
-.0104	-.0079	-.0090	-.0058	-.0012
-.0138	-.0120	-.0141	-.0116	-.0078
-.0187	-.0166	-.0192	-.0179	-.0154
-.0228	-.0208	-.0261	-.0251	-.0243
-.0292	-.0264	-.0329	-.0332	-.0333
-.0389	-.0328	-.0403	-.0406	-.0435
-.3330	-.0413	-.0590	-.0498	-.0537
	-.0555	-.0616	-.0609	-.0664
	-.3330	-.0820	-.0745	-.0799
		-.3330	-.0974	-.0993
			-.3330	-.1274
				-.3330

RUN P, FIELD=11.kG,PORE D=8.0 MICRON

****

900.0	1800.0	3600.0	5400.0	9000.0
0.3330	0.3300	0.3300	0.3300	0.3330
0.0329	0.0536	0.0778	0.0997	0.1317
0.0237	0.0374	0.0562	0.0748	0.0983
0.0167	0.0282	0.0443	0.0587	0.0779
0.0120	0.0208	0.0346	0.0468	0.0634
0.0077	0.0147	0.0264	0.0362	0.0501
0.0043	0.0106	0.0188	0.0284	0.0394
0.0011	0.0061	0.0129	0.0202	0.0293
-.0003	0.0019	0.0067	0.0132	0.0194
-.0039	-.0034	0.0016	0.0064	0.0105
-.0071	-.0074	-.0017	-.0035	0.0021
-.0102	-.0115	-.0069	-.0101	-.0003
-.0134	-.0167	-.0137	-.0170	-.0077
-.0177	-.0229	-.0195	-.0245	-.0170
-.0240	-.0287	-.0260	-.0330	-.0266
-.0321	-.0372	-.0343	-.0421	-.0368
-.3330	-.0492	-.0429	-.0529	-.0467
	-.3330	-.0551	-.0677	-.0586
		-.0731	-.0887	-.0732
		-.3330	-.3330	-.0938
				-.1187
				-.3330

****

RUN H, FIELD = 12.0 kG, PORE D = 8.0 MICRON

900.0	1800.0	3600.0	7200.0	10800.0
0.3300	0.3300	0.3300	0.3300	0.3300
0.0259	0.0494	0.0702	0.1037	0.1156
0.0165	0.0332	0.0509	0.0779	0.0857
0.0105	0.0249	0.0384	0.0587	0.0668
0.0062	0.0176	0.0286	0.0460	0.0522
0.0020	0.0112	0.0202	0.0346	0.0384
-.0040	0.0061	0.0131	0.0246	0.0276
-.0076	0.0013	0.0064	0.0143	0.0156
-.0103	-.0034	0.0011	0.0060	0.0052
-.0133	-.0086	-.0067	-.0043	-.0064
-.0164	-.0124	-.0110	-.0107	-.0152
-.0203	-.0166	-.0172	-.0186	-.0245
-.0247	-.0209	-.0226	-.0267	-.0352
-.0302	-.0268	-.0296	-.0353	-.0455
-.0403	-.0325	-.0369	-.0445	-.0584
-.3330	-.0400	-.0452	-.0554	-.0716
	-.0498	-.0539	-.0663	-.0883
	-.3330	-.0677	-.0789	-.1092
		-.3330	-.0962	-.1332
			-.3330	-.3330

RUN A2, FIELD=0.0 , PORE D=0.8 MICRON

****

900.0	1800.0	3600.0	7200.0	10800.0
0.3300	0.3300	0.3300	0.3300	0.3330
0.0206	0.0335	0.0519	0.0889	0.1149
0.0136	0.0225	0.0371	0.0648	0.0853
0.0076	0.0146	0.0272	0.0484	0.0663
0.0031	0.0093	0.0184	0.0362	0.0513
0.0001	0.0051	0.0114	0.0248	0.0368
-.0039	0.0001	0.0051	0.0160	0.0250
-.0070	-.0059	-.0081	0.0075	0.0138
-.0096	-.0094	-.0134	0.0003	0.0045
-.0128	-.0132	-.0189	-.0093	-.0094
-.0142	-.0173	-.0242	-.0172	-.0184
-.0171	-.0216	-.0304	-.0235	-.0270
-.0155	-.0269	-.0365	-.0315	-.0363
-.0190	-.0323	-.0444	-.0394	-.0459
-.0234	-.0385	-.0513	-.0480	-.0576
-.0272	-.0458	-.0616	-.0573	-.0700
-.0327	-.0567	-.0750	-.0679	-.0823
-.0402	-.0768	-.0906	-.0811	-.0972
-.0562	-.3330	-.3330	-.0961	-.1175
-.3330			-.1214	-.1437
			-.3330	-.3330

****

RUN E2, FIELD= 2.5kG, PORE D=0.8 MICRON

****

915.0	1840.0	3600.0	7200.0	10800.0
0.3300	0.3300	0.3300	0.3300	0.3330
0.0264	0.0412	0.0616	0.1033	0.1394
0.0155	0.0297	0.0466	0.0764	0.1007
0.0100	0.0206	0.0344	0.0574	0.0778
0.0050	0.0143	0.0249	0.0442	0.0611
0.0008	0.0085	0.0170	0.0318	0.0466
-.0057	0.0023	0.0091	0.0216	0.0332
-.0093	-.0031	0.0027	0.0119	0.0219
-.0125	-.0072	-.0093	0.0027	0.0104
-.0158	-.0124	-.0154	-.0059	-.0123
-.0200	-.0169	-.0222	-.0151	-.0226
-.0244	-.0219	-.0288	-.0242	-.0333
-.0288	-.0268	-.0371	-.0343	-.0455
-.0344	-.0335	-.0444	-.0444	-.0564
-.0440	-.0405	-.0537	-.0550	-.0709
-.3330	-.0493	-.0674	-.0673	-.0860
	-.0636	-.0862	-.0819	-.1293
	-.3330	-.3330	-.1017	-.1694
			-.1336	-.3330
			-.3330	

****

RUN C2, FIELD= 5.0kG,PORE D=0.8 MICRON

900.0	1800.0	3600.0	7200.0	10800.0
0.3300	0.3300	0.3300	0.3300	0.3330
0.0273	0.0447	0.0649	0.0921	0.1162
0.0199	0.0318	0.0509	0.0730	0.0889
0.0141	0.0240	0.0387	0.0572	0.0704
0.0093	0.0178	0.0289	0.0464	0.0562
0.0053	0.0124	0.0224	0.0367	0.0430
0.0023	0.0078	0.0158	0.0270	0.0323
-.0041	0.0032	0.0097	0.0171	0.0215
-.0066	-.0042	0.0044	0.0094	0.0121
-.0096	-.0080	-.0022	0.0026	0.0031
-.0123	-.0119	-.0089	-.0014	-.0084
-.0152	-.0156	-.0152	-.0099	-.0168
-.0185	-.0202	-.0191	-.0183	-.0271
-.0219	-.0246	-.0253	-.0254	-.0364
-.0253	-.0294	-.0317	-.0338	-.0463
-.0302	-.0351	-.0378	-.0436	-.0563
-.0358	-.0412	-.0448	-.0526	-.0688
-.0441	-.0490	-.0544	-.0628	-.0821
-.3330	-.0613	-.0648	-.0754	-.0976
	-.3330	-.0794	-.0926	-.1184
		-.3330	-.1105	-.1466
			-.3330	-.3330

RUN D2, FIELD=10.kG, PORE D=0.8 MICRON

****

900.0	1800.0	3600.0	7200.0	10800.0
0.3300	0.3300	0.3300	0.3300	0.3330
0.0222	0.0380	0.0558	0.0959	0.1218
0.0141	0.0260	0.0395	0.0703	0.0915
0.0081	0.0175	0.0295	0.0532	0.0704
0.0031	0.0110	0.0203	0.0405	0.0547
-.0063	0.0057	0.0122	0.0290	0.0398
-.0093	0.0012	0.0053	0.0194	0.0279
-.0122	-.0044	-.0060	0.0105	0.0167
-.0151	-.0076	-.0128	0.0011	0.0006
-.0183	-.0110	-.0179	-.0102	-.0116
-.0213	-.0159	-.0234	-.0181	-.0211
-.0246	-.0197	-.0293	-.0256	-.0305
-.0291	-.0245	-.0358	-.0333	-.0405
-.0340	-.0290	-.0425	-.0414	-.0503
-.0418	-.0340	-.0512	-.0507	-.0630
-.3330	-.0399	-.0617	-.0612	-.0759
	-.0477	-.0780	-.0744	-.0922
	-.0594	-.3330	-.0904	-.1128
	-.3330		-.1171	-.1424
			-.3330	-.3330

****

RUN B2, FIELD = 12.5kG,PORE D=0.8 MICRON

900.0	1800.0	3600.0	7200.0	10800.0
0.3300	0.3300	0.3300	0.3300	0.3330
0.0323	0.0480	0.0695	0.1028	0.1209
0.0222	0.0343	0.0534	0.0787	0.0949
0.0158	0.0257	0.0415	0.0616	0.0754
0.0113	0.0188	0.0322	0.0490	0.0609
0.0072	0.0134	0.0245	0.0387	0.0482
0.0035	0.0083	0.0173	0.0285	0.0365
0.0004	0.0038	0.0119	0.0199	0.0264
-.0056	-.0010	0.0060	0.0119	0.0149
-.0086	-.0053	0.0004	0.0038	0.0062
-.0114	-.0100	-.0003	-.0014	-.0060
-.0143	-.0141	-.0056	-.0098	-.0164
-.0175	-.0183	-.0103	-.0183	-.0258
-.0212	-.0227	-.0160	-.0259	-.0357
-.0245	-.0273	-.0218	-.0340	-.0456
-.0289	-.0326	-.0274	-.0421	-.0569
-.0349	-.0392	-.0339	-.0519	-.0676
-.0434	-.0466	-.0409	-.0626	-.0830
-.3330	-.0602	-.0487	-.0750	-.0994
	-.3330	-.0582	-.0928	-.1209
		-.0698	-.1149	-.1578
		-.0919	-.3330	-.3330

APPENDIX B

Raytracing Refractive Index Profile

Correlation Parameters

This appendix tabulates the coefficients A, b, and m derived from the raytracing computer program for the refractive index profile in each half of the diffusion cell

$$n = m \operatorname{erf}(Ax) + b$$

where x is the location in centimeters, n is refractive index, and A, b and m are determined from the best fit of the refractive index profile corrected for wavefront deflection. The values tabulated for each run are listed in columns under the respective times they are taken, in seconds. The first three rows are the parameters tabulated for the upper half of the diffusion cell, the last three rows corresponding to the lower half of the diffusion cell.

RUN L, FIELD=0.0, PORE SIZE=8.0 MICRON

TIME	900.0	1800.0	3600.0	5400.0	7200.0
M-UP	-0.000446	-0.000493	-0.000553	-0.000603	-0.000617
A-UP	10.557301	7.465138	5.278650	4.310000	3.732570
B-UP	1.331726	1.331776	1.331834	1.331903	1.331930
M-DOWN	-0.000484	-0.000545	-0.000598	-0.000626	-0.000631
A-DOWN	10.557301	7.465138	5.278650	4.310000	3.732570
B-DOWN	1.332232	1.332170	1.332117	1.332089	1.332086

RUN N. FIELD=1 KG. PORE SIZE =8.0 MICRON

TIME	900.0	1800.0	3600.0	5400.0	9000.0
M-UP	-0.000474	-0.000550	-0.000573	-0.000606	-0.000634
A-UP	10.557301	7.465138	5.278650	4.310000	3.338511
B-UP	1.331768	1.331846	1.331869	1.331922	1.331950
M-DOWN	-0.000469	-0.000556	-0.000599	-0.000601	-0.000656
A-DOWN	10.557301	7.465138	5.278650	4.310000	3.338511
B-DOWN	1.332249	1.332161	1.332116	1.332116	1.332058

RUN K, FIELD=2.5 KG, PORE SIZE=8.0 MICRON

TIME	900.0	1800.0	3600.0	5400.0	9000.0
M-UP	-0.000456	-0.000507	-0.000547	-0.000567	-0.000595
A-UP	10.557301	7.465138	5.278650	4.310000	3.338511
B-UP	1.331742	1.331802	1.331847	1.331870	1.331897
M-DOWN	-0.000501	-0.000573	-0.000650	-0.000663	-0.000692
A-DOWN	10.557301	7.465138	5.278650	4.310000	3.338511
B-DOWN	1.332214	1.332144	1.332061	1.332048	1.332017

RUN R, FIELD=4.0 KG, PORE D=8.0 MICRON

TIME	900.0	1800.0	3600.0	5400.0	9000.0
M-UP	-0.000466	-0.000508	-0.000555	-0.000581	-0.000599
A-UP	10.557301	7.465138	5.278650	4.310000	3.338511
B-UP	1.331758	1.331797	1.331852	1.331890	1.331909
M-DOWN	-0.000440	-0.000510	-0.000567	-0.000600	-0.000616
A-DOWN	10.557301	7.465138	5.278650	4.310000	3.338511
B-DOWN	1.332278	1.332208	1.332151	1.332116	1.332100

RUN M, FIELD=10KG, PORE SIZE=8.0 MICRON

TIME	900.0	1800.0	3600.0	5400.0	9000.0
M-UP	-0.000449	-0.000509	-0.000520	-0.000551	-0.000566
A-UP	10.557301	7.465138	5.278650	4.310000	3.338511
B-UP	1.331749	1.331815	1.331823	1.331861	1.331870
M-DOWN	-0.000482	-0.000563	-0.000609	-0.000634	-0.000644
A-DOWN	10.557301	7.465138	5.278650	4.310000	3.338511
B-DOWN	1.332232	1.332150	1.332101	1.332076	1.332067

RUN T, FIELD=10.5 KG, PORE SIZE=8.0 MICRON

TIME	960.0	1800.0	3600.0	5400.0	9120.0
M-UP	-0.000442	-0.000481	-0.000527	-0.000551	-0.000589
A-UP	10.222062	7.465138	5.278650	4.310000	3.316475
B-UP	1.331734	1.331762	1.331827	1.331858	1.331893
M-DOWN	-0.000496	-0.000573	-0.000635	-0.000659	-0.000674
A-DOWN	10.222062	7.465138	5.278650	4.310000	3.316475
B-DOWN	1.332219	1.332143	1.332076	1.332056	1.332040

RUN P, FIELD=11KG, PORE SIZE=8.0 MICRON

TIME	900.0	1800.0	3600.0	5400.0	9000.0
M-UP	-0.000543	-0.000567	-0.000599	-0.000632	-0.000644
A-UP	10.557301	7.465138	5.278650	4.310000	3.338511
B-UP	1.331847	1.331880	1.331915	1.331956	1.331971
M-DOWN	-0.000427	-0.000497	-0.000547	-0.000570	-0.000610
A-DOWN	10.557301	7.465138	5.278650	4.310000	3.338511
B-DOWN	1.332293	1.332220	1.332170	1.332148	1.332106

RUN H, FIELD=12 KG, PORE SIZE=8.0 MICRON

TIME	900.0	1800.0	3600.0	7200.0	10800.0
M-UP	-0.000387	-0.000485	-0.000527	-0.000552	-0.000547
A-UP	10.557301	7.465138	5.278650	3.732570	3.047630
B-UP	1.331684	1.331797	1.331835	1.331866	1.331847
M-DOWN	-0.000558	-0.000573	-0.000600	-0.000644	-0.000663
A-DOWN	10.557301	7.465138	5.278650	3.732570	3.047630
B-DOWN	1.332156	1.332145	1.332120	1.332075	1.332050

RUN A2, FIELD=0.0, PORE SIZE=0.8 MICRON

TIME	900.0	1800.0	3600.0	7200.0	10800.0
M-UP	-0.000352	-0.000411	-0.000439	-0.000517	-0.000537
A-UP	10.557301	7.465138	5.278650	3.732570	3.047630
B-UP	1.331638	1.331691	1.331724	1.331807	1.331837
M-DOWN	-0.000769	-0.000731	-0.000778	-0.000775	-0.000764
A-DOWN	10.557301	7.465138	5.278650	3.732570	3.047630
B-DOWN	1.331936	1.331966	1.331925	1.331935	1.331946

RUN E2, FIELD=2.5 KG, PORE SIZE=0.8 MICRON

TIME	915.0	1840.0	3600.0	7200.0	10800.0
M-UP	-0.000363	-0.000439	-0.000486	-0.000527	-0.000561
A-UP	10.470408	7.383551	5.278650	3.732570	3.047630
B-UP	1.331661	1.331739	1.331787	1.331842	1.331886
M-DOWN	-0.000602	-0.000645	-0.000659	-0.000686	-0.000639
A-DOWN	10.470408	7.383551	5.278650	3.732570	3.047630
B-DOWN	1.332105	1.332062	1.332049	1.332016	1.332068

RUN C2, FIELD=5KG, PORE SIZE=0.8 MICRON

TIME	900.0	1800.0	3600.0	7200.0	10800.0
M-UP	-0.000488	-0.000529	-0.000576	-0.000609	-0.000602
A-UP	10.557301	7.465138	5.278650	3.732570	3.047630
B-UP	1.331779	1.331825	1.331872	1.331903	1.331896
M-DOWN	-0.000671	-0.000707	-0.000717	-0.000713	-0.000756
A-DOWN	10.557301	7.465138	5.278650	3.732570	3.047630
B-DOWN	1.332036	1.332000	1.331997	1.332000	1.331953

RUN D2, FIELD=10KG, PORE SIZE=0.8 MICRON

TIME	900.0	1800.0	3600.0	7200.0	10800.0
M-UP	-0.000317	-0.000418	-0.000441	-0.000525	-0.000526
A-UP	10.557301	7.465138	5.278650	3.732570	3.047630
B-UP	1.331616	1.331709	1.331734	1.331828	1.331841
M-DOWN	-0.000666	-0.000704	-0.000684	-0.000708	-0.000709
A-DOWN	10.557301	7.465138	5.278650	3.732570	3.047630
B-DOWN	1.332044	1.332006	1.332031	1.332006	1.332003

RUN B2, FIELD=12.5 KG, PORE SIZE=8.0 MICRON

TIME	900.0	1800.0	3600.0	7200.0	10800.0
M-UP	-0.000528	-0.000530	-0.000600	-0.000610	-0.000621
A-UP	10.557301	7.465138	5.278650	3.732570	3.047630
B-UP	1.331829	1.331836	1.331903	1.331919	1.331924
M-DOWN	-0.000648	-0.000673	-0.000735	-0.000711	-0.000744
A-DOWN	10.557301	7.465138	5.278650	3.732570	3.047630
B-DOWN	1.332060	1.332037	1.331971	1.332001	1.331963

APPENDIX C

Raytracing Computer Program

```
      IMPLICIT REAL*8(A-H,L,O-Z)
C***********RAYTRACE TRACES RAYS THROUGH OPTICAL SYSTEM ACCOUNTING FOR
C***********RAY BENDING FROM REF INDEX GRADIENT AND FITTING REF INDEX
C***********PROFILE TO AN ERROR FUNCTION CORRELATION*******************
      REAL*8 M
      DIMENSION XO(40),F(40),IV(100),NDOBS(40),PAR(3),XFP(40),
     1LDOBS(40),LREF(40),X7(40),NFRNG(40),V(400),S(40),LDCALC(40)
     2,XSHIFT(40),XOCELL(40)
      COMMON /SET1/Y(40),XF(40)/SET2/RL1,TL1,XL1,RL2,TL2,XL2,
     1ZO,Z1,Z2,Z3,Z5,Z7,NQURTZ,NAIR,NGLASS
      REAL*8 NAIR,NGLASS,NWATER,NQURTZ,LAMBDA,LDCALC,LDOBS
     1 ,NTOP,NBOTTM,NDOBS,NXO,NX1
C*********DEFINE PARAMETERS*************************
      PI=3.14127
      XMAG=.337
      DELXM=.005
      XMAGO=XMAG-.001
      LAMBDA=.6328E-4
      NAIR=1.000276
      NWATER=1.3340
      NQURTZ=1.45709
      NTIMET=0
      NGLASS=1.7499
      DATA M,A,B/-7.D-4,7.D0,1.33D0/
C***************READ IN DATA FOR RUN ***************************
      READ(10,629)NTIME
1       CONTINUE
      ITER=0
      IFLAG=1
C***********SET COUNTER FOR NUMBER OF TIME STEPS DURING EXPERIMENT*****
      NTIMET=NTIMET+1
      NELMT=0
      ISHIFT=0
      IF(NTIMET.GT.NTIME)STOP
C***********READ TITLE AND REFERENCE REFRACTIVE INDICES************
      READ(10,610)NT1,NT2,NT3,NT4,NT5,NT6,NT7,NT8,NT9,NT10,NT11,NT12
      READ(10,629)NPTS,NWATER,NTOP,NBOTTM,TIME
      IF(NTIMET.NE.1)GO TO 589
      WRITE(9,610)NT1,NT2,NT3,NT4,NT5,NT6,NT7,NT8,NT9,NT10,NT11,NT12
      WRITE(9,629)NTIME
589   NELMNT=NPTS
      DO 599 I=1,NPTS
      READ(10,629)NFRNG(I),XO(I)
599   CONTINUE
50    FORMAT('LREF  LDOBS(I)  NDOBS(I) XO(I) X7(I) LL1 LL2')
5       CONTINUE
      NELUP =0
      XMAGO=XMAG
      DO 1000 I=1,NELMNT
610   FORMAT(20A4)
C*******CALCULATIONS FOR TOP HALF OF CELL ARE PERFORMED FIRST ASSUMING
C*******NO BENDING IN REFRACTIVE INDEX GRADIENT*********************
629   FORMAT(I5,4G10.5)
      NDOBS(1)=NTOP
      XOCELL(I)=XO(I)/XMAG
      IF(XOCELL(I).GT.O.)NELUP=NELUP+1
      L12=NQURTZ*(Z2-Z1)
      CALL RTRACE(XOCELL(I),O.DO,REFOPL,X7I)
      X7(I)=X7I
      LREF(I)=NWATER*(Z1-ZO)+REFOPL+L12
```

```
C*******SUM ALL UNDEFLECTED PATH LENGTHS***************
      IF(I.EQ.1)LREFO=LREF(I)
C*******USING OPTICAL PATH LENGTHS FIND INITIAL REF INDEX PROFILE****
C************ASSUMING NO RAY BENDING THROUGH REF INDEX GRADIENT*******
      NDOBS(I)=NTOP + (LAMBDA/(Z1-ZO))*(NFRNG(I)-1)
      NDOBS(1)=NTOP
60    FORMAT(1X,7F10.7)
1000  CONTINUE
      XMAG=X7(1)/XOCELL(1)
      IF(DABS(XMAG-XMAGO).GT..00001)GO TO 5
C ********INITIALIZE BOTTOM  HALF OF CELL************************
      ISTART=NELUP+1
      DO 75 I=ISTART,NELMNT
      NDOBS(I)=NBOTTM-(LAMBDA/(Z1-ZO))*(NFRNG(NELMNT)-NFRNG(I))
75    NDOBS(NELMNT)=NBOTTM
      PRINT 610,NT1,NT2,NT3,NT4,NT5,NT6,NT7,NT8,NT9,NT10,NT11,NT12
      PRINT 55
      DO 76 I=1,NELMNT
76    PRINT 56, NDOBS(I),NFRNG(I),XOCELL(I),X7(I),XO(I)
55    FORMAT(' NINITIAL  FRINGE NO.  XCELL INITIAL  XFOCAL PL. INIT',//)
56      FORMAT(F10.6,I8,3(3X,F10.6))
      RMS=0.0
      NELMAX=NELUP
       PAR(1)=M
      PAR(2)=A
       PAR(3)=B
C******IFLAG IS A FLAG WHICH SIGNALS WHETHER CALCULATIONS ARE BEING PERFORMED
C*******ON UPPER OR LOWER HALF OF CELL,  IFLAG=1 FOR UPPER, -1 FOR LOWER*****
10     IF(IFLAG.LT.0)NELMAX=NELMNT
      ICONV=1
C*******FIT REF INDEX PROFILE TO ERROR FUNCTION**************
      ITER=ITER+1
      IF(ITER.LT.10.)GO TO 57
      PRINT 570
570   FORMAT(//,1X,'PROGRAM FAILED TO CONVERGE IN 10 PASSES',//)
      GO TO 1100
C*************START WITH TOP HALF OF CELL, THEN DO BOTTOM HALF*****
C*************SET FLAGS FOR TOP OR BOTTOM*************************
57    NF=NELMAX
      IF(IFLAG.LT.0)NELMAX=NELMNT-NELUP
      IF(IFLAG.LT.0)ISHIFT=NELUP
      DO 300 IC=1,NELMAX
      Y(IC)=NDOBS(IC+ISHIFT)
300   XF(IC)=XOCELL(IC+ISHIFT)
C*****CALL LINEARIZED ERROR FUNCTION FITTING ROUTINE
      CALL ERRFIT(PAR,NELMAX,TIME)
3000  FORMAT('RETURN CODE =',I5)
      M = PAR(1)
      A = PAR(2)
      B = PAR(3)
      ISTART=ISHIFT+1
      IFINAL=ISHIFT+NELUP
      IF(IFLAG.LT.0)IFINAL=NELMNT
      DO 500 I=ISTART,IFINAL
C*************PERFORM REFRACTIVE INDEX GRADIENT CALCS AND RAYBENDING***
      IF(ITER.EQ.1)NDOLD=NDOBS(I)
      DNDOBS = 2.*M*A*DEXP(-(A*A*XOCELL(I)*XOCELL(I)))/DSQRT(PI)
9999  DX1XO = DNDOBS*(Z1-ZO)*(Z1-ZO)/(2.*NDOBS(I))
      X1=XOCELL(I)+ DX1XO
      NXO = NDOBS(I) - .5*DNDOBS*(DX1XO)
```

```
      S(I) = (DX1XO*DX1XO + (Z1-ZO)*(Z1-ZO))**.5
      SINALP = DNDOBS * S(I)/NDOBS(I)
      LO1=NDOBS(I)*S(I)
      NX1 = NDOBS(I) + DNDOBS*DX1XO
      L12 = NQURTZ*(Z2-Z1)/DCOS(DARSIN((NQURTZ/NX1)*SINALP))
      BETA1 = DARSIN(SINALP*NQURTZ/NX1)
      X2=X1+(Z2-Z1)*DTAN(BETA1)
C***********PERFORM RAYTRACING THROUGH REST OF SYSTEM*****************
      CALL RTRACE(X2,BETA1,OPTPL,XFINAL)
      LDCALC(I)=OPTPL +L12+LO1
      XFP(I)=XFINAL
C********CHECK ERRORS BETWEEN BENT RAY POSITION ON FOCAL PLANE AND
C********ACTUAL FRINGE AND CORRECT REFRACE INDEX PROFILE THEN
C********STARTING ITERATIONS ALL OVER AGAIN UNTIL CONVERGENCE IS OK****
      DELXFP=XO(I)-XFP(I)
      XOCELL(I)=XOCELL(I)+DELXFP/XMAG
      IF(DABS(DELXFP).GT.1.E-6)ICONV=-1
500   CONTINUE
      IF(ICONV.GT.O)GO TO 1100
      GO TO 10
1100   CONTINUE
      IF(IFLAG.GT.O)PRINT 5051
      IF(IFLAG.LT.O)PRINT 5052
      IF(IFLAG.GT.O)
C******WRITE CORRELATION PARAMETERS ON UNIT 9 IF CONVERGENCE HAS BEEN ACHIEVED**
     1WRITE(9,5045)TIME,M,A,B,XOCELL(IFINAL)
      IF(IFLAG.LT.O)WRITE(9,5045)M,A,B,XOCELL(IFINAL)
5045 FORMAT(1X,5E15.8)
       PRINT 5050,   M,A,B
       PRINT 5060
      DO 1105 I=ISTART,IFINAL
      DELXFP=XO(I)-XFP(I)
1105   PRINT 5000,LDCALC(I),LDOBS(I),S(I),DELXFP,NDOBS(I),XOCELL(I),
     1XFP(I)
       IF(IFLAG.LT.O)GO TO 1200
      IFLAG=-1
      ITER=O
      GO TO 10
1200   GO TO 1
5060   FORMAT(//,4X,'LDCALC',1X,' ',5X,'S',5X,'DELXFP ',5X,
     1 'NDOBS',5X,'XOCELL',5X,'XFP',//)
5000   FORMAT(1X,8(1X,F10.6))
5051   FORMAT(//,1X,'TOP HALF OF CELL',//)
5052   FORMAT(//,1X,'BOTTOM HALF OF CELL',//)
5050   FORMAT(//,'M = ',F9.6,'A = ',F9.6,'B = ',F9.6)
      END
      BLOCK DATA
C********INITIALIZE COMMON BLOCKS WITH EQUIPMENT GEOMETRICAL PARAMETERS*****
      IMPLICIT REAL*8(A-H,N,O-Z)
        COMMON /SET1/Y(40),XF(40)/SET2/RL1,TL1,XL1,RL2,TL2,XL2,
     1ZO,Z1,Z2,Z3,Z5,Z7,NQURTZ,NAIR,NGLASS
         DATA RL1,TL1,XL1/99.29,1.0,5.0/
         DATA RL2,TL2,XL2/22.4,1.0,1.5/
        DATA ZO,Z1,Z2,Z3,Z5,Z7/O.,1.,2.,58.2,110.,126.6/
      END
      SUBROUTINE ERRFIT(PAR,NEL,T)
C*******SUBROUTINE ERRFIT FITS REF INDEX PROFILE TO ERROR FUNCTIN CORRELATION
C********N  =  M * ERF(A*X)  +  B   TO FIND PARAMETERS M,A,AND B FOR BEST FIT
      IMPLICIT REAL*8(A-H,O-Z)
      DIMENSION XLIN(40),YFIT(40),WT(40),E1(2),E2(2),P1(2),P2(2)
```

```
     1,PAR(3)
      COMMON /SET1/ Y(40),XF(40) /ICELL/IFLAG
      EXTERNAL AUX
C*****SUBROUTINE ERRFIT FITS REF INDEX PROFILE TO AN ERROR FUNCTION
C*****BY FIRST LINEARIZING ERR FCT THEN FITTING WITH LINEAR CURVE FIT
C*****INITIALIZE PARAMETERS
      IFLAG=1
      IF(XF(2).LT.0.D0)IFLAG=-1
      DO 1 I=1,NEL
      WT(I)=1.D0
C*****IF THE DEFLECTED X VALUE NEAR MEMBRANE IS IN A LOCATION THROUGH
C*****THE MEMBRANE THIS POINT IS IGNORED FOR CORRELATION CALCULATIONS**
1     IF(XF(3).LT.0.D0.AND.XF(1).GT.0.D0)WT(1)=1.D-6
      IF(XF(2).LT.0.D0)WT(NEL)=10.D0
      IF(XF(2).GT.0.D0)WT(1)=1.D0
C******THIS WEIGHTS THE ENDPOINTS 10 TIMES OTHER POINTS******
      ICON=1
      ITER=0
      D=5.D-6
      CUT =1.D-9/DSQRT(D*T)
      TAU = (1.+SQRT(5.))/2.0
      ALOW=0.D0
      AHIGH=3./DSQRT(D*T)
      AT2=(AHIGH-ALOW)/TAU +ALOW
      AT1=(AHIGH-AT2+ALOW)
      EPS=1.D-10
      P1(1)=0.D0
      P1(2)=0.D0
      P2(1)=P1(1)
      P2(2)=P1(2)
      DO 100 I=1,NEL
100   XLIN(I)=DERF(AT1*XF(I))
C******DLQF IS UBC CURVE FITTING LINEAR LEAST-SQUARES CURVE FITTING ROUTINE**
      CALL DLQF(XLIN,Y,YFIT,WT,E1,E2,P1,1.D0,NEL,2,-5,ND,EPS,AUX)
      CALL ERRCAL(Y,YFIT,ERROR1,NEL)
      DO 101 I=1,NEL
101   XLIN(I)=DERF(AT2*XF(I))
      CALL DLQF(XLIN,Y,YFIT,WT,E1,E2,P2,0.D0,NEL,2,-9,ND,EPS,AUX)
      CALL ERRCAL(Y,YFIT,ERROR2,NEL)
10    IF(ERROR1.LE.ERROR2)GO TO 18
11    AHIGH=AT2
      IF(AHIGH-ALOW.LE.CUT)GO TO 21
      AL1=AT1-ALOW
      IF(AHIGH-AT1.LT.AT1-ALOW)GO TO 15
12    AT2=AT1
      AT1=AHIGH-(AT1-ALOW)
      ERROR2=ERROR1
      P2(1)=P1(1)
      P2(2)=P1(2)
      ITER=ITER+1
112   DO 102 I=1,NEL
102   XLIN(I)=DERF(AT1*XF(I))
      CALL DLQF(XLIN,Y,YFIT,WT,E1,E2,P1,1.D0,NEL,2,-5,ND,EPS,AUX)
      CALL ERRCAL(Y,YFIT,ERROR1,NEL)
      GO TO 10
15    AT2=ALOW+(AHIGH-AT1)
115   DO 16 I=1,NEL
16    XLIN(I)=DERF(AT2*XF(I))
      CALL DLQF(XLIN,Y,YFIT,WT,E1,E2,P2,1.D0,NEL,2,-5,ND,EPS,AUX)
      CALL ERRCAL(Y,YFIT,ERROR2,NEL)
```

```
      GO TO 10
18    ALOW=AT1
      IF(AT2-ALOW.LE.CUT)GO TO 21
      IF(AT2-ALOW.LT.AHIGH-AT2) GO TO 20
19    AT1=AT2
      AT2=ALOW+(AHIGH-AT1)
      ERROR1=ERROR2
      P1(1)=P2(1)
      P1(2)=P2(2)
      GO TO 115
20    AT1=AHIGH-(AT2-ALOW)
      GO TO 112
21    CONTINUE
5010  FORMAT(1X,6(1X,F15.6))
      IF(ITER.GT.20)ICON=-1
      IF(ICON.LT.0)GO TO 200
      ERROR=ERROR1
      IF(ERROR1.GT.ERROR2)ERROR=ERROR2
      PAR(2)=AT1
      IF(ERROR1.GT.ERROR2)PAR(2)=AT2
      PAR(3)=P1(2)
      IF(ERROR1.GT.ERROR2)PAR(3)=P2(2)
      PAR(1)=P1(1)
      IF(ERROR1.GT.ERROR2)PAR(1)=P2(1)
      RETURN
200   PRINT 5000
5000  FORMAT(1X,//,'ERRFIT FAILED TO CONVERGE IN 20 PASSES',//)
      RETURN
      END
      SUBROUTINE ERRCAL(Y,YFIT,ERROR,N)
C*******SUBROUTINE ERRCAL CALCULATES RMS ERROR IN FITTED ERROR FUNCTION***
      IMPLICIT REAL*8(A-H,O-Z)
      DIMENSION Y(40),YFIT(40)
      ERROR=0.0
      DO 1 I=1,N
1     ERROR=ERROR+(Y(I)-YFIT(I))*(Y(I)-YFIT(I))
      RETURN
      END
      FUNCTION AUX(P,D,XLIN,L)
C******FUNCTIN AUX CALCULATES PARTIAL DERIVATIVES FOR LINEAR CURVE FITTING
C******ROUTINE USED TO FIT ERROR FUNCTION************************
      IMPLICIT REAL*8(A-H,O-Z)
      COMMON /ICELL/IFLAG
      DIMENSION P(1),D(1)
      D(1)=XLIN
      D(2)=1.D0
      AUX=P(1)*XLIN+P(2)
      RETURN
      END
      SUBROUTINE LNSTRC(XLI,TLI,RLI,XIN,ALPHA1,XOUT,BETA,OPTPL,ZL)
      IMPLICIT REAL*8(A-H,O-Z)
      REAL*8 NAIR,NGLASS
C******SUBROUTINE TO CALCULATE OPTICAL PATH LENGTH THROUGH PLANO-CONVEX***
C******LENS USING GEOMETRICAL OPTICAL RAY TRACING************************
C******TL1=LENS THICKNESS AT THINNEST POSITION*********************
C******RLI=RADIUS OF CURVATURE OF LENS*****************************
C******ZL=Z DISTANCE OF RAY THROUGH LENS***************************
C******XLI=OUTSIDE RADIUS OF LENS**********************
C******XINT=INITIAL X COORDINATE OF RAY ENTERING LENS*****
C******XOUT=FINAL X COORDINATE OF RAY LEAVING LENS******
```

```
C******ALPHA1=ANGLE OF ENTERING RAY NORMAL TO FLAT LENS SURFACE****
C******ALPHA2=ANGLE OF RAY THROUGH LENS MATERIAL************
C******BETA=EXIT ANGLE OF RAY LEAVING LENS***************
C******THETA=ANGLE RAY CUTS WITH TANGENT TO CURVED SURFACE INTERNAL TO LENS**
      N=0
      NAIR=1.000276
      NGLASS=1.57
      IF(XIN.LT.0.)XLI=-XLI
      THETAI=DARSIN(XLI/RLI)
      ZL=TLI
      ZLO=ZL
100   N=N+1
      ALPHA2 = DARSIN((NAIR/NGLASS)*DSIN(ALPHA1))
         XOUT=XIN + ZL*DTAN(ALPHA2)
      THETA=DARSIN(XOUT/RLI)
      ZL=RLI*(DCOS(THETA)-DCOS(THETAI)) + TLI
      OPTPL=(NGLASS/DCOS(ALPHA2))*ZL
      IF(N.GT.20)GO TO 150
      IF(DABS(ZL-ZLO).LT.1.E-8)GO TO 150
55    FORMAT(1X,'N  XOUT  ALPHA2  THETA  ZL  ZLO  OPTPL ')
50    FORMAT(1X,I2,6F10.6)
      ZLO=ZL
      GO TO 100
150   IF(N.GT.20)WRITE(6,40)
40    FORMAT('ERROR IN LNSTRC-DID NOT CONVERGE IN 20 PASSES')
      ALPHAP=ALPHA2-THETA
      BETAP=DARSIN((NGLASS/NAIR)*DSIN(ALPHAP))
      BETA = BETAP+THETA
3000  FORMAT('BETAP = ',F10.6,'BETA  =  ',F10.6)
      RETURN
      END
      SUBROUTINE RTRACE(XIN,ALPHIN,OPTPL,XFINAL)
C********SUBROUTINE RTRACE TRACES A RAY THROUGH OPTICAL SYSTEM FROM
C********DIFFUSION CELL EXIT TO FOCAL PLANE*********************
      IMPLICIT REAL*8(A-H,L,O-Z)
      COMMON/SET2/RL1,TL1,XL1,RL2,TL2,XL2,Z0,Z1,Z2,Z3,Z5,Z7,
     1NQURTZ,NAIR,NGLASS
      REAL*8 NAIR,NGLASS,NQURTZ
      X2 = XIN + (Z2-Z1)*DTAN(ALPHIN)
      ALPHA3 = DARSIN((NAIR/NQURTZ)*DSIN(BETA1))
      L23 = NAIR*(Z3-Z2)/DCOS(ALPHA3)
      X3 = X2 + (Z3-Z2)*DTAN(ALPHA3)
C*****LENS 1 RAY TRACING***********************
      CALL LNSTRC(XL1,TL1,RL1,X3,ALPHA3,X4,BETA4,LL1,ZL1)
C*****LENS 1 TO LENS 2*************************
      Z4=Z3+ZL1
      X5 = X4+ (Z5-Z4)*DTAN(BETA4)
      ALPHA5 = BETA4
      L45 = NAIR*(Z5-Z4)/DCOS(ALPHA5)
C*****LENS 2 RAY TRACING***********************
      CALL LNSTRC(XL2,TL2,RL2,X5,ALPHA5,X6,BETA6,LL2,ZL2)
C*****LENS 2 TO FOCAL PLANE RAY TRACING*********
      Z6=Z5+ZL2
      XFINAL = X6 + (Z7-Z6)*DTAN(BETA6)
      L6FP = NAIR*(Z7-Z6)/DCOS(BETA6)
      OPTPL = L23+LL1+L45+LL2+L6FP
      RETURN
      END
```

APPENDIX D

Mass Flux and Diffusivity Calculation Computer Program

```
      IMPLICIT REAL*8(A-H,O-Z)
C*****DIFFCALC CALCULATES MASS FLUXES, CONCENTRATION PROFILES AND
C*****CONCENTRATION INTEGRALS FROM REFRACTIVE INDEX CORRELATIONS
C*****EVALUATED FROM PROGRAM RAYTRACE AND FIT TO ERROR FUNCTION
C*****CORRELATION*************************************************
      REAL*8 NAXML,NAXMEM,NAXMU,NBXML,NBXMU
      DIMENSION CXDIFF(10),CXML(10),TIME(10),AU(10),BU(10),PMU(10),
     1AL(10),CX(10),CXMLC(10),BL(10),PML(10),PARL(4)
     1,CLSGAR(10),CWATER(10),XSUGAR(10)
      COMMON X(10),Y(10)
C********READ DATA FILE FOR PROFILE CORRELATION PARAMETERS*******
C******READ TITLE*************************************************
      READ(10,500)NT1,NT2,NT3,NT4,NT5,NT6,NT7,NT8,NT9,NT10
C******READ NUMBER OF TIMES DURING RUN*************************************
      READ(10,501)NTIME
500   FORMAT(20A4)
501   FORMAT(I5,3E15.8)
C**********SET PARAMETER VALUES FOR CALCULATIONS**************
      ALPHA=1.D0/49.01621D0
      XBOTTM=-1.8D0
      BETA=-1.331313D0/49.01621D0
      DXM=.0050
      GAMMA=-11.6874423D0
      XML=0.D0
      EPSI=0.0553512015D0
      XTOP=XML
      PI=3.1415927D0
C**********DELTX IS X INCREMENTS FOR WHICH CALCULATIONS ARE PERFORMED IN
C*********;*X POSITION IN DIFFUSION CELL, STARTING AT MEMBRANE SURFACE
C**********AND WORKING DOWN THREE VALUES TO -0.10 CM.*********************
      NINT=3.0
      DELTX=(-.10-XTOP)/NINT
      PRINT 555
555   FORMAT(1X,//,'DIFFCALC WITH CONCENTRATION AT TIME=0',//)
      PRINT 500, NT1,NT2,NT3,NT4,NT5,NT6,NT7,NT8,NT9,NT10
      DO 100 I=1,NTIME
C*******READ VALUES M,A,B FOR REFRACTIVE INDEX PROFILE CORRELATION PARAMETERS
C*******AT EACH TIME VALUE*****************************************************
      READ(10,502)TIME(I),PMU(I),AU(I),BU(I),XUF
      READ(10,502)PML(I),AL(I),BL(I),XLF
100   X(I+1)=TIME(I)
      X(1)=1.D0
C*********PERFORM PROFILES INTEGRALS FOR EACH TIME FROM CONSTANTS****
      DO 105 INT=1,NINT
      DO 106 I =1,NTIME
C******FUNCTION CINTGL CALCULATES CONCENTRATION INTEGRAL IN CELL***************
      CXML(I) = CINTGL(PML(I),AL(I),BL(I),XTOP) -
     1CINTGL(PML(I),AL(I),BL(I),XBOTTM)
C*******EVALUATE CONCENTRATION AT BOTH SURFACES OF MEMBRANE FOR MEMBRANE
C*******DIFFUSIVITY CALCULATIONS*********************************************
      CX(I+1)=CXML(I)
      CX(1)=(XTOP-XBOTTM)*(ALPHA*1.332716+BETA)
106   CONTINUE
C*********FIND CONSTANTS FOR FITTING CONCENTRATION PROFILE VS TIME****
      CALL EQUFIT(CX,PARL,NTIME)
      PRINT 503,XTOP
C*********FIND FLUXES*******************
      PRINT 5000
      PRINT 502,PARL(1),PARL(2),PARL(3),PARL(4)
      PRINT 5002
```

```
      DO 101 I=1,NTIME
C*******FUNCTION DCDT SOLVES FOR PARTIAL DERIVATIVE OF CONCENTRATION INTEGRAL
C*******WRT TO TIME TO DETERMINE MASS FLUX IN CELL AT ANY VALUE X, TIME*****
      NAXML = DCDT(PARL,TIME(I))
C*******NAX IS SUCROSE MOLAR FLUX, NBX IS WATER MOLAR FLUX***************
      NAXMEM=NAXML
      NBXML = GAMMA*NAXML
      CXMLC(I)=PARL(1)+PARL(2)*DERF(PARL(4)/TIME(I)**.5)
     1+PARL(3)*TIME(I)**.5*DEXP(-PARL(4)*PARL(4)/TIME(I))
      CLSGAR(I) = ALPHA*(PML(I)*DERF(AL(I)*XTOP)+BL(I))+BETA
      CWATER(I) = GAMMA*CLSGAR(I) + EPSI
      XSUGAR(I)=CLSGAR(I)/(CWATER(I)+CLSGAR(I))
      DNDY=PML(I)*AL(I)*DEXP(-AL(I)*AL(I)*XTOP*XTOP)/PI**.5
      DSUCDY=ALPHA*DNDY
C*********FIND SUCROSE CONCENTRATION AT MEMBRANE SURFACES FOR
C*********DIFFUSIVTIY CALCULATIONS***************
      CLMEMB=ALPHA*(PML(I)*DERF(AL(I)*XTOP)+BL(I))+BETA
      CUMEMB=ALPHA*(PMU(I)*DERF(-AU(I)*XTOP)+BU(I))+BETA
      DCDMEM=(CUMEMB-CLMEMB)/(DXM+DABS(2.DO*XTOP))
      DMEMB=NAXMEM/DCDMEM
      CDELXA=(1.0-CLSGAR(I)*(1.0+GAMMA)/((1.0+GAMMA)
     1*CLSGAR(I)+EPSI))*DSUCDY
C*******CALCULATE FREE DIFFUSION COEFFICIENTS AND MEMBRANE DIFFUSION COEFF.**
      DNOBLK=-NAXML/CDELXA
      DBULK=(-NAXML+XSUGAR(I)*(NAXML+NBXML))/CDELXA
      CXDIFF(I)=((CXML(I)-CXMLC(I))/CXML(I))*100.0
      PRINT 5001,TIME(I),CLSGAR(I),NAXML,CXML(I),CXMLC(I),
     1DMEMB,DNOBLK,DBULK
101   CONTINUE
502    FORMAT(1X,8E15.8)
5001  FORMAT(1X,F8.2,8(1X,E15.8))

5002  FORMAT(//,1X,'TIME',8X,'SUC CONC',9X,'SUC FLUX',9X,'OBS CINTGL'
     1,4X,'CALC CONCINTGL',7X,'DMEMB',10X,'DNOBULK',10X,'DBULK',//)
5000  FORMAT(//,4X,'APARAMETER',4X,'BPARAMETER',4X,'CPARAMETER',
     14X,'DPARAMETER',//)
503   FORMAT(1X,//,'INTEGRATION LIMITS -1.80 CM TO  ',F10.7,//)
      XTOP =XTOP +DELTX
105   CONTINUE
      STOP
      END
      FUNCTION CINTGL(M,A,B,X)
C*********FUNCTION CINTGL CALCULATES CONCENTRATION INTEGRALS FROM
C*********ERROR FUNCTION PARAMETERS DETERMINED FROM RAYTRACE****
      IMPLICIT REAL*8(A-H,O-Z)
      REAL*8 M
      ALPHA =1.DO/49.01621DO
      BETA=-1.331313DO/49.01621DO
      CINTGL = ALPHA*((M/A)*(A*X*DERF(A*X) +
     1.56418958 * DEXP(-A*A*X*X)) + B*X) + BETA*X
      RETURN
      END
      FUNCTION DCDT(P,T)
C********FUNCTION DCDT FINDS PARTIAL DERIVATIVE WITH RESPECT TO TIME
C********FOR PROFILE CONCENTRATIN INTEGRALS***********************
      IMPLICIT REAL*8(A-H,O-Z)
      DIMENSION P(4)
      DCDT = (P(3)/(2.*T**.5) + P(3)*P(4)*P(4)/(T**1.5)
     1 -P(2)*.56418958*P(4)/(T**1.5))*DEXP(-P(4)*P(4)/T)
      RETURN
```

```
      END
      SUBROUTINE EQUFIT(C,PAR,NTIME)
C*********EQUFIT FITS CONCENTRATION PROFILES AT TIME INTERVALS TO ERROR FUNCT.**
C*********PAR(1)=A**************
C*********PAR(2)=B**************
C*********PAR(3)=C**************
C*********PAR(4)=D**************
      IMPLICIT REAL*8(A-H,O-Z)
      COMMON X(10),Y(10)
      DIMENSION IV(64),C(10),V(400),PAR(4)
      EXTERNAL CALCR,CALCJ
      CALL DFALT(IV,V)
      IV(23)=1
      N=NTIME+1
      M=4
      V(29)=1.D-20
      V(40)=1.D-20
      V(42)=1.D-20
      PAR(1)=6.7D-5
      PAR(2)=1.9D-6
      PAR(3)=-4.1D-8
      PAR(4)=25.6D0
        DO 100 I=1,N
100       Y(I)=C(I)
C******NL2SOL IS UBC CURVE FITTING NON-LINEAR LEAST SQUARES FITTING ROUTINE****
      CALL NL2SOL(N,M,PAR,CALCR,CALCJ,IV,V,IPARM,RPARM,FPARM)
      RETURN
      END
      SUBROUTINE CALCR(N,M,PAR,NF,R,IPARM,RPARM,FPARM)
C**********CALCR CALCULATES ERROR FUNCTION EQU. AND RESIDUALS**********
      IMPLICIT REAL*8(A-H,O-Z)
      COMMON X(10),Y(10)
      DIMENSION PAR(4),R(N)
      DO 100 I=1,N
      FX=PAR(1)+PAR(2)*DERF(PAR(4)/(X(I)**.5))
     1+PAR(3)*(X(I)**.5)*DEXP(-PAR(4)*PAR(4)/X(I))
100   R(I)=FX-Y(I)
      RETURN
      END
      SUBROUTINE CALCJ(N,M,PAR,NF,D,IPARM,RPARM,FPARM)
C*********CALCJ CALCULATES PARTIAL DERIVITIVES OF ERROR FUNCT. CORRELATION**
      IMPLICIT REAL*8(A-H,O-Z)
      COMMON X(10),Y(10)
      DIMENSION PAR(4),D(N,4)
      PI=3.1415927D0
      DO 100 I=1,N
      D(I,1)=1.D0
      D(I,2)=DERF(PAR(4)/(X(I)**.5))
      D(I,3)=(X(I)**.5)*DEXP(-PAR(4)*PAR(4)/X(I))
      D(I,4)=DEXP(-PAR(4)*PAR(4)/X(I))*2./(X(I)**.5)
     1*(PAR(2)/PI**.5 - PAR(4)*PAR(3))
100     CONTINUE
      RETURN
      END
```